USE OF EQUIVALENT SINGLE POROSITY MEDIUM AND AUTOMATED LUMPED FLUID COMPOSITION IN NATURALLY FRACTURED GAS CONDENSATE RESERVOIR SIMULATIONS

A THESIS SUBMITTED TO
THE GRADUATE SCHOOL OF NATURAL AND APPLIED SCIENCES
OF
MIDDLE EAST TECHNICAL UNIVERSITY

BY

MEHMET CİHAN ERTÜRK

IN PARTIAL FULFILLMENT OF THE REQUIREMENTS
FOR
THE DEGREE OF DOCTOR OF PHILOSOPHY
IN
PETROLEUM AND NATURAL GAS ENGINEERING

JUNE 2018

Approval of the thesis:

USE OF EQUIVALENT SINGLE POROSITY MEDIUM AND AUTOMATED LUMPED FLUID COMPOSITION SIMULATION IN NATURALLY FRACTURED GAS CONDENSATE RESERVOIRS

submitted by **MEHMET CİHAN ERTÜRK** in partial fulfillment of the requirements for the degree of **Doctor of Philosophy in Petroleum and Natural Gas Engineering Department, Middle East Technical University** by,

Prof. Dr. Halil Kalıpçılar
Dean, Graduate School of **Natural and Applied Sciences** _____

Prof. Dr. Serhat Akın
Head of Department, **Petroleum and Natural Gas Engineering** _____

Assoc. Prof. Dr. Çağlar Sınayuç
Supervisor, **Petroleum and Natural Gas Engineering Dept., METU** _____

Examining Committee Members:

Assoc. Prof. Dr. Uğur Murat Leloğlu
Geodetic and Geographic Information Technologies, METU _____

Assoc. Prof. Dr. Çağlar Sınayuç
Petroleum and Natural Gas Engineering Dept., METU _____

Assoc. Prof. Dr. Murat Çınar
Petroleum and Natural Gas Engineering Dept.,
İstanbul Technical University _____

Asst. Prof. Dr. İsmail Durgut
Petroleum and Natural Gas Engineering Dept., METU _____

Asst. Prof. Dr. Tuna Eren
Petroleum and Natural Gas Engineering Dept.,
İzmir Katip Çelebi University _____

Date: 08.06.2018

I hereby declare that all information in this document has been obtained and presented in accordance with academic rules and ethical conduct. I also declare that, as required by these rules and conduct, I have fully cited and referenced all material and results that are not original to this work.

Name, Last name : Mehmet Cihan Ertürk

Signature :

ABSTRACT

USE OF EQUIVALENT SINGLE POROSITY MEDIUM AND AUTOMATED LUMPED FLUID COMPOSITION SIMULATION IN NATURALLY FRACTURED GAS CONDENSATE RESERVOIRS

Ertürk, Mehmet Cihan

Ph.D., Department of Petroleum and Natural Gas Engineering

Supervisor: Assoc. Prof. Dr. Çağlar Sınayuç

June 2018, 108 pages

Each naturally fractured gas condensate reservoir is unique and needs special interests for an accurate modelling study. Ordinarily, it is a very difficult task to conduct a fast and well-characterized simulation study and predict the performance of such reservoirs in view of the complicated thermodynamic behavior, the complex fluid composition, dual porosity behavior and significant computational time requirement. The numerical simulation of fractured gas condensate reservoirs offer remarkable potential for understanding of the field development strategies even though it is a challenging process due to the aforementioned reasons.

The conventional simulation study of naturally fractured gas reservoirs is carried out with dual porosity and/or permeability models and the compositional simulation methodology. The main issues concerning the fractured gas condensate reservoirs are dealing with a large number of components that form the condensate fluid composition and also the need for a large amount of grid cells because of the nature of dual medium approach. They both have adverse impact on the execution time and give rise to various instabilities and convergence problems; hence the efficiency of the simulation study is affected in a negative manner.

In this work, it is aimed to attain not only a physically representative but also numerically time-efficient novel modeling approach that is required especially for the time consuming studies such as the sensitivity, uncertainty and optimization analysis. By using the proposed systematic lumping methodology based on the phase diagram comparison considering all the available schemes under the physical constraints and then to calculate the RMS error of each scenario compared to that of original quality lines of phase plot with isothermal depletion assumption, one can reduce the number of the components that represents the original fluid composition. Construction of an equivalent single porosity medium approach, which is not used for this type of reservoirs before, by averaging of variables such as porosity and permeability and weighting of some curves such as relative permeability curves instead of a traditional dual media technique reduces the number of cells, hence the simulation run time. In an attempt to validate the proposed lumping methodology and the equivalent single porosity technique, a naturally fractured gas condensate reservoir is evaluated by the traditional dual media and compositional simulation technique at first and then, additional near wellbore modeling approaches such as velocity dependent relative permeability and generalized pseudo pressure methods are incorporated into the model. The weaknesses and strengths of modeling approaches are assessed. Finally, the proposed new concepts are compared with the results of the conventional cases with respect to the accuracy and the run time of simulation. As a result, it is shown that the proposed lumping methodology and the equivalent single porosity are beneficial and adequate tools to be used for the modeling of naturally fractured gas-condensate reservoirs by saving considerable time.

Keywords: naturally fractured reservoir, gas condensate reservoir, equivalent single porosity system, dual porosity system, near wellbore modeling, component lumping

ÖZ

DOĞAL ÇATLAKLI GAZ KONDENSAT REZERVUARLARINDA EŞDEĞER TEK GÖZENEKLİ ORTAM VE OTOMATİK TOPLU AKIŞKAN KOMPOZİSYONU SİMÜLASYONU KULLANIMI

Ertürk, Mehmet Cihan

Doktora, Petrol ve Doğal Gaz Mühendisliği Bölümü

Tez Yöneticisi: Doç. Dr. Çağlar Sınayuç

Haziran 2018, 108 sayfa

Her doğal çatlaklı gaz kondensat rezervuarı eşsizdir ve doğru bir şekilde modellenmesi için özel bir ilgiye gereksinimi vardır. Genellikle, hızlı ve iyi karakterize edilmiş bir simülasyon çalışması yapmak ve böyle rezervuarların performansını tahmin etmek karmaşık termodinamik davranışları, kompleks akışkan kompozisyonu ve belirgin hesaplama zamanı gereksiniminden dolayı çok zor bir görevdir. Bahsi geçen nedenlerden dolayı çatlaklı gaz kondensat nümerik simülasyonu zorlu bir süreç olmasına rağmen, saha geliştirmenin anlaşılması için kayda değer bir potensiyel sunmaktadır.

Doğal çatlaklı gaz kondensat rezervuarlarının geleneksel simülasyonu çift gözenek ve/veya geçirgenlik modellleri ve kompozisyonel simülasyon metodolojisi ile gerçekleştirilir. Çatlaklı gaz kondensat rezervuarları ile ilgili ana sorun ikili ortam yaklaşımının doğası gereği ızgara yapısında cok sayıda hücre ve kondensat akışkan kompozisyonunu oluşturan çok sayıdaki bileşendir. Her ikisinin de simülasyon yürütme zamanı üzerine olumsuz etkisi olup çeşitli yakınsama ve dengesizlik sorunlarına neden olurlar. Bu nedenle, simülasyon çalışması olumsuz bir biçimde etkilenir.

Bu çalışmada özellikle duyarlılık, belirsizlik ve optimizasyon analizi gibi zaman alıcı çalışmalar için gerekli olan fiziksel olarak temsili, aynı zamanda hesaplama zamanı açısından verimli yeni bir modelleme yaklaşımı elde edilmesi amaçlanmıştır. Önerilen sistematik bir araya getirme metodolojisi, faz eğrisi kıyaslaması baz alınarak fiziksel kısıtlar altındaki tüm mevcut şemaları göz önünde bulunduran ve daha sonra izotermal tükenme varsayımıyla orijinal faz çiziminin kalite eğrilerine kıyasla her bir senaryonun kök ortalama kare hatasını hesaplayarak asıl akışkan kompozisazyonunu temsil eden bileşen sayısının azaltılabilmesidir. Gözeneklilik ve geçirgenlik gibi değişkenlerinin ortalaması alınarak ve göreli geçirgenlik eğrileri gibi eğriler ağırlandırılarak, geleneksel çift gözenekli bir ortam yerine bu tür rezervuarlar için daha evvel kullanılmamış olan eş değer tek gözenekli ortam yaklaşım modelini oluşturulması ızgara sayısını ve dolayısıyla simülasyon zamanını azaltır. Önerilen bir araya getirme metodolojisi ve eş değer tek gözenek tekniğinin geçerliliğini denetlemek amacıyla, doğal çatlaklı bir gaz kondensat rezervuarı öncelikle geleneksel ikili ortam ve komposizyonel simulasyon tekniği ile değerlendirilecek daha sonra hıza bağımlı göreli geçirgenlik ve genellenmiş sözde basınç metodları gibi ilave kuyu yakını modelleme yaklaşımları mevcut modele dahil edilerek bunların zayıf ve güçlü yönleri incelenecektir. Son olarak, önerilen yeni kavramlar simülasyon zamanı ve doğruluna göre geleneksel durumların sonuçları ile kıyaslanacaktır. Sonuç olarak, önerilen bir araya getirme metodolojisi ve eş değer tek gözeneklilik yaklaşımı büyük ölçüde zaman tasarrufu sağlayıp doğal çatlaklı gaz kondensat rezervuarlarını modellemek için kullanıbilecek yararlı ve yeterli araçlar olarak gösterilecektir.

Anahtar Kelimeler: doğal çatlaklı rezervuar, gaz kondensat rezervuar, eşdeğer tekli gözenek sistemi, çift gözenek sistemi, kuyu yakını modellemesi, bileşen bir araya getirme

To My Wife Tuğçe

ACKNOWLEDGEMENTS

I am sincerely grateful to my supervisor Assoc. Prof. Dr. Çağlar SINAYUÇ for his valuable suggestions, guidance, support and encouragement. He has always been accessible and willing to help throughout my work. Without his supervision, this study would not have been accomplished. I was honored to work with him.

I would like to thank to my monitoring committee members Assoc. Prof. Dr. Uğur Murat Leloğlu and Asst. Prof. Dr. İsmail Durgut for their support and guidance throughout this research and also for their feedback which helps making this work better.

I would like to extent my sincere thankfulness to Prof. Dr. Fevzi Gümrah for his friendship and support in my personal, professional and school life since my undergraduate years.

I am heartily thankful to my wife Tuğçe, and her patience, understanding and caring support which has been my source of strength and inspiration. As a result, this tough period became smooth and rewarding for me.

I would like to express my great gratitude and respect to my family for their endless support, trust, love and understanding in every stage of my life.

TABLE OF CONTENTS

ABSTRACT v
ÖZ vii
ACKNOWLEDGEMENTS x
TABLE OF CONTENTS xi
LIST OF TABLES xiii
LIST OF FIGURES xiv
NOMENCLATURE xvi
CHAPTERS
1. INTRODUCTION 1
2. LITERATURE REVIEW 5
2.1 Gas Condensate Reservoirs 5
2.1.1 Gas-Condensate Flow Behavior 5
2.1.1.1 Phase Behavior 5
2.1.1.2 Behavior of Condensate Blockage Phenomena 7
2.1.2 Modeling of Gas-Condensate Reservoirs 11
2.1.2.1 Compositional Simulation 11
2.1.2.2 Lumping of Components 11
2.2 Naturally Fractured Reservoirs 12
2.2.1.1 Modeling of Naturally Fractured Reservoirs 13
3. STATEMENT OF PROBLEM 19
4. METHODOLOGY 21
4.1 Model Properties and Input Data 21
4.2 Modeling of Naturally Fracture Reservoirs 23
4.2.1. Equivalent Single Porosity Model 24
4.2.1.1. Grid Property Modification 24
4.2.1.2. Pseudo Relative Permeability Generation 25
4.2.1.3. Treatment of Wells 28

4.2.2. Dual Porosity Model 28
4.2.3. Local Grid Refinement Modeling 31
4.3 Simulation of Gas Condensate Reservoirs 32
4.3.1. Use of Compositional Simulation Model 33
4.4 Treatment of Gas Flow Near Wellbore Region 33
4.4.1. Non-Darcy Flow 34
4.4.2. Velocity Dependent Relative Permeability Method 35
4.4.2.1 Capillary Number 35
4.4.3. Generalized Pseudo-Pressure Method 39
4.5 PVT Analysis of Gas Condensate Reservoirs 43
4.5.1. PVT Experiments 43
4.5.1.1 Constant Composition Expansion 43
4.5.1.2. Constant Volume Depletion 44
4.5.2. Flash Calculations 45
4.5.2.1. Flash Equations 46
4.5.3. Equation of State Calculation & Characterization 48
4.5.4. PVT Simulation and Lumping 48
4.5.4.1 Splitting 48
4.5.4.2 Grouping 49
4.5.5. PVT Data and Results 50
4.5.6. Automated Lump Approach 56
4.5.6.1 Estimating the Error of Lumped Fluid Models 59
5. RESULTS & DISCUSSION 61
6. CONCLUSION 95
REFERENCES 97
CURRICULUM VITAE 107

LIST OF TABLES

TABLES

Table 4.1 Model Variables 23
Table 4.2. Composition of Reservoir Fluid Sample 51
Table 4.3 Pressure Volume Relations of Reservoir Fluid at 200 F° (CCE) 52
Table 4.4 Condensation during Gas Depletion at 200 F° (CVD) 53
Table 4.5 Stepwise pseudoization of reservoir fluid sample 55
Table 5.1 Simulation Time of Some Cases 80
Table 5.2 Number of Component of Cases 80
Table 5.3 Error Values of Lumped Plus Fraction for Component Reduction Level 1 82
Table 5.4 Error Values of Lumped Plus Fraction for Component Reduction Level 2 82
Table 5.5 Error Values of Lumped Plus Fraction for Component Reduction Level 3 83
Table 5.6 Error Values of Lumped Plus Fraction for Component Reduction Level 4 84
Table 5.7 Error Value of Lumped Plus Fraction for Component Reduction Level 584
Table 5.8 Error Value of Lumped Isomers 85
Table 5.9 Error Value of Lumped Non-Hydrocarbons 85
Table 5.10 Error Values of Final Lumping Schemes 86
Table 5.11 Composition of Second Fluid Sample 91
Table 5.12 Error Values of Lumped Plus Fraction for Component Reduction Level 1 92
Table 5.13 Error Values of Lumped Plus Fraction for Component Reduction Level 2 92
Table 5.14 Error Values of Lumped Plus Fraction for Component Reduction Level 3 93
Table 5.15 Error Values of Lumped Plus Fraction for Component Reduction Level 4 93
Table 5.16 Error Value of Lumped Isomers 93
Table 5.17 Error Value of Lumped Non-Hydrocarbons 93
Table 5.18 Error Values of Final Lumping Schemes 93

LIST OF FIGURES

FIGURES

Figure 2.1 Phase diagram of a retrograde gas. (Ahmed 2007). 6
Figure 2.2 Typical liquid dropout curve of gas condensate. (Ahmed 2007). 7
Figure 2.3 Schematic representation of three region flow theory (Roussennac 2001). 8
Figure 2.4 Illustration of Positive Coupling Effect. 10
Figure 2.5 Classification of naturally fractured reservoirs (Nelson 2001). 13
Figure 2.6 Idealization of a fractured system (Warren and Root, 1963). 15
Figure 2.7 Idealization of the heterogenous porous medium (Gilman 1993). 16
Figure 2.8 Representation of Discrete Fractures (Petrel Manual 2013). 17
Figure 4.1 Dual Porosity Model. 22
Figure 4.2 Equivalnet Single Porosity Model. 22
Figure 4.3 Dual Porosity Model (Warren & Root, 1963). 29
Figure 4.4 Simulation model of a fractured system (Eclipse 2012). 30
Figure 4.5 View of a simple dual porosity system (Eclipse 2012). 31
Figure 4.6 Illustration of Local Grid Refinement Grids (Eclipse 2012). 32
Figure 4.7 Gas relative permeability curve. 39
Figure 4.8 Schematic of constant composition expansion experiment (CCE). 44
Figure 4.9 Schematic of constant volume depletion experiment (CVD). 45
Figure 4.10 Phase diagram of a gas condensate system. 52
Figure 4.11 Relative Total Volume in Constant Composition Expansion at 200 F°. 53
Figure 4.12 Liquid drop-out curve. 54
Figure 4.13 Phase Diagrams of some lumped fluid samples. 56
Figure 4.14 Successive approximation method of automated lumping process. 58
Figure 4.15 Detailed Representation of Proposed Methodology 58
Figure 5.1 Field Pressure of Dual Porosity and Equivalent Single Porosity Models. 62
Figure 5.2 Average Field Pressure of Dual and Equivalent Single Porosity Models. 62
Figure 5.3 Bottom Hole Pressure of Dual and Equivalent Single Porosity Models. 64
Figure 5.4 Cumulative Condensate Production of both Models. 65
Figure 5.5 Average Grid Pressure of Dual Porosity Models. 65
Figure 5.6 Bottom-hole Pressure of Dual Porosity Models. 66
Figure 5.7 Cumulative Condensate Production of Dual Porosity Models. 67
Figure 5.8 Effect of Fracture to Matrix Permeability Ratio on Average Grid Pres. . 68
Figure 5.9 Effect of Fracture to Matrix Permeability Ratio on BHP. 68
Figure 5.10 Effect of Fracture to Matrix Permeability Ratio on Average Grid Pres. 69

Figure 5.11 Effect of Fracture to Matrix Permeability Ratio on BHP. 69
Figure 5.12 Average Grid Pressure of Dual Porosity Lumped Models. 71
Figure 5.13 Bottom Hole Pressure of Dual Porosity Lumped Models. 71
Figure 5.14 Average Grid Pressure of Equivalent Single Porosity Lumped Models. 72
Figure 5.15 Bottom Hole Pressure of Equivalent Single Porosity Lumped Models. 72
Figure 5.16 Average Grid Pressure of all Lumped Models for Dual Porosity. 73
Figure 5.17 Average Grid Pressure of all Lumped Models for Single Porosity. 74
Figure 5.18 Cumulative Condensate Production of Dual Porosity Lumped Models. 75
Figure 5.19 Cumulative Condensate Production of Equivalent Single Porosity Lumped Models. 75
Figure 5.20 Elapsed time of Equivalent Single Porosity and Dual Porosity Models. 77
Figure 5.21 Elapsed time of Dual Porosity System with Different Lumped Samples. 77
Figure 5.22 Elapsed time of Single Porosity System with Different Lumped Samples 78
Figure 5.23 Elapsed Time vs. # Component Number for Single Porosity System. .. 79
Figure 5.24 Elapsed Time vs. # Component Number for Dual Porosity System. 79
Figure 5.25 Simulation Time vs Cases. 81
Figure 5.26 RMS Error vs. Number of Pseudo Components (sample 1)..... 87
Figure 5.27 RMS Error vs. Number of Pseudo Components (sample 2)..... 88
Figure 5.28 RMS & Simulation Error vs. Number of Pseudo Components 89
Figure 5.29 RMS & Simulation Error vs. Number of Pseudo Components 89
Figure 5.30 RMS vs Simulation Error 90
Figure 5.31 Phase diagram of second fluid sample (gas condensate)..... 92

NOMENCLATURE

Latin

k_m: matrix permeability

k_f: fracture permeability

k_b: modified grid block permeability

n_f: the number of fractures present in the fractured block

d_f: cumulative fracture aperture

d_b: grid block spacing

$M_{T,\,ij}$: transmisivity multiplier

$T_{ij,\,m}$: transmissibility of the matrix only between grid blocks i and j

$T_{ij,\,b}$: transmissibility of the matrix between grid blocks i and j after incorporation of the fracture permeability

l_f: the cumulative length of the fractures in the given grid block

$S_{gr,\,m}$: residual gas saturation in the matrix

$S_{gr,\,f}$: residual gas saturation in the fracture

$S_{cr,\,m}$: residual condensate saturation in the matrix

$S_{cr,\,f}$: residual condensate saturation in the fracture

$k_{ge,\,m}$: end point relative permeability to gas in the matrix (at the residual condensate saturation)

$k_{ge,\,f}$: end point relative permeability to gas in the fracture

$k_{ce,\,m}$: end point relative permeability to condensate in the matrix (at the residual gas saturation)

$k_{ce,\,f}$: end point relative permeability to condensate in the fracture

$M_{PI,i,n}$: local productivity index multiplier for perforated grid block I of well n

k_b : permeability of matrix plus fracture in grid block i

C_n : global multiplier for all perforated grid blocks of well n

N_{cp} = capillary number, as defined by the model selected

v_g : gas velocity

S_p : saturation of phase p, in the cell of calculation

N_{cnp} : normalized capillary number of phase p

S_p : normalized hydrocarbon phase saturation

F_p : Scaling parameter between the miscible and immiscible relative permeability

X_p : Fractional reduction of the trapped saturation in phase p

$S_{pTrapped}$: trapped saturation of phase p on the original relative permeability curves

S_{max} : max. hydrocarbon saturation

k_{rpMax} : the max. permeability on the original, entered permeability curves at S_{Max}

$k_{rpImmisc}$: relative permeability of phase p, under immiscible relative permeability

k_{rpMisc}: relative permeability of phase p, under straight line relative permeability

$k_{rpCombined}$: the result of the interpolation between the miscible and immiscible curves

h = height of the homogenous radial media

k = permeability

r = radius

Q_j = in-situ volumetric flow rate

n_i: component phase molar rate

M_i: molar mobility

M_T: total molar mobility

F_{Bi}: flow blocking factor

F_B: total dimensionless flow blocking factor

k_j = phase relative permeability

dP/dr = pressure gradient

V_{jm} : phase molar volume

x_{ij} : mole fraction of the i^{th} component in the j^{th} phase

r_B : Peaceman pressure equivalent radius

r_w : Peaceman pressure equivalent well radius

T : well connection factor

S : skin factor

P_b: block pressure

P_w: bottom-hole pressure

P_{dew}: dew point pressure

P_{res}: reservoir pressure

Z_{pi}: composition of the flowing fluid

CGMM: component generalized molar mobility

TGMM: total generalized molar mobility

DP: Dual Porosity

ESM: Equivalent Single Medium

CCE: Constant Composition Expansion

CVD: Constant Volume Depletion

RMS: Root Mean Squared

Greek

ϕ_m: matrix porosity

ϕ_f : fracture porosity

ϕ_b: modified grid block porosity

α_f: the contribution of fracture volume to the total mobile porosity in a grid block

$\beta_{f,c}$: the contribution of fracture to the maximum grid block relative permeability to condensate

$\beta_{m,g}$: the contribution of fracture to the maximum grid block relative permeability to gas

μ_g : gas viscosity

μ_j = phase viscosity

σ_{go} : gas-oil surface tension

CHAPTER 1

INTRODUCTION

A significant amount of hydrocarbon fluid resides in naturally fractured reservoirs all over the world. Representation of such systems in a proper way is crucial to obtain efficient and effective reservoir management strategies. To do this, reservoir simulation is one of the widely preferred techniques however modeling and simulation of naturally fractured reservoirs present unique challenges compared to conventional single porosity systems due to their geological complexity (Vo et al., 1989). That is commonly honored in practice by utilizing flow modeling procedures based on dual porosity approach involving twice the number of grid cells (Bourbiaux et al. 2002; Beckner 1990).

The type of fluid in place, i.e., gas condensate is another challenging point in respect to reservoir simulation (Coats, 1982). In general, that kind of fluid flow model applies to compositional simulation methodology which is generally used to model fluids near the critical point where changes in the pressure and temperature of the compositional system can result in very different fluid behavior. There are also a number of issues that may be needed to be taken into account while running a compositional model. The most remarkable one is the computing time which drastically differs from the black oil simulation (Bengherbia and Tiab, 2002).

The gas condensate reservoirs also differ from other type of gas reservoirs which have very special characteristics in terms of their flow and phase behaviors (Whitson et al., 1982). When the reservoir pressure falls below the dew point pressure, the condensate drops out of the gas in the system and this

causes substantial productivity loss (El-Banbi et al., 2000; Hinchman and Barree, 1985) which is an issue associated with the condensate banking (Barker, 2005) that occurs around the well. The behavior of condensate blockage can be simulated properly with the help of additional near wellbore modeling techniques such as velocity dependent relative permeability (Henderson et al., 2000), generalized pseudo pressure method (Whitson and Fevang, 1997), and local grid refinement that might contribute to accurate fluid flow through the near wellbore area.

The change of reservoir conditions with time is investigated by determining average values in each simulation cell during successive small time steps. At each time step, equilibrium condition is determined for each grid block by exhaustive flash calculations. For a large reservoir, the total number of equilibrium flashes may exceed many millions, consuming a large computational time and making the simulation expensive. As the number of equations in conventional flash calculation increases with the number of components, the number of components characterizing the fluid is commonly reduced by lumping to reduce the computational time. As stated in the cases above, computing time of a simulation highly depends on selected modelling techniques such as dual porosity and compositional models. In this regard, this study aims at generating an equivalent single porosity medium replacing commonly used dual porosity model with/without near wellbore modeling techniques and also making use of a proposed novel automated lumping procedure to generate a minimum equivalent lumped composition that represents the full composition of the system as an alternative to using any heuristic lumping techniques. In doing so, the simulation study of the naturally fractured gas condensate field with a real data set will be performed by means of a commercial simulator. Results of conventional and proposed approaches are compared with one another to observe the consistency and the range the margin of difference is minimum.

Last but not least, the methods are investigated in terms of run time of simulation; revealing the time that could be saved with the proposed techniques and whether they are adequate or not.

To sum up, the effects of using equivalent models with the lumped fluid compositions both in geological and fluid properties will be analyzed in terms of their advantages and disadvantages in order to understand the error range versus computational time relationship.

CHAPTER 2

LITERATURE REVIEW

2.1 Gas Condensate Reservoirs

Gas-condensate reservoirs consist of a significant amount of hydrocarbon resources and exhibit very complex flow and thermodynamic behaviors. Therefore, the optimization of hydrocarbon recovery of gas-condensate reservoirs needs having a good understanding of phase behavior, reservoir properties, planning and management (Allen and Roe, 1950).

Most of the gas condensate systems are found as single phase gas at the prevailing reservoir conditions of pressure and temperature at the time of discovery. Once the well flowing bottom-hole pressure drops below the dew point pressure, condensation begins to occur and liquid hydrocarbon phase is formed while its saturation builds up around the wellbore leading significant reduction in well deliverability. This negative impact, so-called condensate banking (or condensate blockage), on the inflow performance of the well is the main challenge of a gas condensate system due to the decrease in the effective gas permeability (Wheaton and Zhang, 2000). Build-up of condensate saturation around the well is a dynamic process and varies as a function of time, location (distance to wellbore) and phase behavior owing to the compositional variation and relative permeability constraints.

2.1.1 Gas-Condensate Flow Behavior

2.1.1.1 Phase Behavior

A typical phase envelope or P-T diagram of retrograde gas is given in Figure-2.1. It demonstrates that if the initial pressure is above the dew point pressure and located at

point-1 and also the reservoir temperature is between the critical temperature and cricondentherm of the reservoir fluid where the gas-condensate is initially present as a gaseous phase. When the production starts under the isothermal conditions, reservoir pressure decreases and exhibits a dew-point pressure point-2. The attraction between the molecules of the light and heavy components gets weakened and that results in a split between the heavy and light components hence it increases the attraction between the molecules of heavy components and gives rise to condensation of fluid (Ahmed, 2007). The process of condensation proceeds with the reservoir pressure depletion until the liquid dropout comes to its maximum accumulation value (Figures 2.1 and 2.2). If the pressure keeps decreasing, the heavier molecules start to vaporize and more gas molecules leave the liquid phase rather than entering it and the process continues until the lower dew-point pressure at which the fluids of system is totally in the vapor phase (Ahmed, 2007 and Whitson and Brule 2000).

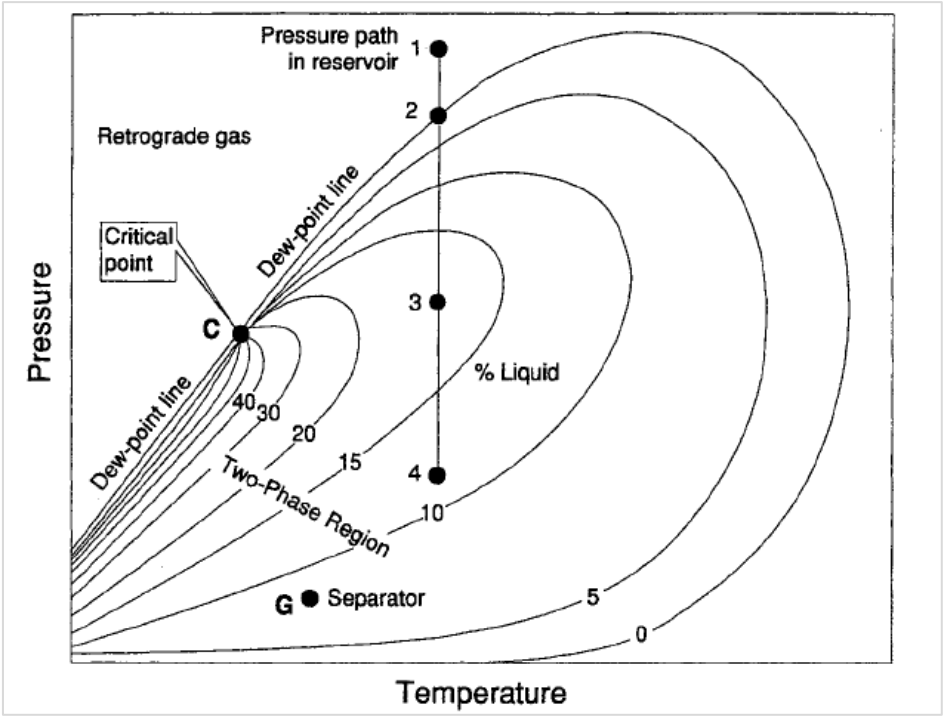

Figure 2.1 Phase diagram of a retrograde gas (Ahmed 2007).

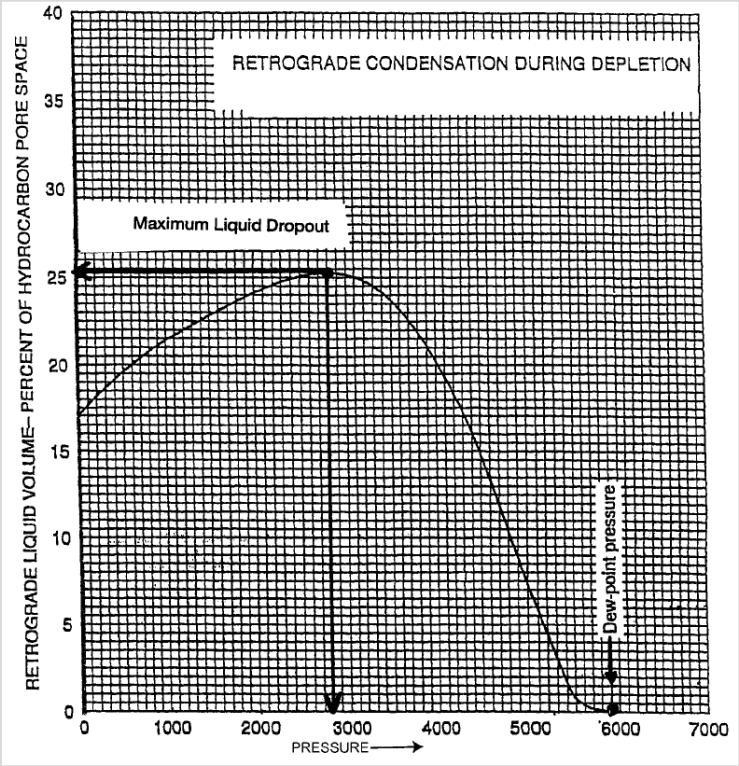

Figure 2.2 Typical liquid dropout curve of gas condensate (Ahmed 2007).

2.1.1.2 Behavior of Condensate Blockage Phenomena

The gas condensate reservoirs differ from the other type of gas reservoirs and they have very special characteristics in terms of their flow and phase behaviors. When the reservoir pressure falls below the dew point pressure, the condensate drops out of the gas in the system and that causes to substantial productivity loss associated with the condensate banking occurs around the well (Shi et al., 2006). According to Afidick et al. (1994) and Barnum et al. (1995), the well productivity may reduce 50% or even more due to condensate build-up. First studies regarding the deliverability reduction were conducted in the 1930s however it has been still a long standing problem. Muscat (1949) accounted for the radius of the condensate blockage with a function including time, gas rate, rock and fluid properties. The two numerical models were developed to estimate the saturation and pressure near the wellbore by Kniazeff and Naville in 1965 separately. O'Dell and Miller (1967) announced a method to calculate the condensate volume in the vicinity of the producing well and its impact on the production rate with steady-state flow concept. Later on, Roebuck et al. (1968) presented the first model for each component and by taking into account mass transfer

between phases. Modified version of the model was utilized by Fussel (1973) and his results indicated that the productivity of the well may be reduced by a factor three compared to O'Dell and Miller's predictions (1967). Fevang and Whitson (1996) touched upon the significance of the physics of condensate blockage and proposed the three flow region theory for flow of gas condensate into a producing well from a reservoir undergoing depletion under the steady-state flow conditions. Figures 2.3 shows the three flow region theory in a proper way.

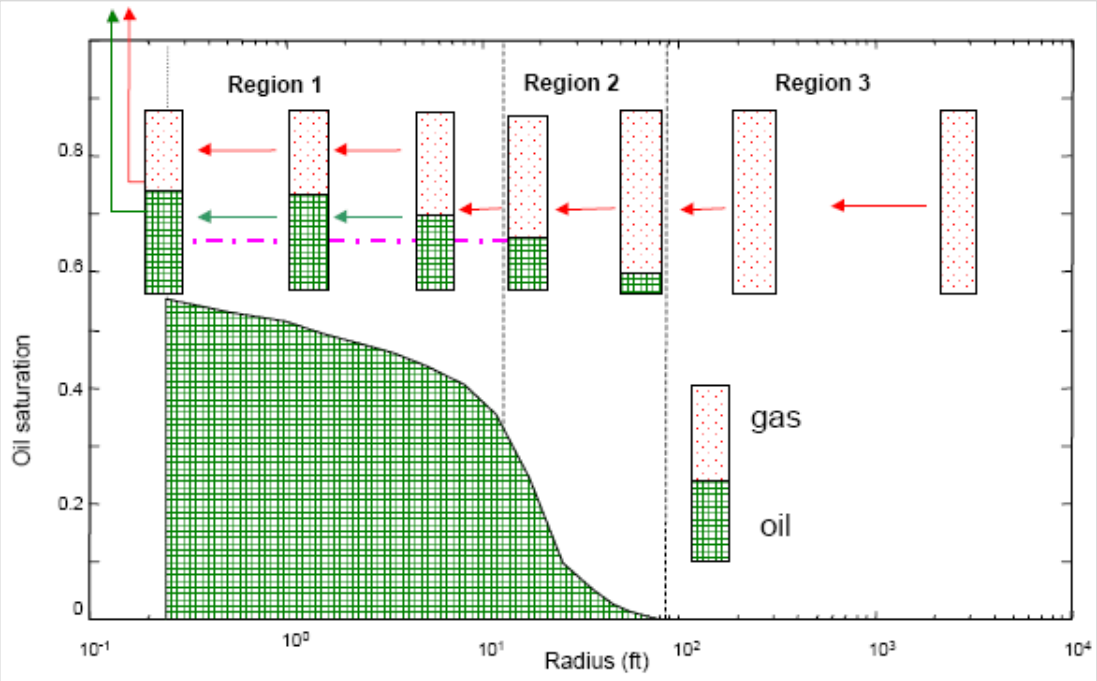

Figure 2.3 Schematic representation of three region flow theory (Roussennac 2001).

Region 1: An inner near-wellbore region where the condensate saturation is above the critical saturation and both gas and condensate are mobile thereby they flow simultaneously (with different velocities). The composition of the producing wellstream is almost constant throughout this region (Roussennac, 2001). In other words, the overall composition of the flowing fluid has the same composition with the single phase gas and dew point pressure at the outer edge of Region 1. The fluid properties can be estimated by the constant composition expansion (CCE) of the producing mixture (Fevang, 1995).

The main reason behind the well deliverability loss is the sharp decrease in the gas relative permeability due to the high oil saturation in Region 1. With ongoing production, the radius of Region 1 increases provided that the bottom hole flowing pressure stays below the dew-point pressure at all times. Moreover, the amount of the dropped out liquid is dependent on the production rate and PVT properties of the reservoir fluid in Region 1.

Region 2: It is the intermediate region, in which the condensate first starts to drop out of the gas in the reservoir. It means that the flowing pressure declines the dew-point pressure and the first droplet of liquid condensate is formed at the boundary between Region 2 and Region 3. The effect of the gas relative permeability reduction is limited on the well productivity because the liquid phase does not flow due to being zero or low oil mobility. On the other hand, the only flowing phase is gaseous and it leaves its intermediate and heavier components in the liquid / oil phase hence it becomes leaner and leaner with the changing composition (Riemens and Jong, 1985). Saturation of condensate can be approximated by means of the liquid dropout curve from the constant volume depletion (CVD) experiment which is corrected for water saturation. At the early stage of condensation process, the size of Region 2 is largest but it decreases with time as Region 1 expands. The net condensate accumulation is also defined in Region 2.

Region 3: An outer part of the reservoir or the region farthest away from the well where the pressure is above the dew-point pressure of the reservoir fluid. In Region 3, fluid is in single gas phase and the composition of fluid is constant and represents the original reservoir gas. The properties of fluid could be approximated by CCE experiment.

In addition to that positive coupling, velocity coupling, or velocity stripping effect was introduced in 2000 by Henderson et al. The phenomenon that creates a new mobility region in the nearest vicinity of the wellbore is related to the relative permeability increase of the gas and condensate phase while increasing velocity due to the capillary number effects which turn out to be miscible flow partially. Figure 2.4 illustrates the positive coupling effect of a well producing gas with condensate.

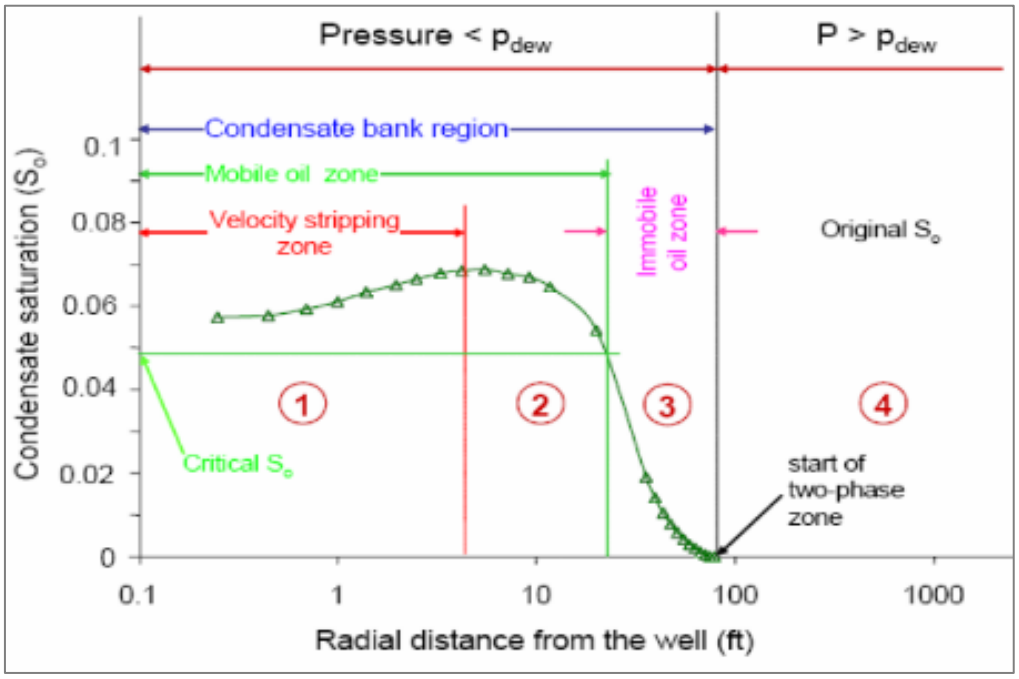

Figure 2.4 Illustration of Positive Coupling Effect.

Two techniques, the single-phase and two-phase pseudo-pressure, are used to estimate the actual fluid gas condensate reservoirs. The former one was proposed by Al Hussainy et al. (1966) to linearize the real gas flow equation and it works well for dry gas and also gas condensate wells that produce above the dew-point pressure. The latter one is divided into two models such as steady-state and three-region model. O'Dell and Miller (1967) developed the steady state saturation pressure model so-called two-region model around the wellbore without transition zone. This model includes inner and outer region. In the inner region below the dew-point pressure, gas and condensate exhibit together. For the outer region above the dew-point pressure, only single phase gas flows. The model was also improved by Chopra and Carter (1985) and Jones and Raghavan (1989) to approximate the pressure-saturation relationship assuming a hypothetical steady-state flow. The three-region model is already explained in detail in the previous part of this chapter.

2.1.2 Modeling of Gas-Condensate Reservoirs

The idea behind the reservoir simulation is to divide the reservoir into a number of discrete units in the desired dimensions and model the progression of reservoir and fluid properties through space and time in a series of discrete steps to quantify and interpret physical phenomena with the ability to extend these to project future performance.

2.1.2.1 Compositional Simulation

The compositional simulation models have a number of features in common with the black oil simulation model to account for the effects of composition on phase behavior, miscible displacement, etc. On the contrary, the latter one is not capable of providing the adequate reservoir description especially for such cases: Enhanced Oil Recovery processes that involves a miscible displacement, cases where gas injection/re-injection into an oil producers a large compositional changes in the fluids, if condensate are recovered using gas cycling and the composition of injected gas is significantly different from the composition of any free gas in the reservoir.

Despite the fact that the compositional simulation enables the comprehensive description of reservoir processes in a number of circumstances, there are several difficulties which would need to be taken into account while running a compositional simulation model. The computing time is the most serious of them.

2.1.2.2 Lumping of Components

The equilibrium condition over a time step is determined by flash calculation in each grid block. As reservoir calculations are generally iterative, more than one equilibrium flash calculation per each grid-block at a time step is required. For a large reservoir, the total number of equilibrium flashes may exceed millions, consuming a large computational time and making the simulation expensive. As the number of equations in conventional flash calculation increases with the number of components, the number of components characterizing the fluid is commonly reduced by lumping to reduce the computational time. An important consideration in phase behavior

modeling of reservoir studies is wide ranges of composition and pressure which are to be modelled (Jacoby et al., 1959; and Li et al., 1988).

The concept of lumping has long been employed in fluid description, but this is conducted commonly because of limitations in the compositional analysis. The most famous technique is to determine the hydrocarbon mixture with discrete components to normal pentane and hexanes each as a single carbon group and lump all the heavy fractions as the heptane plus (C_{7+}) (Behrens et al., 1986). That is not an efficient method of describing a reservoir fluid, particularly in compositional simulation studies, where it is desirable to minimize the number of components while still retaining the reliability of predicted values by phase behavior models.

Many investigators (Hong, 1982; Schlijper, 1984; and Montel and Gouel, 1984) recommended selecting the number of pseudo components (groups). A simple approach is to add nitrogen and carbon dioxide to methane and ethane respectively, and to combine iC_4 with nC_4 and iC_5 with nC_5. The plus fraction is also characterized by a number of pseudo-components and included. The boundary between the consecutive groups are based on the molecular weights and mole fractions (Gonzalez et al., 1986). The selection of pseudo-components are generally performed with the help of heuristic methods such as trial and error. The use of statistical approach can play an important role to minimize the number of components and optimize the lumped fluid models.

2.2 Naturally Fractured Reservoirs

Most of the oil and gas reservoirs are affected in some way by natural fractures all over the world, yet the effects of fractures which have a significant role on reservoir performance are often poorly understood and largely underestimated. The reservoirs having fractures are generally coupled with background rock matrix and characterized with respect to two continua media. Nelson (2001) classified four types of naturally fractured reservoirs according to storage capacity and permeability. In Type-1 fractured reservoirs; the fractures provide the essential storage capacity and permeability in the reservoir. The matrix has very low porosity and permeability and

also it does not contain any recoverable hydrocarbon. In Type-2 reservoirs, the fractures act to further increase the permeability of the reservoir. The matrix is responsible for the main storage capacity and has low permeability, but it may have low, moderate, or even high porosity. In Type-3 systems, the matrix permeability and porosity are relatively high and the fracture contributes to the flow capacity of the reservoir. In Type-4 reservoirs, the fractures that are sealed with clays create barriers to flow and impact on the system permeability in a negative way however the matrix has high permeability and porosity in such reservoirs. Figure 2.5 demonstrates the relationship between percent reservoir porosity and percent permeability (percent due to matrix versus percent due to fracture)

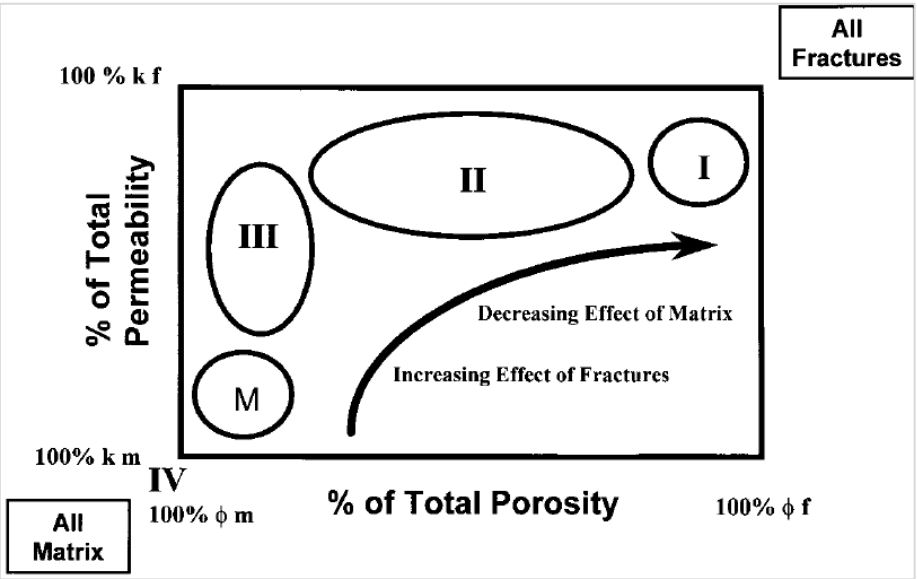

Figure 2.5 Classification of naturally fractured reservoirs (Nelson 2001).

2.2.1.1 Modeling of Naturally Fractured Reservoirs

In the literature, there are several approaches to simulate the fluid flow in naturally fractured reservoirs such as equivalent single continuum, dual porosity, and discrete fracture network models.

The equivalent single porosity approach treats the matrix and fracture media as single entity and attempts to include the respective contribution of each system variables

such as transmissibility and porosity. The parameters involving into the flow equations are averaged corresponding to the nature of the property and also the pseudo-curves are described especially for capillary pressure and relative permeabilities. With the help of this methodology, the flow can be modeled with the accurate fluid flux through the naturally fractured reservoirs.

From the reservoir simulation engineering point of view, naturally fractured reservoirs are generally represented with the dual porosity continuum models. The foundation of this phenomenon was introduced by Barenblatt (1959). His formula was composed of the flow equations for each continuum using conservation of mass principles and source or transfer functions, and also the pseudo-steady state flow assumption of a fluid between the set of fractures and the matrix blocks as distinct but interacting continua.

In 1963, Warren and Root proposed an idealized form of Barenblatt's model to account for the hydraulic behavior of a fractured reservoir with a simplified system of stacked or sugar cube model. Figure 2.6 illustrates the schematic of this model. The reservoir model is formed by two porosity regions as primary and secondary associated with matrix and fracture respectively. The matrix blocks are defined by the primary porosity of the system that contains the remarkable amount of the reservoir pore volume and is assumed to be homogenous and isotropic. The fractures are represented by the secondary porosity of the system that is responsible for the majority of the flow capacity and assumed to be orthogonally connected (continuous) and it also surrounds the matrix blocks by penetrating a set of identical rectangular matrix blocks. The single-phase fluid flow only occurs between the matrix and fractures but not within the matrix under the pseudo-steady state conditions in this approach.

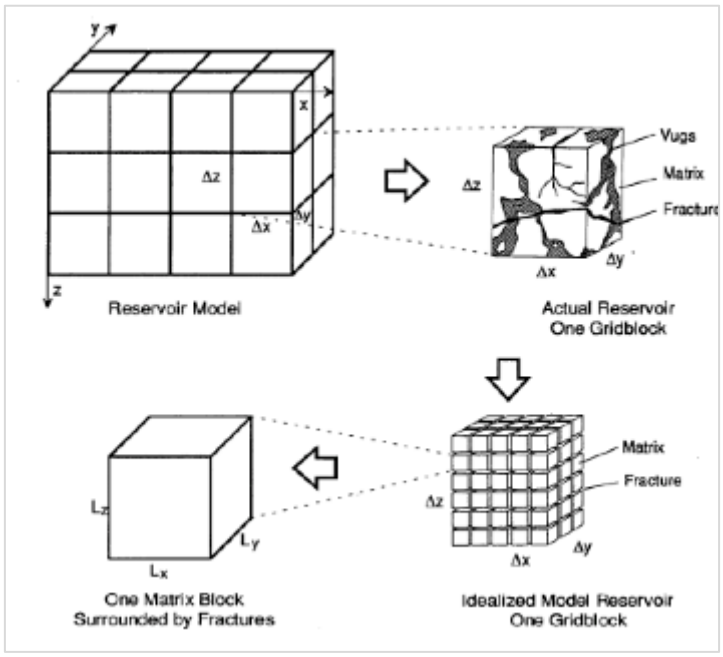

Figure 2.6 Idealization of a fractured system (Warren and Root, 1963).

Kazemi (1969) developed a new model considering the unsteady-state or transient single-phase flow between the matrix and the fracture network in 1969 and he also used the slab dual porosity model, which is comprised of a system of horizontally stacked matrix layers being divided by a set of horizontal fractures, instead of the famous sugar cube one. The model has the similar assumptions with the Warren and Root's model but the main difference is the circular shape of the reservoir. Figure 2.7 shows the Kazemi's Slab model configuration.

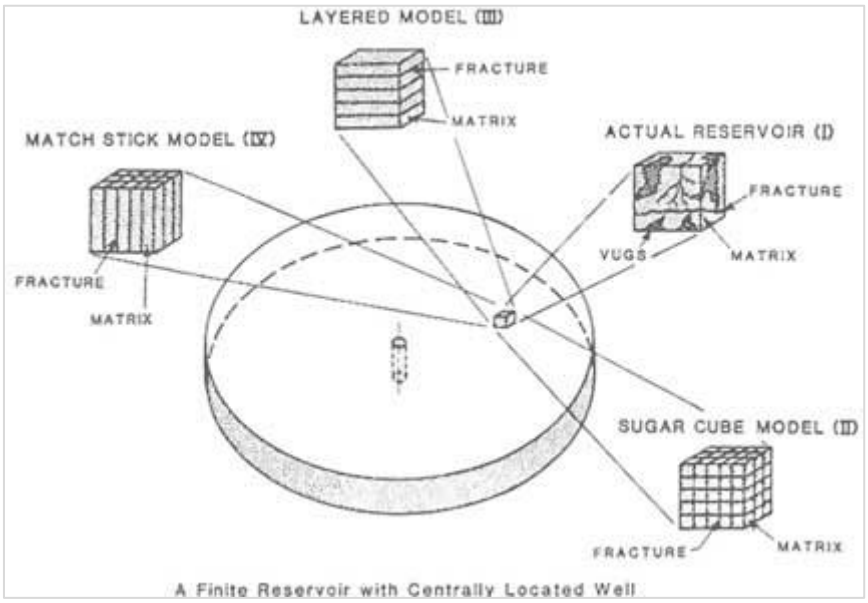

Figure 2.7 Idealization of the heterogenous porous medium (Gilman 1993).

Unfortunately, the idealized systems mostly do not honor the geological characteristics of the naturally fractured reservoirs properly since they are highly heterogeneous and anisotropic systems, thus the main drawback of the dual porosity systems is inconsistencies created by uniform assumptions of matrix and fracture properties.

The discrete fracture network (DFN) model relies on the constructing of a network of planar surfaces representing the fractures/joints and faults in three dimensions (Figure 2.8). The main advantage of the model over the previous one (dual medium or porosity) is to take into consideration the framework of fracture geometry details and each individual fracture attributes explicitly. The DFN model concept was suggested in 1970s (Bear 1972) and developed in 1980s. The initial models were simple and created in a deterministic way. Later, the approach was reviewed and extended by several authors to achieve a stochastic model (Dershowitz and Einstein 1988). In 1998, Dershowitz and Doe enhanced the stochastic methodology successfully and presented the up-to-date/current DFN modeling in a less generalized way based on interactive discrete feature data analysis and geometric modeling. In spite of its powerful structure, the building of a DFN model does not need extensive

characterization work and more computational cost in terms of CPU and memory, therefore the use of this method is practical industrially in particular for large-scale fields.

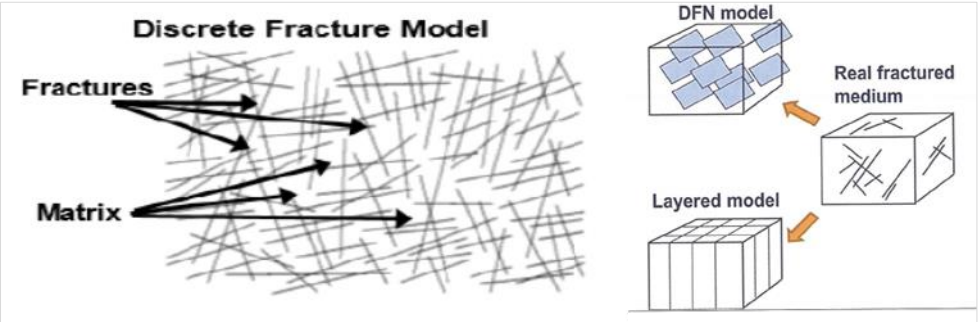

Figure 2.8 Representation of Discrete Fractures (Petrel Manual 2013).

CHAPTER 3

STATEMENT OF PROBLEM

The conventional simulation study of naturally fractured gas condensate reservoirs is carried out with dual porosity and/or permeability models and the compositional simulation methodology. Simulation of naturally fractured gas condensate reservoirs is more time demanding and computationally more expensive not only due to their doubled number of cells representing the dual-medium matrix/fracture system but also because of having high number of components forming the complex hydrocarbon composition. The simulations might frequently be exposed to several numerical instabilities and convergence problems, thus the efficiency of the simulation is affected in a negative manner.

In this work, a naturally fractured gas condensate reservoir is evaluated by the traditional dual media and compositional simulation techniques at first and then, the velocity dependent relative permeability and generalized pseudo pressure methods are incorporated into the current model and also explored to assess their weaknesses and strengths. The lumping procedure of fluid components are commonly conducted in a heuristic way such as trial and error procedure and all possible grouping schemes are not described and analyzed independently. That mostly depends on the experience thus it may seem to be impractical to achieve an optimal solution. For the purpose of reducing the components of the fluid composition statistically, the number of optimum component is endeavored to be adjusted by the proposed automated lumping procedure. After that, all the necessary steps like averaging of variables and weighting of some curves such as relative permeability curve are accomplished to construct an equivalent single porosity model for the same lumped fluid composition.

Finally, the proposed new concept is compared with the results of the other cases with respect to the accuracy and run time of simulation and it is validated as beneficial and adequate tool. As a result, the main objective of the thesis is to attain a physically representative and numerically efficient novel modeling approach with the help of proposed lumping algorithm.

CHAPTER 4

METHODOLOGY

Most hydrocarbon reservoirs contain fractures at various scales and those have a strong influence on the preferential flow directions and the pressure profile of the porous media. If the fluid composition of such systems is complex such as gas condensate, modeling and simulation studies become more difficult and numerous challenges should be dealt with to represent the fluid flow properly through these systems. In this part, the implemented methodology and details of the constructed model will be explained.

4.1 Model Properties and Input Data

The starting point in the study was to create two different 3D layered model grids, and distribute the petrophysical properties and make necessary adjustments by pre-processer. Later on, the original fluid sample was analyzed and lumped in terms of their similar properties by means of PVTi (2010.1) package and then each case was prepared by modifying the base models. In the final step, numerical compositional simulator, Eclipse 300 (2010.1), was employed to investigate each case.

The following figures represent the constructed two models dual porosity and equivalent single medium one. The former one has 32000 cartesian blocks ((Nx=40, Ny=40, Nz=10) built with ten zones having thickness of 10 meters. The latter one has 16000 cartesian blocks ((Nx=40, Ny=40, Nz=10) built with ten zones having thickness of 10 meters. Areal extent of both models are the same; 4 km to 4 km in x and y directions.

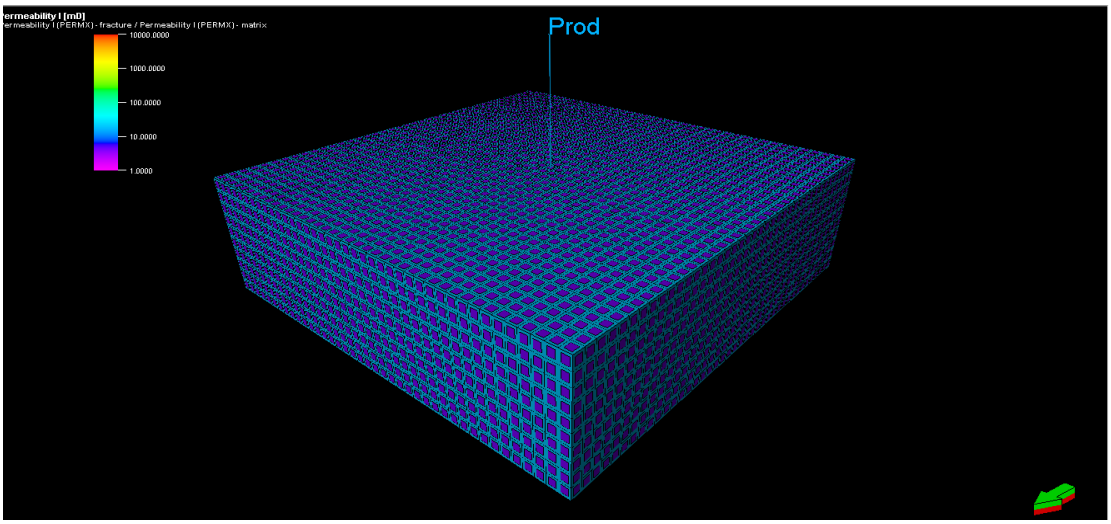

Figure 4.1 Dual Porosity Model.

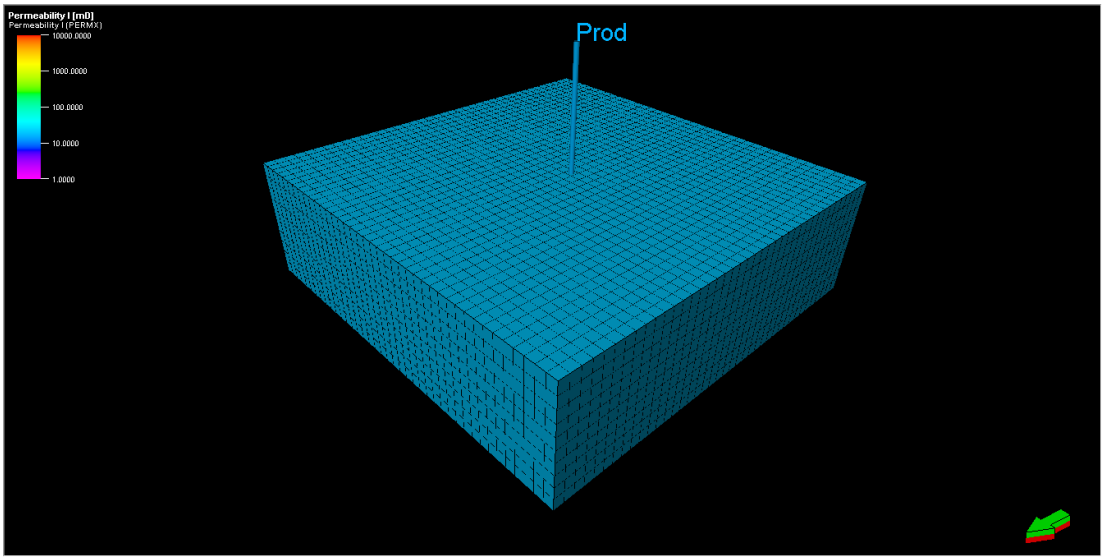

Figure 4.2 Equivalnet Single Porosity Model.

Table-1 illustrates the simulation dataset for dual porosity and equivalent single medium models.

Table 4.1 Model Variables

	DP	ESM
k_{mx}, mD	4	45.2
k_{my}, mD	2	23.4
k_{mz}, mD	1	12.7
k_{fx}, mD	200	-
k_{fy}, mD	100	-
k_{fz}, mD	50	-
$Ø_m$, %	4	4.35
$Ø_f$, %	0.4	-
P_{res}, psia @ reservoir top	4786	4876
P_{dew}, psia	3442	3442

For the sake of clarity, it is needed to make some necessary arrangements before the simulations of both models are run. For example, the original gas in place, fracture orientation and properties, and transmissibility values in each direction should be identical. The fractures of equivalent single medium are also spaced and distributed in each direction taking into account the value of the fracture transfer function in dual porosity model. In addition to that both models are constructed as homogenous and non-isotropic.

4.2 Modeling of Naturally Fracture Reservoirs

The naturally fractured reservoirs differ from the conventional non-fractured ones in terms of conductivity and storage characteristics (Sognesand, 1991). Each naturally fractured reservoir system has special characteristics that should be integrated into the model accordingly to achieve the acceptable and reliable simulation results (Bourbiaux et al., 2002). In the study, the issue will be handled with widely used two methods relied on the homogenization of fracture properties.

4.2.1. Equivalent Single Porosity Model

The equivalent single porosity approach is based on the incorporation of the effects of conductive fractures into a single effective continuum by virtue of the modification of grid properties and the generation of pseudo tables without using any dual system of porosities or permeabilities. It was put forward by Van Lingen et al, (2001) as an alternative dual porosity formulation in literature.

The following procedures explain the implementation of the technique in three subsequent main areas.

4.2.1.1. Grid Property Modification

The grid block properties are modified to take account of the physical void introduced by fractures. The conductivity and porosity values are increased by appropriate averaging technique.

The equivalent conductivity is calculated in the two-step procedure. First, the permeability of the grid blocks containing fractures is averaged and then the transmissivities of the corresponding grid blocks are reset using a transmissivity multiplier.

Estimation of Conductivity:

$$k_b = k_m + \frac{k_f n_f d_f}{d_b} \quad (1)$$

Where

k_m: matrix permeability

k_f: fracture permeability

k_b: modified grid block permeability

n_f: the number of fractures present in the fractured block

d_f: cumulative fracture aperture

d_b: grid block spacing

$$M_{T,ij} = \frac{T_{ij,m}}{T_{ij,b}} \quad (2)$$

Where

$M_{T,\,ij}$: transmisivity multiplier

$T_{ij,\,m}$: transmissibility of the matrix only between grid blocks i and j

$T_{ij,\,b}$: transmissibility of the matrix between grid blocks i and j after incorporation of the fracture permeability (using the first equation)

$$T_{ij} = \frac{2k_i k_j}{d_b(k_i + k_j)} \quad (3)$$

Estimation of Porosity: The following arithmetic averaging estimates the average porosity of the grid block with fractures.

$$\phi_b = \phi_m + \frac{\phi_f l_f d_f}{d_b^2} \quad (4)$$

Where:

ϕ_m: matrix porosity

ϕ_f : fracture porosity

ϕ_b: modified grid block porosity

l_f: the cumulative length of the fractures in the given grid block

4.2.1.2. Pseudo Relative Permeability Generation

The saturation curves of the fractures and affected grid blocks are combined under the assumption that the fracture volume of a grid block is filled with gas before any condensate is displaced from the matrix volume of a grid block.

First, the pseudo end-points are calculated by changing the effective residual saturations and end-point relative permeabilities of the grid blocks in the presence of fractures.

Estimation of Residual Saturations:

The effective residual gas saturation of the fractured grid blocks, $S_{gr,\,b}$, is calculated as follows:

$$S_{gr,b} = \frac{S_{gr,m}\phi_m d_b^2 + S_{gr,f}\phi_f l_f d_f}{\phi_m d_b^2 + \phi_f l_f d_f} \quad (5)$$

Where

$S_{gr,\,m}$: residual gas saturation in the matrix

$S_{gr,\,f}$: residual gas saturation in the fracture

The similar calculations are made for the residual condensate or oil saturation, $S_{cr,\,b}$.

$$S_{cr,b} = \frac{S_{cr,m}\phi_m d_b^2 + S_{cr,f}\phi_f l_f d_f}{\phi_m d_b^2 + \phi_f l_f d_f} \quad (6)$$

Where:

$S_{cr,\,m}$: residual condensate saturation in the matrix

$S_{cr,\,f}$: residual condensate saturation in the fracture

then, the effective end-point relative permeability $k_{ge,\,b}$ to gas and $k_{ce,\,b}$ to condensate are calculated as:

$$k_{ge,b} = \frac{k_{ge,m} k_m d_b + k_{ge,f} k_f n_f d_f}{k_m d_b + k_f n_f d_f} \quad (7)$$

Where

$k_{ge,\,m}$: end point relative permeability to gas in the matrix (at the residual condensate saturation)

$k_{ge,\,f}$: end point relative permeability to gas in the fracture

$$k_{ce,b} = \frac{k_{ce,m}k_m d_b + k_{ce,f}k_f n_f d_f}{k_m d_b + k_f n_f d_f} \quad (8)$$

Where

$k_{ce,m}$: end point relative permeability to condensate in the matrix (at the residual gas saturation)

$k_{ce,f}$: end point relative permeability to condensate in the fracture

The matrix and fracture relative permeability curves are combined to generate one single pseudo curve. Initially, the original matrix and facture curves are normalized between 0 and 1 both with respect to the saturation and the end point relative permeability. The three parameters are required to do this procedure.

α_f: the contribution of fracture volume to the total mobile porosity in a grid block

$$\alpha_f = \frac{(1-S_{gr,f}-S_{cr,f})l_f d_f \phi_f}{(1-S_{gr,f}-S_{cr,f})l_f d_f \phi_f} + \frac{(1-S_{gr,f}-S_{cr,f})l_f d_f \phi_f}{(1-S_{gr,m}-S_{cr,m})d_b^2 \phi_m} \quad (9)$$

$\beta_{f,c}$: the contribution of fracture to the maximum grid block relative permeability to condensate

$$\beta_{f,c} = \frac{k_f k_{rce,f} n_f d_f}{k_f k_{rce,f} n_f d_f + k_m k_{rce,m} d_b} \quad (10)$$

$\beta_{m,g}$: the contribution of fracture to the maximum grid block relative permeability to gas

$$\beta_{m,g} = \frac{k_m k_{rge,m} d_b}{k_m k_{rge,m} d_b + k_f k_{rge,m} n_f d_f} \quad (11)$$

The points of the original matrix curves are adjusted with the following transformations:

$$S_{cn,b} = S_{cn,m}(1- \alpha_f)+\alpha_f \quad (12)$$

$$k_{rcn,b} = k_{rcb,m}(1-\beta_{f,c})+\beta_{f,c} \quad (13)$$

$$k_{rgn,b} = \beta_{f,g} k_{rgn,m} \quad (14)$$

Also, the two points are considered to create the grid block pseudo relative permeability curves:

$k_{rcn,b}\ (S_{cn,b} = 0) = 0$ (15)

$k_{rgn,b}\ (S_{cn,b} = 0) = 1$ (16)

4.2.1.3. Treatment of Wells

The well completed in the grid blocks containing fractures may be subjected to enhanced flow conditions owing to the increased effective permeability (i.e. both the permeability and the relative permeability changes) once it intersects any fractures. If not so, two modifications are made to specify the case. The first modification is to reverse the changes in permeability with the well productivity or injectivity index multiplier and the second one is to revert the connection cell saturation table to that of the original matrix block.

$$M_{PI,i,n} = C_n \left(\frac{k_m}{k_b}\right)_{i,n} \quad (17)$$

Where

$M_{PI,i,n}$: local productivity index multiplier for perforated grid block I of well n

k_m : matrix permeability of grid block i

k_b : permeability of matrix plus fracture in grid block i

C_n : global multiplier for all perforated grid blocks of well n

4.2.2. Dual Porosity Model

The general idea and progress of the dual medium approach was given chronologically in chapter-2. As for the use of that in numerical simulator, the reservoir is represented by two overlapping continua - fracture networks acting as main flow channels and matrix blocks serving as a major storage source that is shown in figure 4.3. The interaction between the two continua is controlled through a transfer function called

shape or coupling factor (σ) that can be evaluated with typical dimensions of the matrix blocks or distances between fractures.

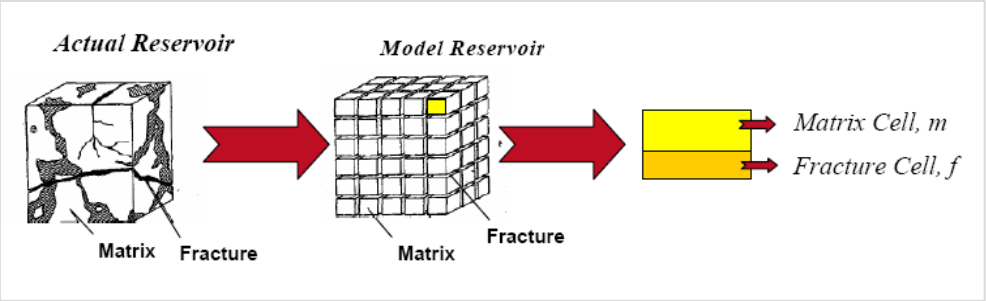

Figure 4.3 Dual Porosity Model (Warren & Root, 1963).

The shape factor may be expressed by analytical derivations, numerical derivations, and time-dependent functions. Several authors proposed shape factor constant but Kazemi and Gilman (1992) type of shape factor is mostly utilized in the numerical simulators since it is easy to apply.

The shape factor (σ) accounts for the matrix-fracture interface area per unit bulk volume and Kazemi has proposed the following form for σ:

$$\sigma = 4\left[\frac{1}{L_x^2} + \frac{1}{L_y^2} + \frac{1}{L_z^2}\right] \quad (18)$$

Where L_x, L_y, and L_z are typical X, Y and Z dimensions of the blocks of material making up the matrix volume and they refer to fracture spacing in represented directions and also L_x, L_y, and L_z are thus not associated to the simulation grid dimensions. It describes how the fluid flows between the matrix and fracture cells of a dual porosity model at the same location.

In the above equation, σ is second order and distance-related parameter which is inversely proportional to the fracture spacing. Consequently, the higher fracture spacing is in the system, the smaller shape factor is calculated.

In a dual porosity reservoir, fluids exist in two interconnected systems:

1. The rock matrix, which usually provides the bulk of the reservoir volume
2. The highly permeable rock fractures.

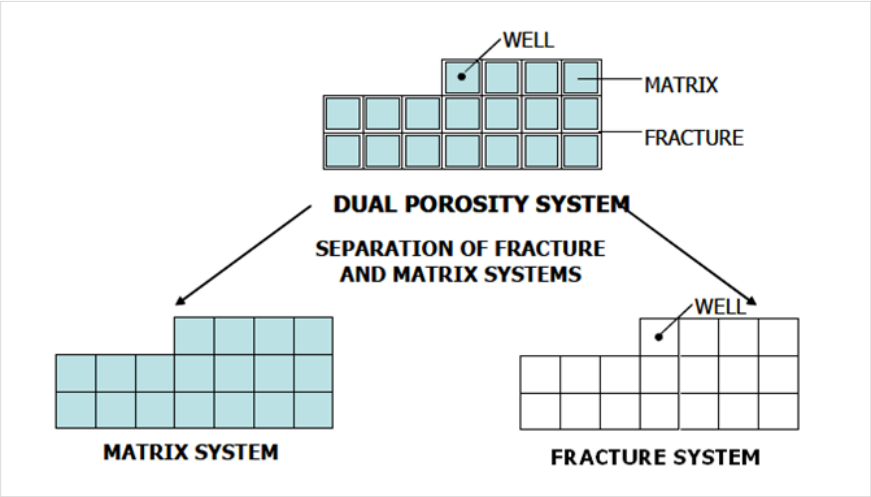

Figure 4.4 Simulation model of a fractured system (Eclipse 2010).

The Dual porosity model consists of two interconnected systems representing the matrix and the permeable rock fractures as shown in figure 4.4. The matrix blocks are linked only through the fracture system regarded as a dual porosity single permeability system, since fluid flow through the reservoir takes place only in the fracture network with the matrix blocks acting as sources and there is no flow between neighboring matrix blocks.

To model such systems, two simulation cells are associated with each block in the geometric grid, representing the matrix and fracture volumes of the cell. In a dual porosity run of Eclipse (2010.1), the number of layers in the Z-direction is doubled and Eclipse automatically assigns the first half of the grid with the matrix blocks, and the second half with the fractures as represented in figure 4.5. In such case, the number of layers (NDIVIZ) should be even and for the dual porosity model to be activated.

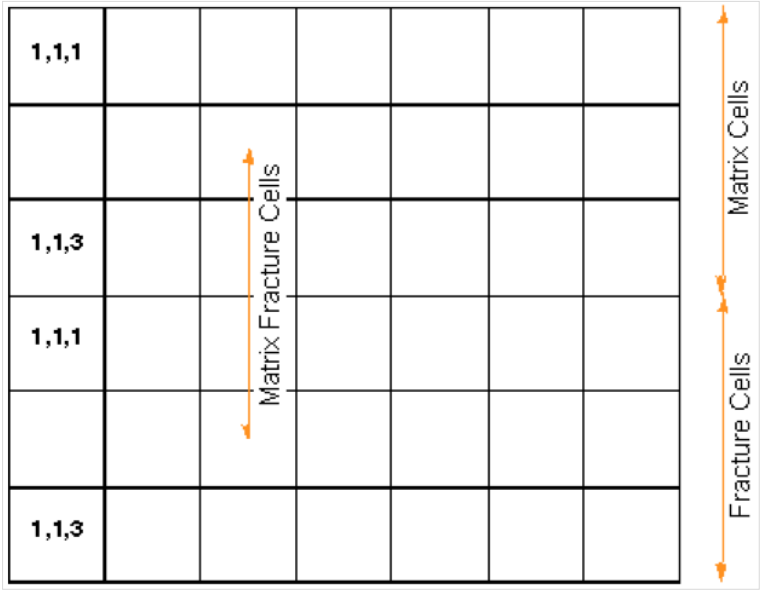

Figure 4.5 View of a simple dual porosity system (Eclipse 2010).

The following restrictions apply to dual porosity runs in Eclipse:

- ✓ Wells connect only to fracture cells – not to matrix cells.
- ✓ Non-neighbor connections (NNC) may not be used with matrix cells.
- ✓ Each active matrix cell must connect with an active fracture cell.

4.2.3. Local Grid Refinement Modeling

The local grid refinement (LGR) technique was proposed initially by Von Rosenberg (1982) to model the unit mobility ratio flow in one quarter of a five-spot pattern. The results indicated that the use of local grid refinement in the vicinity of a well improves the accuracy of the numerical solution without any remarkable increase in the total number of gridblocks. Just after that the local grid refinement facility has appeared in the commercial reservoir simulators.

The low resolution grid is usually sufficient for the most part of the simulation models. However, in many different situations, the higher grid resolution is required to capture the large changes in the solution variables (i.e., fluid saturations) over the course of the simulation, or to give additional model definition around a particular feature of interest such as the area surrounding a pilot study.

The local grid refinement allows describing a local grid in an area of interest having a different resolution to the original global (coarser) grid. The properties of the cells in the local grid might be inherited either from the global grid or specified explicitly for the refined cells.

The local grid refinements, which are the cartesian and cylindrical types, are utilized to simulate and model the many cases (i.e., large pressure changes near the wellbore, coning and supping, condensate dropout, undulating horizontal wells, areas of high well density, etc.). Figure 4.6 depicts the two different types of LGR.

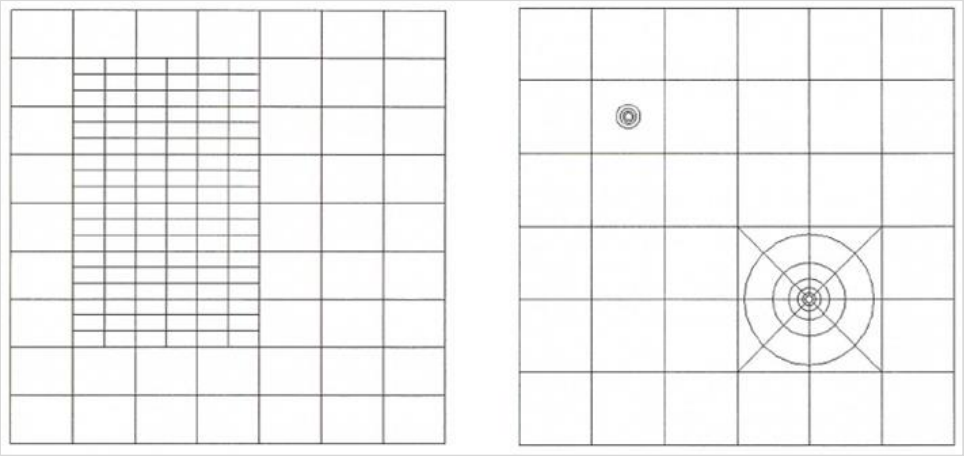

Figure 4.6 Illustration of Local Grid Refinement Grids (Eclipse 2010).

In our model, the grid block including the production well acts as a host cell and it is refined locally with 10 by 10 grids.

4.3 Simulation of Gas Condensate Reservoirs

Simulation of gas condensate reservoirs are generally performed by compositional simulators to represent their complicated thermodynamic behavior and the complex fluid composition accordingly. The most challenging part of that is to conduct the simulation study in an acceptable timeframe and at reasonable cost.

4.3.1. Use of Compositional Simulation Model

If the reservoir fluid stays as a single phase oil or gas during its entire production life and it is far away from the critical point, the black oil simulation models are adequate. For some cases, the compositional effects may exist especially for two-phase fluid flow at the prevailing reservoir conditions that can be approximated with varying gas-oil and oil-gas ratios and modelled by black oil simulators as well (Coats 1988). However, once the reservoir temperature and pressure are close to the critical point of the reservoir fluids or they approach each other during the management of the reservoir in view of the gas injection, the compositional simulation models must be performed. Even if there is no gas injection into the reservoir, the compositional simulation could be required for some special situations such as large compositional with depth, temperature variations with depth and large compositional variation in the lateral direction. Actually, the main difference between the black-oil and compositional simulation is the fluid PVT description. Whilst the fluid properties is taken from a table of physical properties versus pressure in a black oil model, the flash calculation and Equation of State have to be solved in a compositional model to identify what components are present at the given pressure and temperature (Spivak and Dixon 1973). In other words, the physical properties of the reservoir fluid is only function of pressure in a black oil model, however, the compositional model confirms the number of phases present first. If there are more than one phase, and it ascertains the composition of each phase. Lastly the physical properties of the fluid are computed in as much as the assigned compositions.

4.4 Treatment of Gas Flow Near Wellbore Region

The flow behavior of gas is affected somehow in the near well-region with regard to the high gas velocities leading to the turbulent and positive coupling or velocity stripping effects (Nikravesh and Soroush 1996; Ali et al., 1997). In addition to that gas condensate drop-out would change in situ saturations that would influence the relative permeabilities (Whitson et al., 2003). For instance, the turbulence flow that causes additional pressure drop is modeled successfully with Forchheimer correction (Lai et al., 2009). However, the mobility increase of oil and gas must be considered

with various different options such as capillary number model by virtue of the reduced interfacial tension (Barker, 2005).

4.4.1. Non-Darcy Flow

Darcy's Law is unable to capture the fluid flow accordingly at the high flow rates. In 1901, Forchheimer observed the deviations and expanded Darcy's linear form into a quadratic flow equation so-called Forchheimer Equation. The non-Darcy flow or the inertia effects due to high velocity that may occur around the gas wells or in high permeability regions such as fractures is taken into consideration with Forchheimer parameter in the simulation studies (Wu et al., 2009).

Darcy flow is given by:

$$q = \left(\frac{kA}{\mu}\right)\frac{dP}{dx} \tag{19}$$

or

$$\frac{dP}{dx} = \left(\frac{\mu}{kA}\right)q \tag{20}$$

Where

q = volumetric flow rate (cm^3/s)

k = permeability (Darcys)

A = area of flow (cm^2)

dP/dx = pressure gradient (Atm/cm)

Forchheimer Equation is given by:

$$\frac{dP}{dx} = \left(\frac{\mu}{kA}\right)q + \beta\rho\left(\frac{q}{A}\right)^2 \tag{21}$$

Where:

ρ = fluid density, (g/cm^3)

β = non-Darcy flow coefficient or Forchheimer parameter

4.4.2. Velocity Dependent Relative Permeability Method

The concept of velocity dependent relative permeability was developed to investigate the velocity stripping effect corresponding to increase in relative permeability due to increase in velocity that can lessen the impact of inertia on well deliverability. The phenomenon is mostly related to miscibility between the flowing phases because of the low interfacial tension in high velocity flow regimes (Henderson et al., 1995). In this regard, several empirical models depended on the capillary number concept were suggested to determine correlations between interstitial velocity in the reservoir, interfacial tension and viscosity (Blom and Hagoort, 1997).

4.4.2.1 Capillary Number

The capillary number, which is function of fluid viscosity (μ), velocity (v), and the interfacial tension (σ), is a dimensionless parameter defined as the ratio of viscous to capillary forces (indication of the relative strength of viscous stripping to capillary trapping). (App and Mohanty, 2002) Many researchers have worked to compute the capillary number effects on residual saturations and relative permeabilities and proposed various models which are empirical in origin. The capillary number is mostly expressed in the literature as:

$$N_c = \frac{v\mu}{\sigma} \qquad (22)$$

In gas condensate reservoirs, the interfacial tension between gas and condensate could be very low (smaller capillary forces). The viscous forces might be the same order of magnitude with the capillary forces thereby the phase distribution is affected by the viscous force even on the pore scale and therefore the macroscopic flow properties such as residual saturation and relative permeability are dependent on both forces. (Bourbiaux and Limborg, 1994)

At higher capillary numbers, the residual saturation is reduced because of the enhancement of the viscous forces compared to the capillary forces. It is also identified that the relative permeabilities of both phases are improved by the lower interfacial tension.

The velocity dependent relative permeability calculations are made according to the following flowchart for all three of the capillary number models. (Henderson et al., 2000 and Whitson et al., 1999) and final gas relative permeability curve which is attained by flowchart is given in figure 4.7.

Models in Eclipse

Model 1:

$$N_{cp}{}^{(1)} = \frac{v_g \mu_g}{\sigma} \quad (23)$$

Model 2:

$$N_{cp} = \frac{Kk_{rvp} \Delta p_P}{\sigma L} \quad (24)$$

Model 3:

$$N_{cp} = \left(2 \phi S_p Kk_{rvp}\right)^{\frac{1}{2}} \frac{\Delta p_P}{\sigma} \quad (25)$$

The subscript p indicates phase and these equations are calculated for the gas and condensate phases separately.

1) Calculate the capillary number based on the definition selected

2) Normalize the capillary number versus the base capillary number, which is a fitting parameter of the model, and is in the numerator

3) Calculate the normalized saturation (without water)

4) Calculate the miscibility factor, F_p, with n1p and n2p. This is one of the main factors that will change the relative permeability

5) Calculate the multiplier of the trapped (critical) endpoint, X_p. This is the second main factor that affects the relative permeability

6) Calculate the lookup saturation for the immiscible K_r via the endpoint scaling process (with X_p) and then use the lookup saturation to interpolate for K_{rp}_Immisc on the original kr curves

7) Calculate the miscible K_{rp} based on a scaled straight line

8) Combine the miscible and immiscible K_{rs} with F factor from step 4

9) To arrive at the final relative permeability, we need to add the effect of water in the normal way if the water is available in the system

$$N_{cp}{}^{(1)} = \frac{v_g * \mu_g}{\sigma} \tag{26}$$

$$N_{cnp} = \frac{N_{cbp}}{N_{cp}} \tag{27}$$

$$S'_p = \frac{S_p}{1 - S_w} \tag{28}$$

$$n_p = n1_p * S'p^{n2p} \quad , \quad F_p = N_{cnp}{}^{\left(\frac{1}{np}\right)} \tag{29}$$

$$X_p = 1 - \exp\left(-m_p * N_{cnp}\right) \tag{30}$$

$$SLookup = S_pTrapped + \frac{(S_p - X_p * S_pTrapped) * (S_{max} - S_pTrapped)}{(S_{max} - X_p * S_pTrapped)} \tag{31}$$

$$k_{rp}Misc = k_{rp}Max * \frac{(S_p - X_p * S_pTrapped)}{\left((1 - S_w) - X_p * S_pTrapped\right)} \tag{32}$$

$$k_{rp}Misc = k_{rp}Max * \frac{(S_p - X_p * S_pTrapped)}{\left((1 - S_w) - X_p * S_pTrapped\right)} \tag{33}$$

$$K_{rpImmisc} = K_{rpTables}(SLookup) \tag{34}$$

$$k_{rg} = \frac{S_o k_{rgo} + (S_w - S_{wco}) k_{rgw}}{S_o + S_w - S_{wco}} \quad , \quad k_{ro} = \frac{S_g k_{rog} + (S_w - S_{wco}) k_{row}}{S_g + S_w - S_{wco}} \tag{35}$$

Items in blue are fitted or calibrated parameters, ones in green are scaling parameters or results.

N_{cp} = capillary number, as defined by the model selected

v_g = gas velocity

μ_g = gas viscosity

σ_{go} = gas-oil surface tension

S_p = saturation of phase p, in the cell of calculation

Calculated Parameters:

N_{cnp} = normalized capillary number of phase p

S'_p = normalized hydrocarbon phase saturation (water removed)

Fitted Parameters (determined by laboratory or well testing)

$N_{cbp,}$ m_p, $n1_p$, $n2_p$ for each hydrocarbon phase (p)

Scaling Parameters (results of the calculation that act on the relative permeability behavior)

F_p = Scaling parameter between the miscible and immiscible relative permeability curves

X_p = Fractional reduction of the trapped saturation in phase p

Relative Permeability Parameters

$S_{pTrapped}$ = The trapped saturation (critical) of phase p on the original relative permeability curves. $S_{gTrapped}$ = SGCR, or ISGCR if imbibition curves are present

S_{max} = maximum hydrocarbon saturation, 1-SWL (see figure 4.7)

k_{rpMax} = the maximum permeability on the original, entered permeability curves at S_{Max} (see figure 4.7) S_{wco}: Sama as SWCR

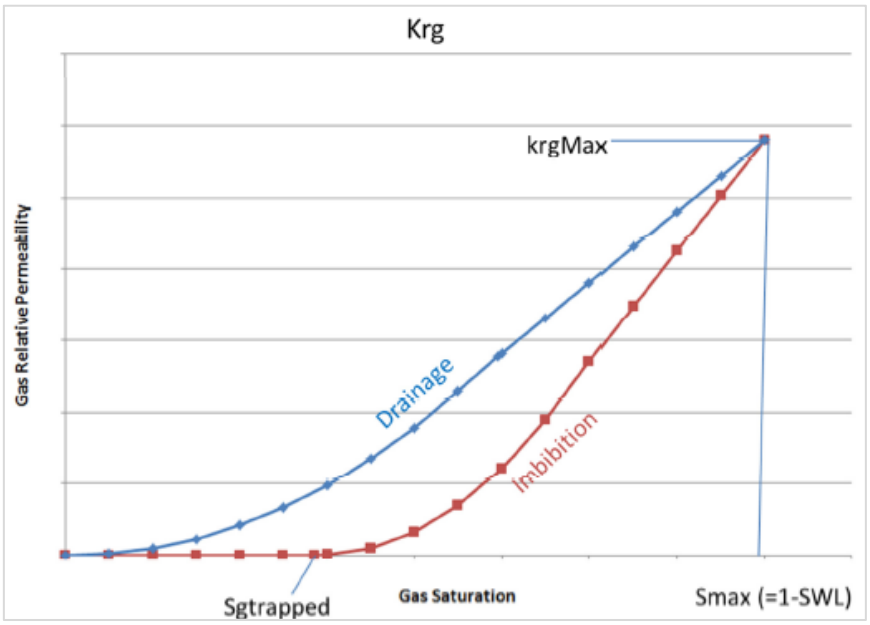

Figure 4.7 Gas relative permeability curve.

$k_{rpImmisc}$: relative permeability of phase p, under immiscible relative permeability curves (scaled to changed trapped saturation = ($S_{pTrapped}$*X_p)

k_{rpMisc}: relative permeability of phase p, under straight line relative permeability curves (scaled to k_{rpmax} and changed trapped saturation)

$k_{rpCombined}$: the result of the interpolation between the miscible and immiscible curves

k_{rg}, k_{ro}: the final relative permeability of the hydrocarbon phases after weighting by the water present.

4.4.3. Generalized Pseudo-Pressure Method

The generalized pseudo pressure (GPP) is another way to model the effects of gas condensate dropout on the fluid mobilities in the field scale simulation. This approach is convenient for relatively coarse grids as an alternative to make use of the local grid refinement modeling for the condensate blockage issue near the wellbore (Fevang and Whitson 1996).

The initial study on the gas condensate pseudo pressure technique was conducted by Fevang and Whitson in 1996 and further results were published by Singh and Whitson on the same topic in 2008. The GPP method is commonly recommended to be used

with coarse grids and the grid block containing the well should be small enough to represent the near-well steady-state flow region accordingly.

The pseudo pressure methodology is based on the assumption that the flowing composition of produced fluid is known from a grid cell at a given time step. The corresponding rate with reference to bottom hole flowing pressure and average grid cell pressure are related to each other by means of the fluid composition, appropriate relative permeabilities, and PVT calculations. (Whitson and Fevang, 1997)

Derivation:

$$v_j = \frac{Q_j}{2\pi rh} = \frac{KK_{rj}}{\mu_j}\frac{dP}{dr} \quad (36)$$

Where

Subscript j represents the flow of phase (oil, gas)

h = height of the homogenous radial media

K = permeability

r = radius

Q_j = in-situ volumetric flow rate

K_j = phase relative permeability

μ_j = phase viscosity

dP/dr = pressure gradient

if the phase volumetric flow rate is written as follows.

$Q_j = n_j V_{mj}$

Where

Vjm is phase molar volume. Combining and re-arranging gives:

$$n_j \frac{dr}{r} = 2\pi Khx_{ij}\frac{K_{rj}b_j}{\mu_j}dp \quad (37)$$

where x_{ij} is the mole fraction of the i^{th} component in the j^{th} phase.

Integrating between the Peaceman pressure equivalent radius r_B and the well radius r_w gives

$$n_{ij}\int_{r_W}^{r_B}\frac{dr}{r} = \ 2\pi Kh\int_{P_W}^{P_B} x_{ij}\frac{K_{rj}b_j}{\mu_j}dp \tag{38}$$

Summing component phase molar rates in the oil and gas phases for component i:

$$\left(n_{io}+n_{ig}\right)\left[\ln\left(\frac{r_B}{r_W}\right)+S\right] = 2\pi Kh\int_{P_W}^{P_B}\left[x_i\frac{K_{ro}b_o}{\mu_o}+y_i\frac{K_{rg}b_g}{\mu_g}\right]dp \tag{39}$$

or:

$$n_i = T\int_{P_W}^{P_B} M_i(p)\,dp \tag{40}$$

where the well connection factor, T, including the skin factor, S, is given by:

$$T = \frac{2\pi Kh}{In\left(\frac{r_B}{r_W}\right)+S} \tag{41}$$

and the component generalized molar mobility (CGMM) is given by:

$$M_i = x_i\frac{K_{ro}b_o}{\mu_o}+y_i\frac{K_{rg}b_g}{\mu_g} \tag{42}$$

Usually, the pressure dependency is not considered in the integral and the CGMM is computed at the block pressure.

$$\int_{P_W}^{P_B} M_i(p)\,dp \rightarrow \ M_i(P_B)[P_B - P_W] \tag{43}$$

For a gas condensate system, the block pressure may be approximated poorly and the inconsistency between the well and block pressure leads to remarkable reduction in the gas relative permeability. In such cases, the integral should be performed in more detail and the ratio of component generalized molar mobility (CGMM) for component i to the total generalized molar mobility (TGMM) should be a constant to prevent the accumulation of moles in the completion cell.

$$z_{pi} = \frac{M_i}{M_T} \tag{44}$$

where

$$M_T = \sum_i M_i \tag{45}$$

therefore, it can be written:

$$n_i = Tz_{pi} \int_{P_W}^{P_B} M_T(p)\, dp \tag{46}$$

where

$$M_T = \frac{K_{ro} b_o}{\mu_o} + \frac{K_{rg} b_g}{\mu_g} \tag{47}$$

If the block pressure (Pb) exceeds the dew point pressure, the composition of the flowing fluid z_{pi} is equal to the total hydrocarbon composition in the block. If the P_b is less than the dew point pressure, the composition of the production stream is calculated by CGMM equation for both oil and gas phase.

Once the generalized pseudo-pressure model is implemented, the typical well inflow equation can be modified with the flow blocking factor, F_{Bi}, as an additional dimensionless component and then the equation is given:

$$n_i = TF_{Bi} M_i(p)[P_B - P_W] \tag{48}$$

where

$$F_{Bi} = \frac{1}{M_i(P_B)} \frac{1}{(P_B - P_W)} z_{pi} \int_{P_W}^{P_B} M_T(p) dp \tag{49}$$

and then it can be written:

$$M_i(P_B) = z_{pi} M_T(P_B) \tag{50}$$

thus, the total dimensionless flow blocking factor, FB, is described

$$F_B = \frac{1}{M_T(P_B)} \frac{1}{(P_B - P_W)} \int_{P_W}^{P_B} M_T(p) dp \tag{51}$$

Finally, the modified inflow equation becomes:

$$n_i = TF_B M_i(p)[P_B - P_W] \tag{52}$$

4.5 PVT Analysis of Gas Condensate Reservoirs

PVT measurement of retrograde gas condensate reservoir systems plays a crucial role to estimate the fluid properties accurately and that should be paid special attention to model the complex flow behavior of these systems.

4.5.1. PVT Experiments

The physical properties of the gas condensate fluids are highly sensitive to temperature and pressure changes. Therefore, it is required to know how the fluid behaves within the reservoir, wells, and at the surface conditions, etc. The performed laboratory experiments are adequate to some extent however they are not capable of measuring all the things needed to know regarding the fluid properties. Herein, the Equation of State (EOS) comes into picture to compensate the inability of the lab results and match its observations. The details of the PVT simulation procedure are explained in the later sections.

Essentially, gas condensate fluid is analyzed by carrying out two fundamental experiments; Constant Composition (Mass) Expansion (CCE/CME) is close to what happens after the hydrocarbon reaches the well and Constant Volume Depletion (CVD) represents the conditions encountered in the reservoir.

4.5.1.1 Constant Composition Expansion

The schematic diagram of a Constant Composition Expansion, which is also called flash vaporization, is shown in figure 4.8. The experiment begins charging a laboratory cell with a known amount of gas condensate sample at a pressure above the initial reservoir pressure and then the cell pressure is reduced in a stepwise manner by expanding the cell volume while keeping the temperature constant. The volume at each pressure step is measured once the system equilibrium is attained. The overall composition of the cell contents remains same during the experiment since no gas and condensate are removed from the cell.

The CCE experiment is often conducted to determine the dew point of a gas and estimate the relative volume defined as the volume of the fluid at any given pressure per the volume of the fluid at the saturation pressure. For the single phase state, the vapor Z-factor or liquid density can be calculated from the other fluid properties.

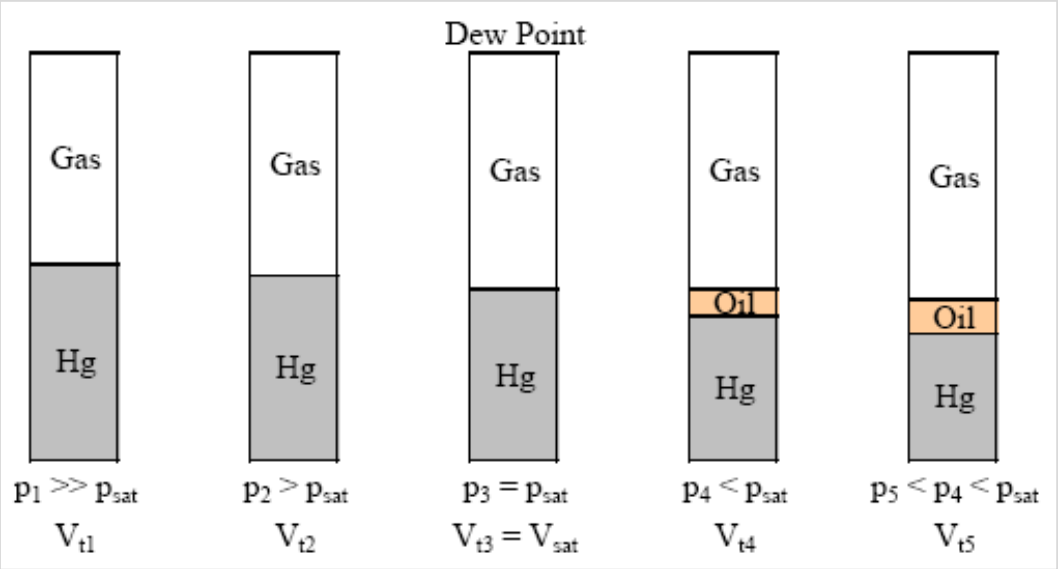

Figure 4.8 Schematic of constant composition expansion experiment (CCE).

4.5.1.2. Constant Volume Depletion

The schematic diagram of a Constant Volume Depletion is shown in figure 4.9. The CVD experiment is commenced by bringing the sample of reservoir fluid in the laboratory cell to the dew point and setting the temperature to the reservoir temperature. The volume is noted at the dew point and all subsequent volumes are referred to it. The cell volume is increased by reducing the pressure and the gas is expelled at the constant pressure until the volume of the cell become equal to the volume at the dew point. The liquid volume is recorded at each stage (liquid drop-out is calculated (V_T^L/V_T^{dew})) and the withdrawn gas is analyzed in terms of composition. The pressure is further reduced and the process is repeated for several times until a low pressure (close to ambient) is reached.

In theory, the composition of remaining fluid in the cell can be determined by means of material balance provided that knowing the number of moles that is present at the initial condition. Some laboratory reports have that sort of routine checks to smooth

the reported composition. In fact, it is useful to make the material balance calculations on a CVD experiment data just before any EOS matching.

The CVD experiment represents the reservoir depletion provided that the condensate phase is immobile which is valid only if the condensate saturation does not exceed the critical condensate saturation. In addition, it should be borne in mind that the liquid drop-out estimation does not take into account the condensate accumulation in the reservoirs and it has nothing to do with the direct indication of the maximum possible gas condensate occurrence at the reservoir conditions.

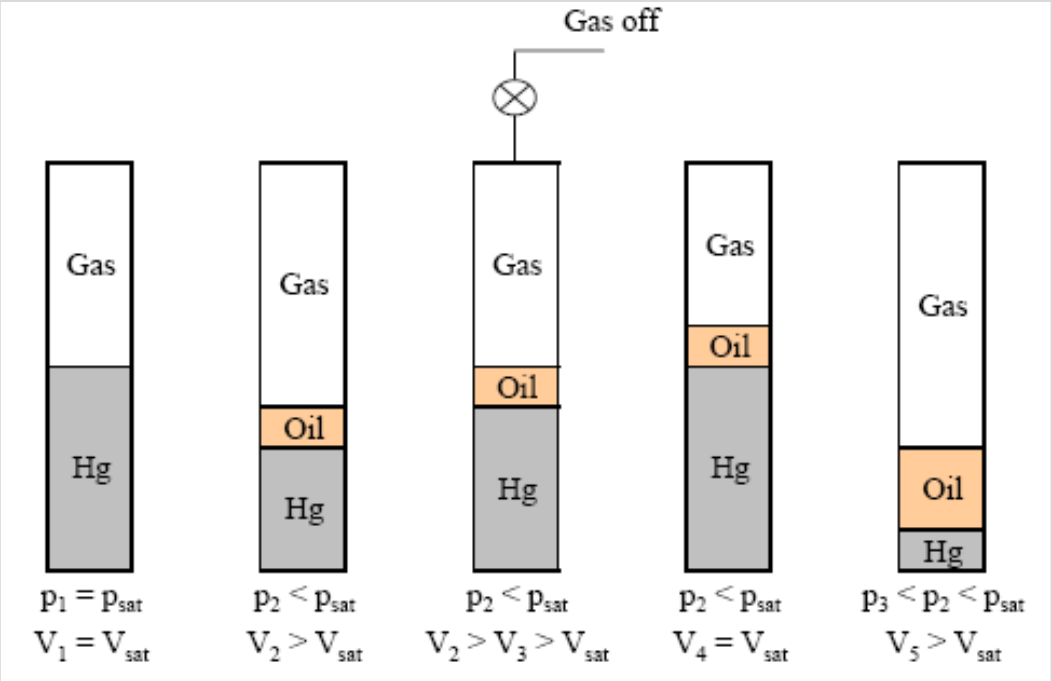

Figure 4.9 Schematic of constant volume depletion experiment (CVD).

4.5.2. Flash Calculations

The physical properties of the oil and gas are just the function of pressure and given as an input table in a black oil simulation model, but the only known is the present components of the hydrocarbon for a compositional simulation model and that makes the situation more complicated thus a series of calculation is necessary to work out the physical properties of the fluid. The flash calculation is one of them and a process of making decision how many phases are present at the desired pressure and

temperature. In other words, it determines the amount and composition of the vapor and liquid at the equilibrium.

4.5.2.1. Flash Equations

If we take one mole of a fluid of composition z_1, $z_2 \ldots z_N$ is split into L moles of liquid of composition x_1, $x_2 \ldots x_N$ and V moles of vapor composition y_1, $y_2 \ldots y_N$ at the given temperature and pressure.

$$L + V = 1 \tag{53}$$

$$Lx_i + Vy_i = z_i \tag{54}$$

$$\sum_{i=1}^{N} x_i = \sum_{i=1}^{N} y_i = \sum_{i=1}^{N} z_i = 1 \tag{55}$$

Substituting of L in equation 54

$$(1 - V)x_i + Vy_i = z_i \tag{56}$$

To define the K-value of the i^{th} component:

$$K_i = \frac{y_i}{x_i} \tag{57}$$

Then, the mole fractions of each component in the liquid and vapor phases are defined as:

$$x_i = \frac{z_i}{1+V(K_i-1)} \tag{58}$$

and

$$y_i = \frac{K_i z_i}{1+V(K_i-1)} \tag{59}$$

$$\sum_{i=1}^{N}(y_i - x_i) = \sum_{i=1}^{N} \frac{z_i(K_i-1)}{1+V(K_i-1)} = 0 \tag{60}$$

The final form of the equation, which is also known as the Rachford-Rice equation;

$$\sum_{i=1}^{N} \frac{z_i(K_i-1)}{1+V(K_i-1)} = 0 \tag{61}$$

The calculations start with an estimate of the K-value and refine it during the solution of the Rachford-Rice equation. Also, stability test (Michelsen, 1982) test for the minimum of the Gibbs free energy and numerical solution is carried out to define the number of phase available for the specified pressure, temperature, and composition.

The detailed workflow for a flash calculation is given as follows:

Firstly, the component K-values are estimated, and then molar faction of vapour V is found solving the Rachford Rice equation that is monotonically decreasing function. Later on, the composition of the oil and gas phase is determined using the found V. If there is more than one phase, the component fugacities in the liquid and vapor phases should be equal. The fugacities can be calculated by means of the equation of state (Peng Robinson EOS Equation.) and the ratio of them has to be close to one. If it is not, the Rachford Rice equation must be solved with the new estimates of K which are the old estimates times the ratio of fugacities (Peng and Robinson 1976).

$$\ln \frac{f_i}{y_i p_i} = \ln \varphi_i = \frac{B_i}{B}(Z - B) - \frac{A}{2\sqrt{2}B} \ln \left[\frac{Z + (1+\sqrt{2})B}{Z - (1-\sqrt{2})B} \right] \quad (62)$$

Where

f_i: fugacity of the i-th component

yiPi: partial pressure of i-th component

∂i: Fugacity coefficient of i-th component

Z: compressibility factor

A: the parameter of the attractive forces between molecules

B: the parameter of the finite (non-zero) volume of the molecules

$$f_i^L = f_i^V \quad i = 1,2,3 \ldots\ldots n_c \quad (63)$$

Where

f_i^L: the fugacity of the liquid phase

f_i^V: the fugacity of the vapour phase

$$\sum_{i=1}^{n_c} \left(\frac{f_{iL}}{f_{iV}} - 1\right)^2 < \varepsilon \quad (64)$$

with $\varepsilon \approx 10^{-12}$

$$K_i^{New} = K_i^{Old} * \left[\frac{f_{iL}}{f_{iV}}\right] \quad (65)$$

4.5.3. Equation of State Calculation & Characterization

An equation of state is an analytic equation which expresses the relationship between pressure, temperature and volume of a fluid. The cubic equations of state (EOS) such as Peng-Robinson (PR) and Soave-Redlich-Kwong (SRK) are widely used in today's commercial reservoir simulators for the representation of volumetric and phase equilibria due to their simplicity and solvability (Coats, 1980).

4.5.4. PVT Simulation and Lumping

The simulation of the experiments that have been performed in the lab on a set of fluid samples and prediction of the experimental observations are vital steps to have a realistic lumped physical model of reservoir fluid sample prior to using them in compositional reservoir simulation runs since the high number of components poses a problem in terms of CPU time and simulator cost (Pedersen and Christensen, 2007). Thus, it is desirable to reduce the number of components before performing any equilibrium calculation based on the equation of state and flash calculation. Mostly, PVT laboratory reports are not in good format for use in an EOS model and some additional manipulations such as splitting and grouping are required to characterize the plus fraction and similar hydrocarbons of the fluid sample (Ahmed, 2007).

4.5.4.1 Splitting

The plus fraction composition and properties which subject to change during the regression are the most uncertain because the laboratories tend to give very limited analysis to them. In other respects, they have great importance on the gas condensate reservoirs and appropriate description of heavier hydrocarbons increases the accuracy of PVT predictions even if their mole fractions are relatively small.

The main reason behind the splitting is that the heavier ends tend to remain in solution so that the molar distribution of components within the plus fraction alters and any EoS model making use of a single component of such a plus fraction is not able to model the CVD experiment which represent the reduction in the mole weight and specific gravity of the plus fraction of the removed gas with decreasing pressure.

It requires a numerical procedure as Whitson's technique (1982) that relates the mole fraction to mole weight and adjust the correlation to fit any available data and change into a set of components for an EOS Model is the most widely used.

4.5.4.2 Grouping

The primary purpose of grouping the components is to speed up the compositional simulator since the large number of components increases not only the execution time spent to solve the flow equations but also the computing time required to solve the flash equations drastically.

The main principle of the grouping procedure is to achieve a pseudoised set of components for a compositional simulation with the similar properties such as the same log of K values as a function of pressure trend, molecular weights, etc (Joergensen and Stenby, 1995). Newly and Merrill (1984) suggested a method of grouping based on minimizing the difference between the apparent equilibrium ratio (K-value) of the pseudo–component and those of the original components. After grouping the components with respect to above considerations, the shape of the phase envelope of the grouped components should match up with that of the original one and if it seems to be acceptable then the regression analyses of the laboratory results to obtain the new grouped components are able to be performed (Coats and Smart, 1986). If the original compositional simulation model gives the identical results with the lumped compositional simulation model, it means that the number of components is sufficient (Li and Nghiem, 1982).

4.5.5. PVT Data and Results

The gas condensate fluid sample used in the simulation has been taken from SPE-3 dataset that has been investigated and grouped as different fluid models with the help of commercial fluid PVT package. The Whitson and Coats techniques have been used for splitting and lumping fluid components. The Equation of State (EOS) models for the fluid sample has been constructed with the Peng-Robinson (PR) EOS. The EOS parameters have been tuned by regression methodology that is based on choosing as few EOS parameters as possible, varying properties of poorly defined components, i.e. plus fraction(s) (highest uncertainty), maintaining the monotonicity (proper increasing/decreasing trend) properties, weighting important measurements, etc. to have a good match between the calculated values and observed data points. The critical properties of the plus components have been put in the tuning process as regressed variables. The dataset and related plots regarding PVT analysis and simulation procedure are given as tables and figures. Table 4.2 shows the hydrocarbon analyses of the original fluid sample having 16 components.

Table 4.2. Composition of Reservoir Fluid Sample

Component Name		**mol %**
CO2	Carbon Dioxide	1.21
N2	Nitrogen	1.94
C1	Methane	65.99
C2	Ethane	8.69
C3	Propane	5.91
IC4	Isobutane	2.39
NC4	n-Butane	2.78
IC5	Isopentane	1.57
NC5	n-Pentane	1.12
C6	Hexanes	1.81
C7	Heptanes	1.44
C8	Octanes	1.5
C9	Nonanes	1.05
C10	Decanes	0.73
C11	Undecanes	0.49
C12+	Dodecanes plus	1.38
Plus fraction - MW: 161, SG: 0.805		

The phase diagram of the original fluid sample is illustrated in figure 4.10. Blue and red lines represent the bubble and dew point lines respectively. The other colored lines given by V letter demonstrate the vapor lines as fraction.

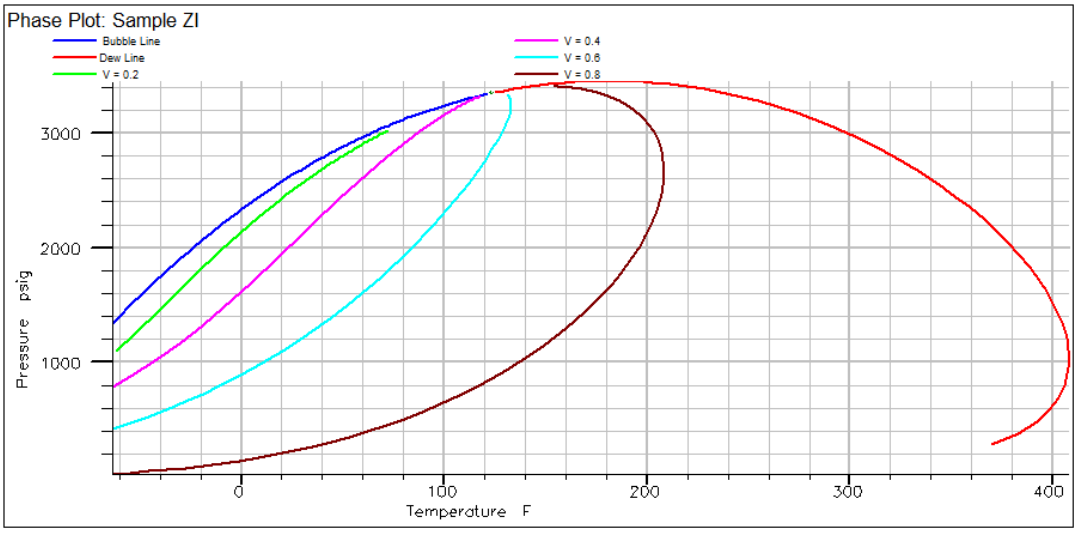

Figure 4.10 Phase diagram of a gas condensate system.

Table 4.3 Pressure Volume Relations of Reservoir Fluid at 200 F° (CCE)

Pressure (psia)	Relative Volume	Deviation Factor, Z
6014.7	0.8045	1.129
5514.7	0.8268	1.063
5014.7	0.853	0.998
4514.7	0.8856	0.933
3614.7	0.9745	0.869
3442.7	1.0000	0.822
3414.7	1.0043	
3364.7	1.0142	
3214.7	1.0468	
3014.7	1.0997	
2814.7	1.1644	
2414.7	1.3412	
2014.7	1.6113	
1614.7	2.0412	
1314.7	2.5542	
1044.7	3.2925	
850.7	4.1393	

Table 4.3 gives the relative volume and deviation factor values with respect to pressure. This represents the constant composition expansion experiment at 200 F degrees.

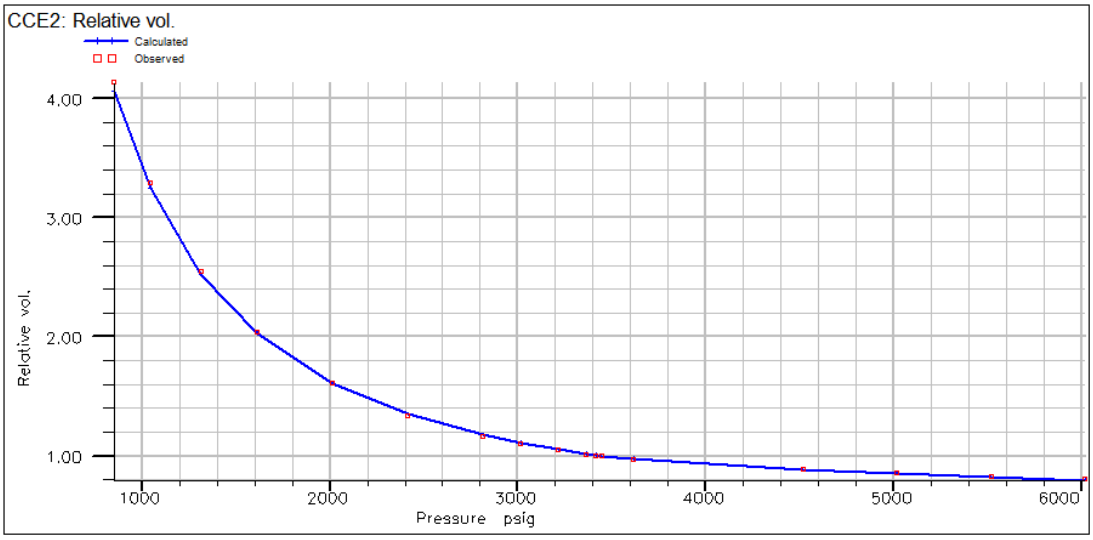

Figure 4.11 Relative Total Volume in Constant Composition Expansion at 200 F°.

Figure 4.11 demonstrates the relation between the observed and simulated relative volume data of the constant composition expansion experiment. The estimated values of that match fairly good with the observed ones.

Table 4.4 Condensation during Gas Depletion at 200 F° (CVD)

Pressure (psia)	Liquid drop out %
3442.7	0
3014.7	15
2414.7	19.9
1214.7	17.1
714.7	15.2

Table 4.4 indicates liquid drop-out percentage versus pressure values of the constant voume depletion experiment for the original fluid sample.

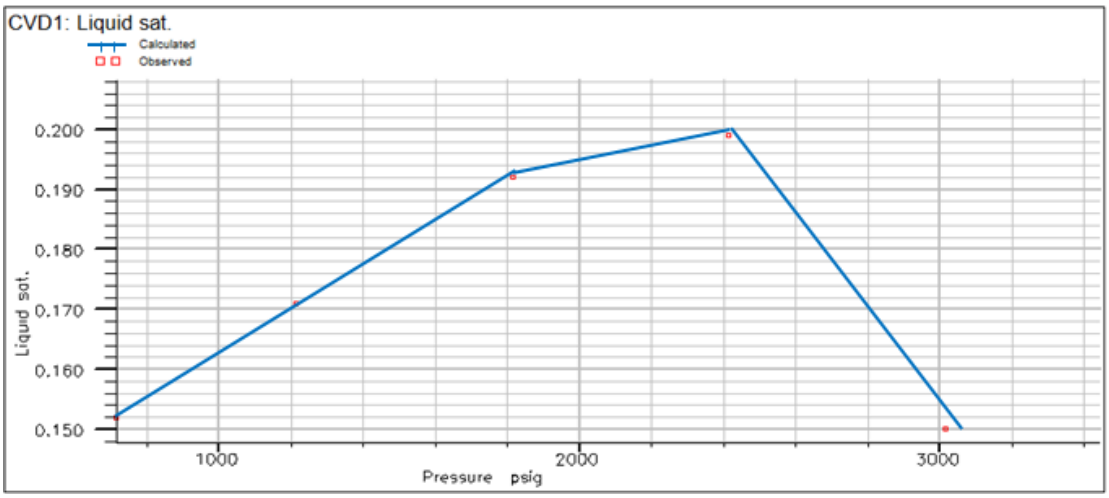

Figure 4.12 Liquid drop-out curve.

Figure 4.12 shows the relation between observed and calculated liquid drop-out percentage values of the constant volume depletion experiment.

Table 4.5 depicts the some of the grouped fluid models in a step-wise manner. The theory behind the grouping is given in the previous section.

Table 4.5 Stepwise pseudoization of reservoir fluid sample

<table>
<tr><th>Group I</th><th>Group II</th><th>Group III</th><th>Group IV</th><th>Group V</th><th>Group VI</th></tr>
<tr><td>C1</td><td>'C1'</td><td rowspan="2">'X1+'</td><td rowspan="2">'X1+'</td><td rowspan="2">'X1+'</td><td rowspan="4">'C1+'</td></tr>
<tr><td>N2</td><td>'N2'</td></tr>
<tr><td>CO2</td><td>'CO2'</td><td rowspan="2">'X2+'</td><td rowspan="2">'X2+'</td><td rowspan="2">'X2+'</td></tr>
<tr><td>C2</td><td>'C2'</td></tr>
<tr><td>C3</td><td>'C3'</td><td>'C3'</td><td>'C3'</td><td rowspan="3">'C3+'</td><td rowspan="6">'C3+'</td></tr>
<tr><td>IC4</td><td>'IC4'</td><td>'IC4'</td><td rowspan="2">'C4+'</td></tr>
<tr><td>NC4</td><td>'NC4'</td><td>'NC4'</td></tr>
<tr><td>IC5</td><td>'IC5'</td><td>'IC5'</td><td rowspan="2">'C5+'</td><td rowspan="3">'C5+'</td></tr>
<tr><td>NC5</td><td>'NC5'</td><td>'NC5'</td></tr>
<tr><td>C6</td><td>'C6'</td><td>'C6'</td><td>'C6'</td></tr>
<tr><td>C7</td><td rowspan="2">'C7+'</td><td rowspan="2">'C7+'</td><td rowspan="2">'C7+'</td><td rowspan="2">'C7+'</td><td rowspan="2">'C7+'</td></tr>
<tr><td>C8</td></tr>
<tr><td>C9</td><td rowspan="2">'C9+'</td><td rowspan="2">'C9+'</td><td rowspan="2">'C9+'</td><td rowspan="2">'C9+'</td><td rowspan="2">'C9+'</td></tr>
<tr><td>C10</td></tr>
<tr><td>C11</td><td rowspan="2">'C11+'</td><td rowspan="2">'C11+'</td><td rowspan="2">'C11+'</td><td rowspan="2">'C11+'</td><td rowspan="2">'C11+'</td></tr>
<tr><td>C12+</td></tr>
</table>

After implementing the lumping methodology, the phase diagrams of the different fluid models are shown in figure 4.13. The important point and indicator of the good grouping is the change of phase diagram before and after grouping. If the change is too large, it means that the group is not good. Another significant check point is to have the similar simulation results regardless of the component numbers. That will also be discussed through the result and discussion section. As it is seen from the figure 4.13, the phase diagrams of the five lumped fluid models look alike and the main shapes and critical points of phase diagrams are very close to those of the original fluid sample, thus, the good simulation results can be expected by considering aforementioned circumstances. However, the last grouped fluid sample is out of the acceptable range and the deviation or change on the phase diagram is too much. It will not give satisfactory results owing to the lack of representation of the original reservoir fluid sample.

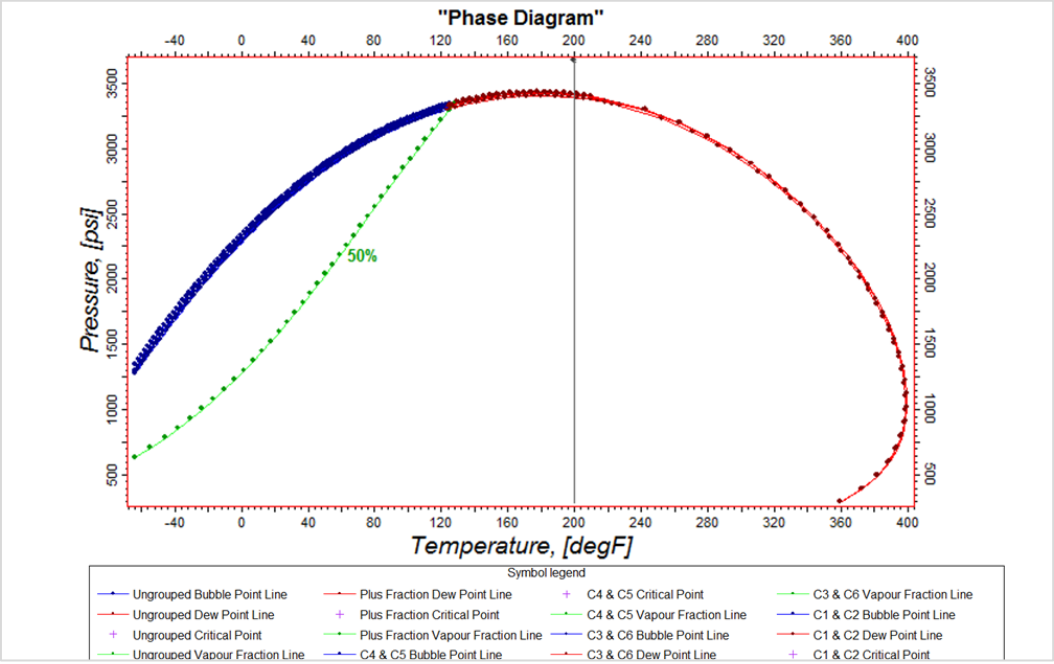

Figure 4.13 Phase Diagrams of some lumped fluid samples.

4.5.6. Automated Lump Approach

The lumping procedure that may subject to too much alternatives is actually based on some criteria but mostly subjective and that may change from user to user. The proposed approach aims at grouping components automatically. It is certainly the most important aspect of finding an optimal lumped EOS model that honors the specifics of a particular fluid system Liu (2001). For this purpose, the mismatch of phase diagrams and the use of compositional simulation to verify the grouped fluid samples, underlie the suggested procedure which follows an algorithm consisting of four phases: Each phase handles the some part of the reservoir fluid sample separately. The detail of methodology is as follows:

Phase 1: The heaviest component is found and it gets together with its one lighter neighbor then that is compared to the original fluid sample. It continues in descending order for each couple components. Once all couple is grouped separately, triple grouping strategy comes into picture and all alternatives are conducted. It goes on increasing grouped components until the number of plus fraction component is reached.

Phase 2: If there are isomers in the fluid sample, the related component and its isomer is grouped together and then that is done for the other component having isomers respectively. At last, all components with its isomers are lumped and this phase is finalized.

Phase 3: Most of the reservoir fluid contains some inorganic components such as carbon dioxide, nitrogen, those are generally grouped with lighter hydrocarbons with respect to their K-values. Each non-hydrocarbon component is kept as pure compound and forced to be grouped in a specific manner.

Phase 4: The most representative lumped models, which brings the least amount of error, of each phase are combined. If there is any single or multiple light component/s available, they are lumped with their contiguous carbon number in a stepwise manner. For this phase, the lumping of carbon numbers can be done using contiguous isomer-ranked components.

The deviation or error of each grouped fluid sample's phase diagram to original one is estimated by applying RMS method.

To apply above workflow and keep the possible lumping schemes physically correct, a few constraints has been introduced on lumping.

Firstly, the lumping of non-hydrocarbons with hydrocarbons have been restricted: e.g. N_2 only with C_1 and CO_2 only with C_2.

Secondly, hydrocarbons have been lumped only by contiguous carbon numbers, e.g. $C_{12}+C_{11}+C_{10}$. The following grouped components have not been allowed. e.g. C_8+C_{10} and C_7+C_{12}. For isomers with the same carbon number, it is recommended the contiguous ordering of the original components. The successive approximation method is shown schematically in figure 4.14. The figure 4.15 demonstrates the detailed representation of proposed lumping methodology. RMS error vs. number of component plot is drawn and the intersection of two different trends is determined in order to obtain the optimum number of lumped components.

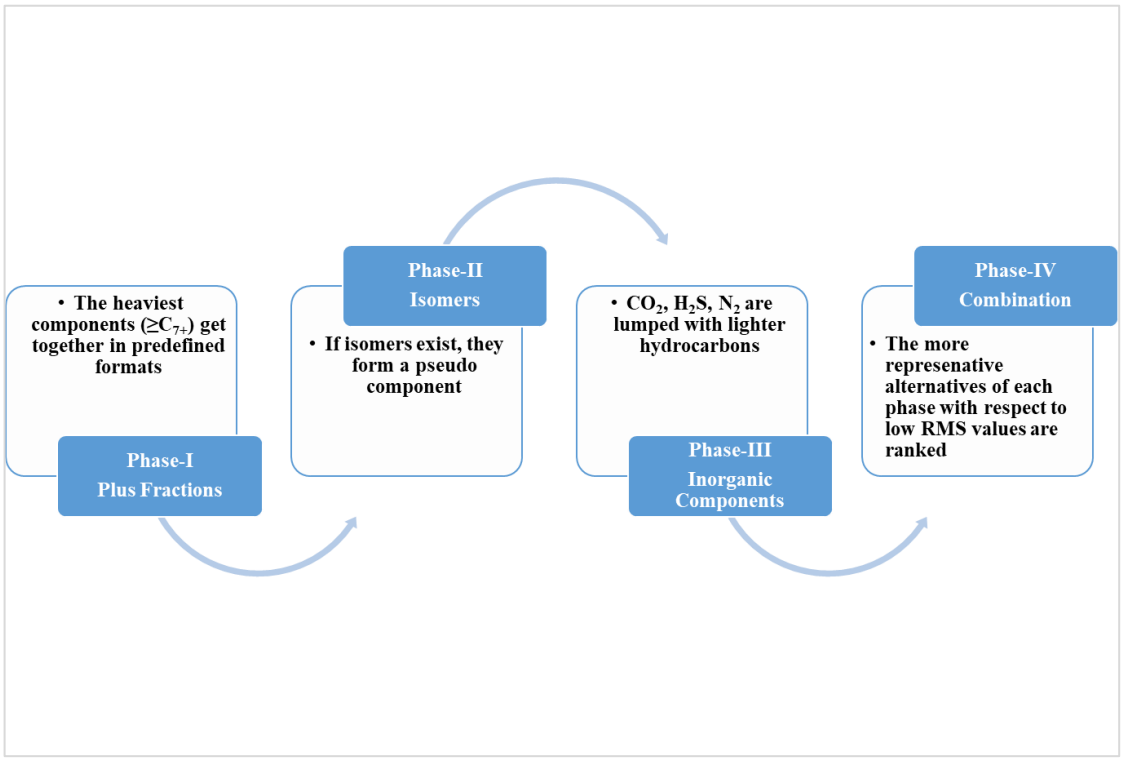

Figure 4.14 Successive approximation method of automated lumping process.

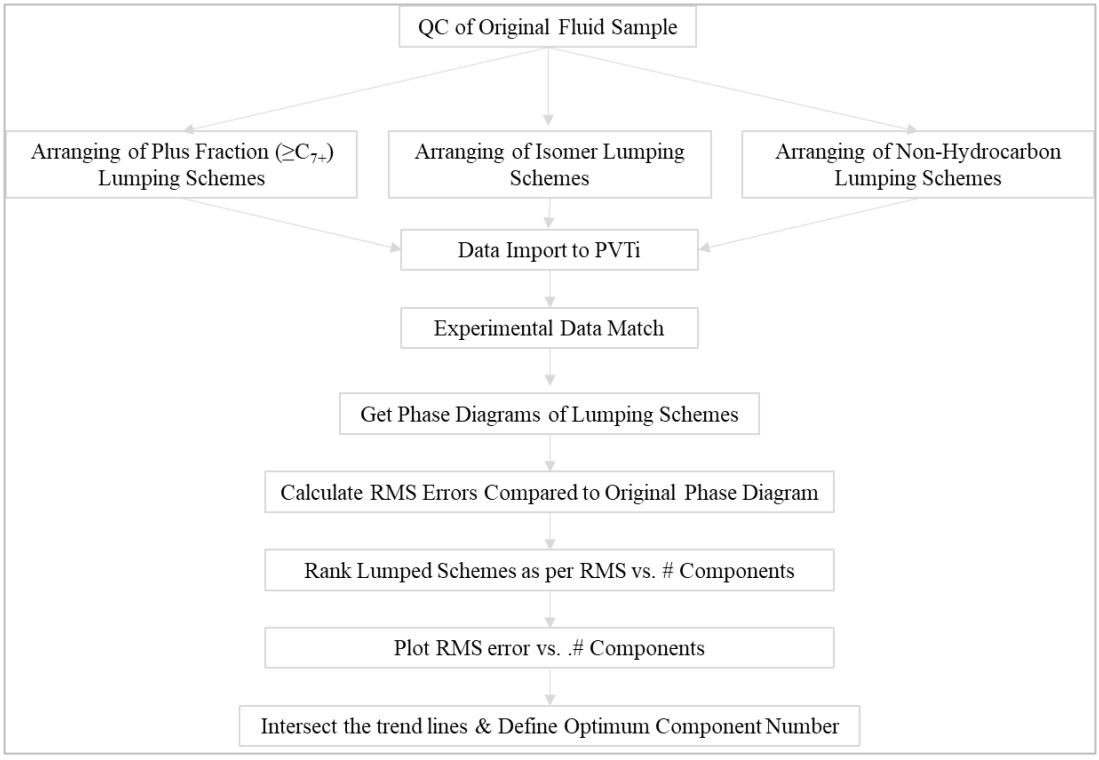

Figure 4.15 Detailed Representation of Proposed Methodology

4.5.6.1 Estimating the Error of Lumped Fluid Models

Once all the physical lumped fluid models are obtained, they have been analyzed statistically to validate their deviations and define the more accurate alternatives. For this reason, root mean square (RMS) has been used to analyze how close the estimated grouped samples are with respect to original fluid model (McKeen et al., 2005 and Savage et al. 2013). The RMS is defined as the arithmetic mean of the squares of a set of values.

The regression line predicts the average y value associated with a given x value. Firstly, the residuals that are the difference between the actual and the predicted values are determined to find RMS error. In our approach, the reservoir is depleted isothermally and the actual values which intersect the relevant quality lines comes from the phase diagram of the original fluid composition having 16 components. The predicted values are taken from the phase diagram of the lumped fluid models similarly.

$$\text{Residual} = \hat{y}_i - yi \tag{66}$$

Where

$\hat{y}i$: observed value

yi : predicted value

To obtain RMS error, residuals are squared and each squares are averaged. Finally, that is reached by taking the square root of averages.

$$\text{RMS Error} = \sqrt{\frac{\sum_{i=1}^{n}(\hat{y}_i - yi)^2}{n}} \tag{67}$$

CHAPTER 5

RESULT & DISCUSSION

In this section of the thesis, all simulation cases for each system are analyzed and discussed. Firstly, dual porosity and equivalent single medium systems will be compared with the original fluid sample and then the analysis will be made with automated lumped/grouped fluid samples with respect to accuracy of results and simulation time efficiency. In addition to that the effects of near wellbore modeling techniques such as local grid refinement, velocity dependent relative permeability, and generalized pseudo pressure for naturally fractured gas condensate system are investigated.

The main challenge of naturally fractured gas condensate reservoirs is to simulate the fluid flow properly in the most time efficient manner. If we are able to represent these complex systems with less amount of grid and components, that will provide us an opportunity to make the huge amount of sensitivity, optimization and uncertainty analysis in a short period of time, consequently, it leads to improvement of the reservoir management quality by permitting to better understand these types of hydrocarbon systems.

5.1 Comparison of Dual Porosity and Equivalent Single Medium Models

The equivalent single porosity model might mimic the dual porosity model. For example, fracture orientation and properties are kept similar and constant in each direction so that the porosity and permeability values can be adjusted to those of the dual porosity model.

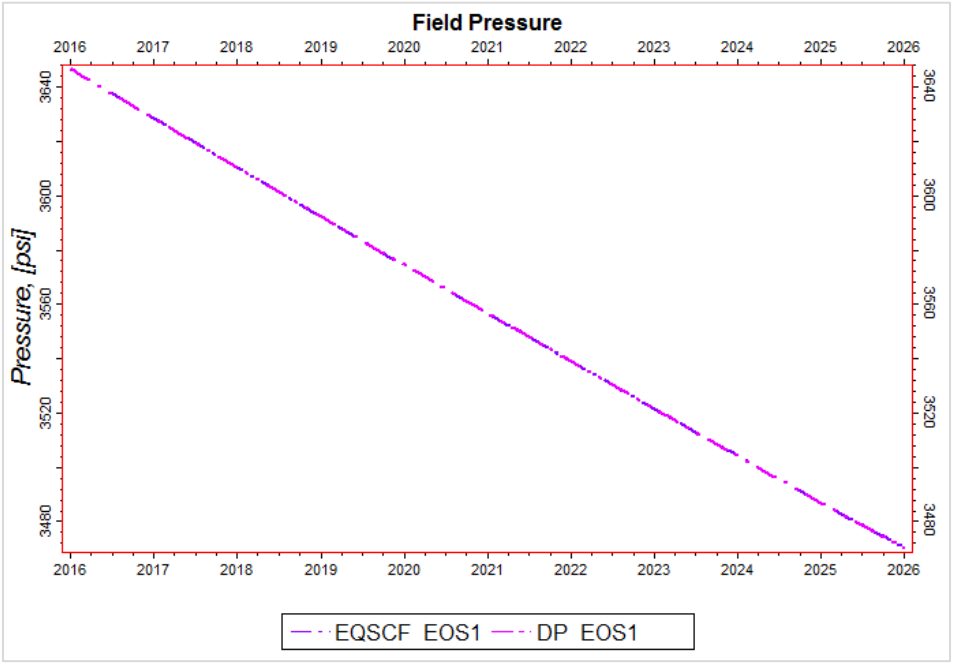

Figure 5.1 Field Pressure of Dual Porosity and Equivalent Single Porosity Models.

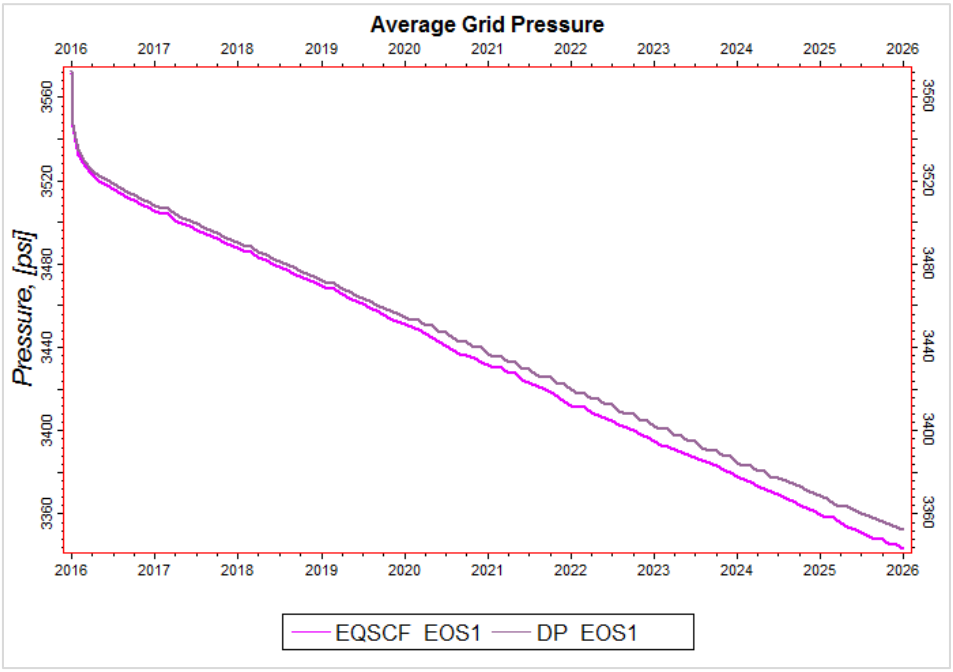

Figure 5.2 Average Field Pressure of Dual and Equivalent Single Porosity Models.

As it is seen in figures 5.1 and 5.2, the equivalent single porosity and dual porosity models show very similar results for the base case scenario that was run with the original fluid composition. The trends of average block pressure and field pressure decline are identical for both models under the gas rate control mode.

The reservoir pressure decreases sharply for both cases and then it follows a regular decline trend until the end of production period. In fact, the results of both models are in good agreement with each other until the average reservoir/grid pressure falls below the dew point pressure of the system. In other words, the equivalent single medium approach represents the gas flow very well in a grid block and field scale before the starting of multi-phase flow. As the gas condensation begins in the early of year-2020, the deviation starts on the plot of average grid pressure. The representation of equivalent single medium approach gives satisfactory results with respect to the average block pressure and field pressure. However, the trend of the bottom hole pressure behavior of the equivalent single porosity model differs from the dual porosity one and it does not provide a reasonable result without using any near wellbore modeling techniques that comes out as a necessity for a good agreement on the bottom-hole pressure. By considering this deviation, it is suggested that the effect of near wellbore techniques may be analyzed to obtain a rational behavior of the bottom-hole pressure. Once generalized pseudo pressure and velocity dependent relative permeability models are added to the base case equivalent single medium model, it is realized that there is a remarkable enhancement on the bottom-hole pressure with the generalized pseudo pressure approach that approximates the bottom-hole pressure up to 20 psia and reduces the error margin from 3 % to 0.15. Indeed, the discretization of fractures in equivalent single medium approach pretend to act dual media but it may fail to satisfy the matrix to facture transfer for low ratios of fracture to matrix permeability. It is in line with the working principle of the generalized pseudo pressure. For instance, if the pressure distribution is less sharp around the well, the pressure drop will extend for a longer instance and drop-out occur further from the well therefore there is no need for the generalized pseudo pressure. On the other hand, the velocity dependent relative permeability method is able to make some contribution to bottom-hole pressure but it is limited because it is very sensitive against the saturation changes. The local grid refinement facility is not evaluated for the equivalent single medium method since it is not compatible with this module. The improvement of the bottom-hole pressure trend is demonstrated in Figure 5.3.

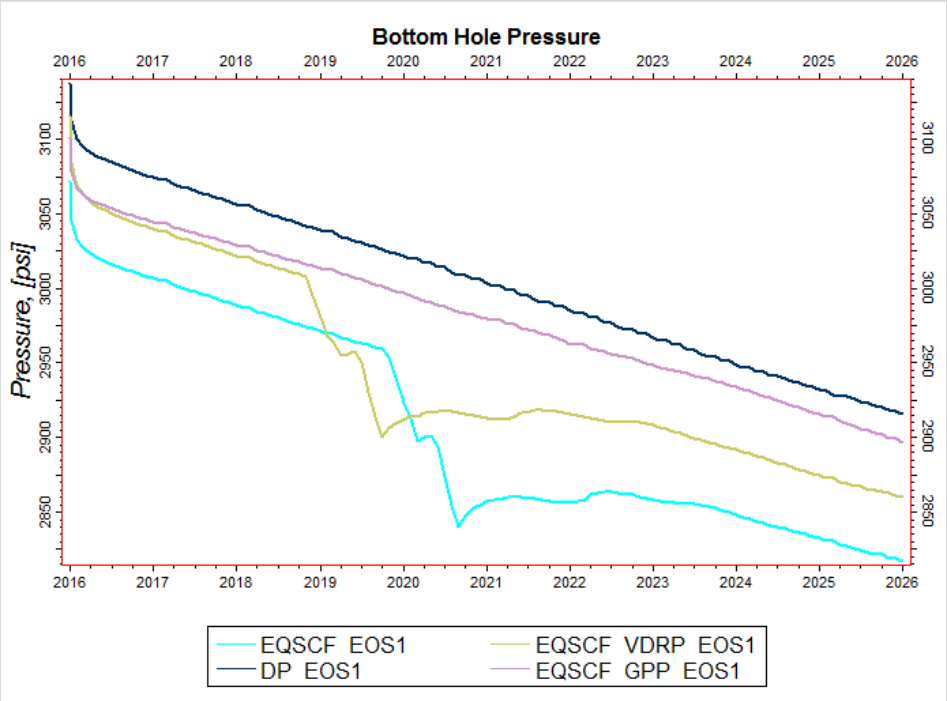

Figure 5.3 Bottom Hole Pressure of Dual and Equivalent Single Porosity Models.

The generalized pseudo pressure technique approximates the cumulative condensate production of dual porosity model with less than 0.1 % error at the end of 10-year production period under the gas rate control mode. Figure 5.4 represents the relationship between equivalent single medium with the generalized pseudo pressure and dual porosity model.

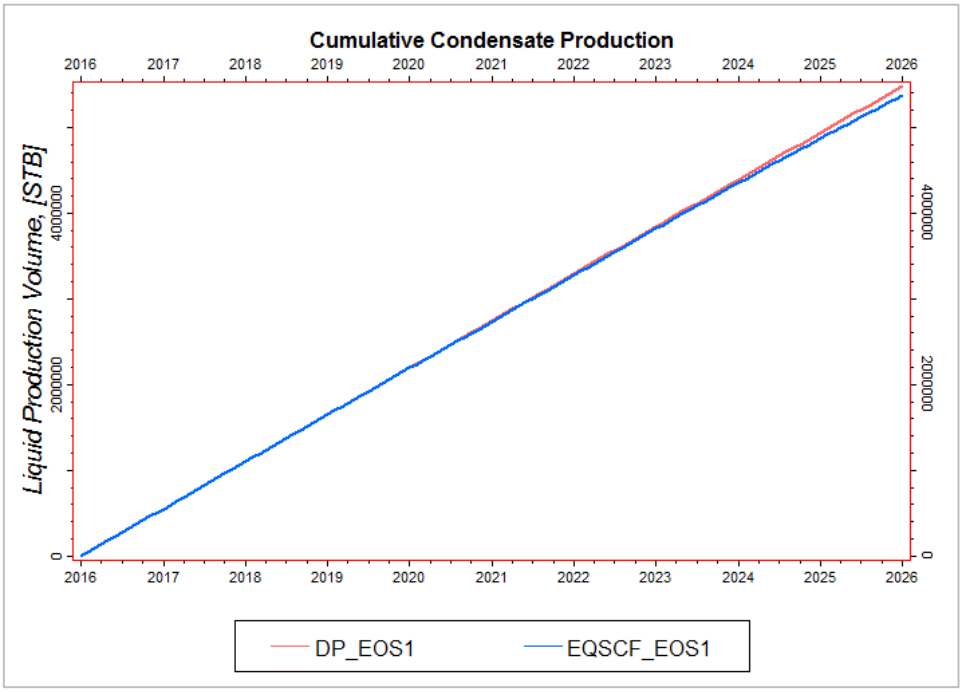

Figure 5.4 Cumulative Condensate Production of both Models.

The average grid block pressures of dual porosity case coincide with each other during the production period for generalized pseudo pressure and velocity dependent relative permeability techniques. The result of the local grid refinement is not drawn on this plot since it takes a different size to calculate the average grid block pressures.

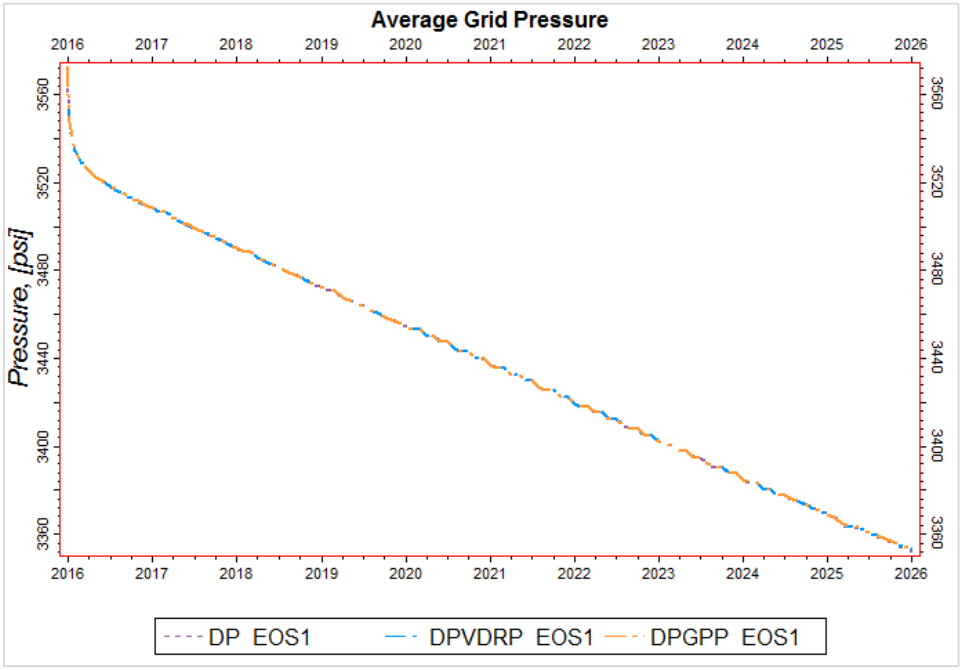

Figure 5.5 Average Grid Pressure of Dual Porosity Models.

Actually, the sudden pressure drop on the bottom-hole pressure is generally expected for the conventional retrograde gas condensate reservoirs when the reservoir pressure is just below the dew point pressure. This issue is mainly related to mobility reduction for the system since the condensate comes into solution and that causes the productivity loss on the well performance. If the reservoir system has conductive natural fractures that act as flow corridors, they can improve the conductivity and minimize the mobility problem, thus the drastic decline on the bottom-hole pressure is not observed. For those systems, the near well bore modeling techniques may not be considered after several quality check analyses are made. Local grid refinement and generalized pseudo pressure methods almost fit into one another and underestimate the bottom-hole pressure within the range of 1-15 psia and they differ from the original base case and velocity dependent relative permeability models in Figure 5.5. In our dual porosity case, the results of all of those are very close and satisfactory to that of the base case dual porosity model and it is thought that it arises from the nature of dual porosity system. Figures 5.5 and 5.6 support above explanation and depict the similarities for dual porosity cases.

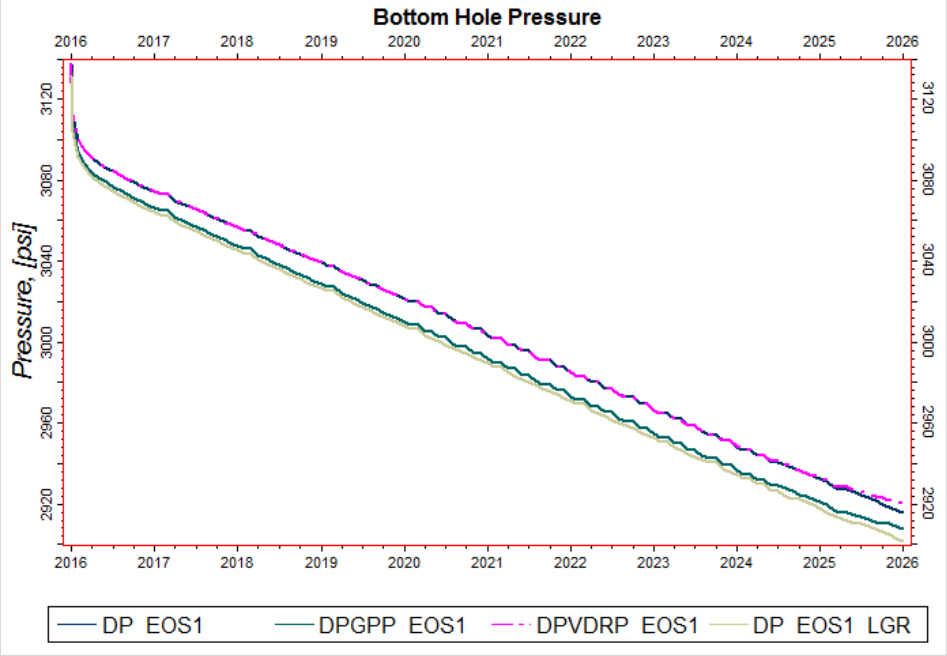

Figure 5.6 Bottom-hole Pressure of Dual Porosity Models.

Having a look at the cumulative condensate production, the results of all dual porosity models with near wellbore techniques are very close to base case dual porosity model and each other. They produce almost the same amount of condensate during all the production period. Figure 5.7 demonstrates the cumulative condensate production amount of all cases.

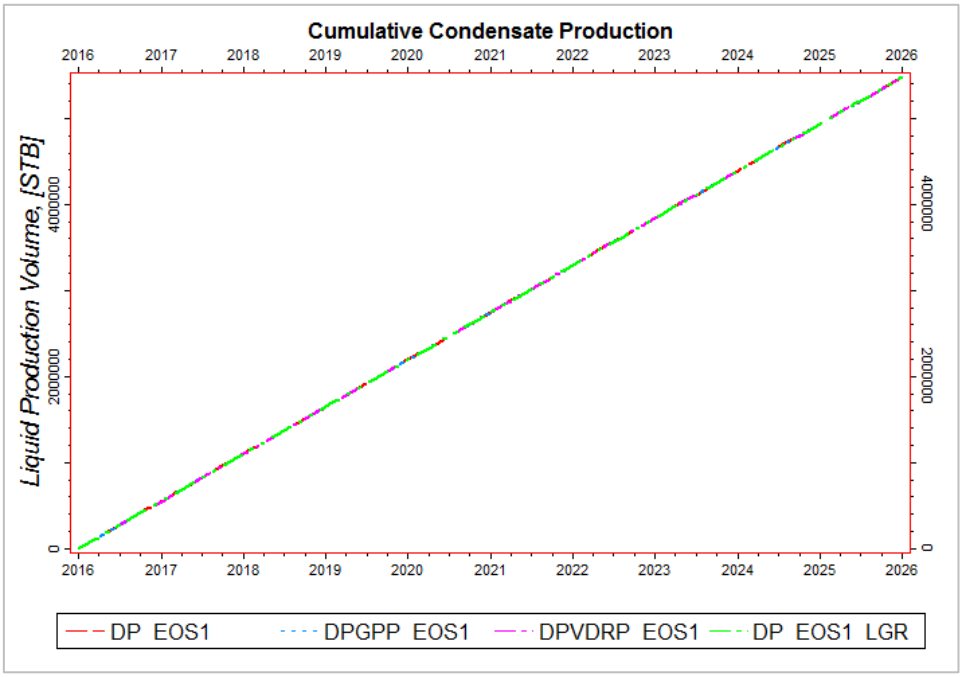

Figure 5.7 Cumulative Condensate Production of Dual Porosity Models.

In order to observe the effect of fracture to matrix permeability ratio on the equivalent single medium approach, the actual ratio is increased by 5 times and 10 times respectively. It is noted that all runs are performed with original fluid composition having 16 components for these cases. As it is seen on the figure 5.8 and 5.9, the fracture to matrix permeability increase in each direction extra 5 times compared to original one show still favorable agreement with the dual porosity model for both average grid and bottom-hole pressure.

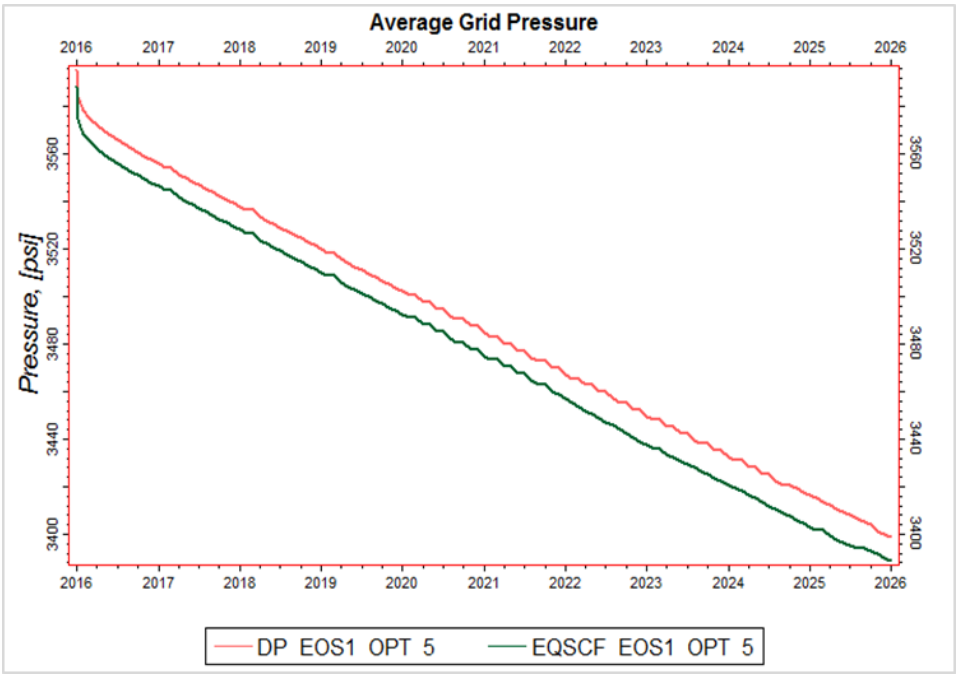

Figure 5.8 Effect of Fracture to Matrix Permeability Ratio on Average Grid Pres.

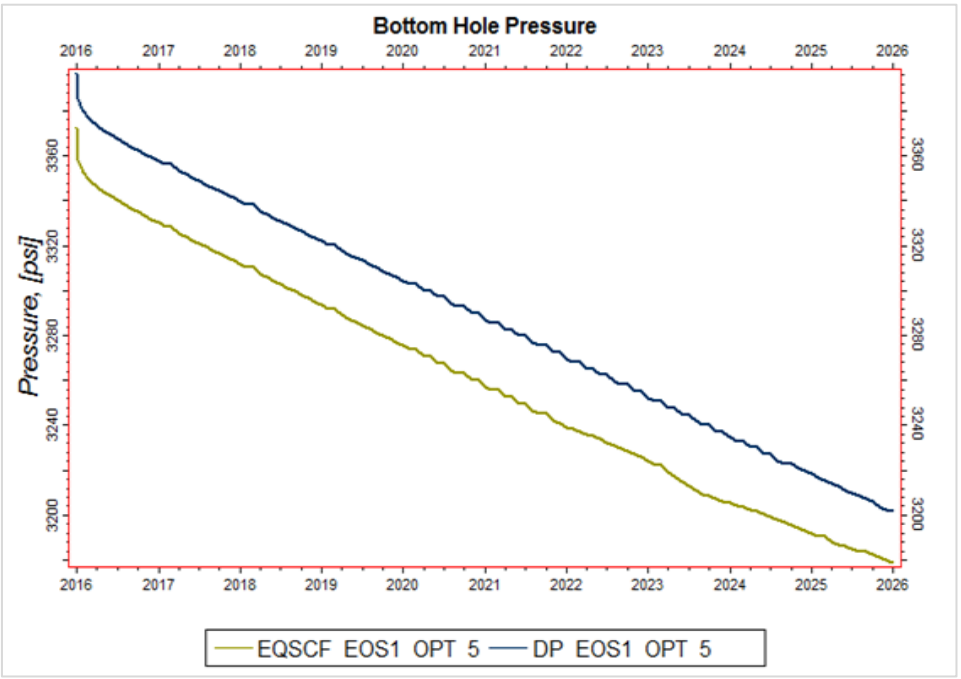

Figure 5.9 Effect of Fracture to Matrix Permeability Ratio on BHP.

If the ratio is kept increasing in each direction by 10 times compared to the original case, the equivalent single medium approach starts to represent the dual porosity model in an inadequate way in terms of the average grid and bottom hole pressures. The results are depicted in figure 5.10 and 5.11 respectively.

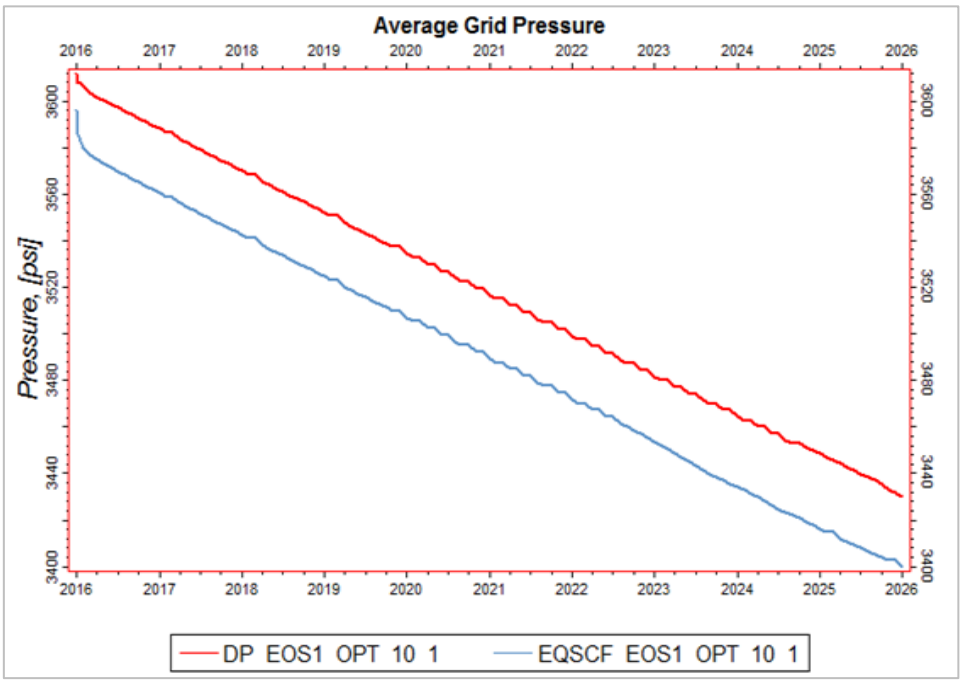

Figure 5.10 Effect of Fracture to Matrix Permeability Ratio on Average Grid Pres.

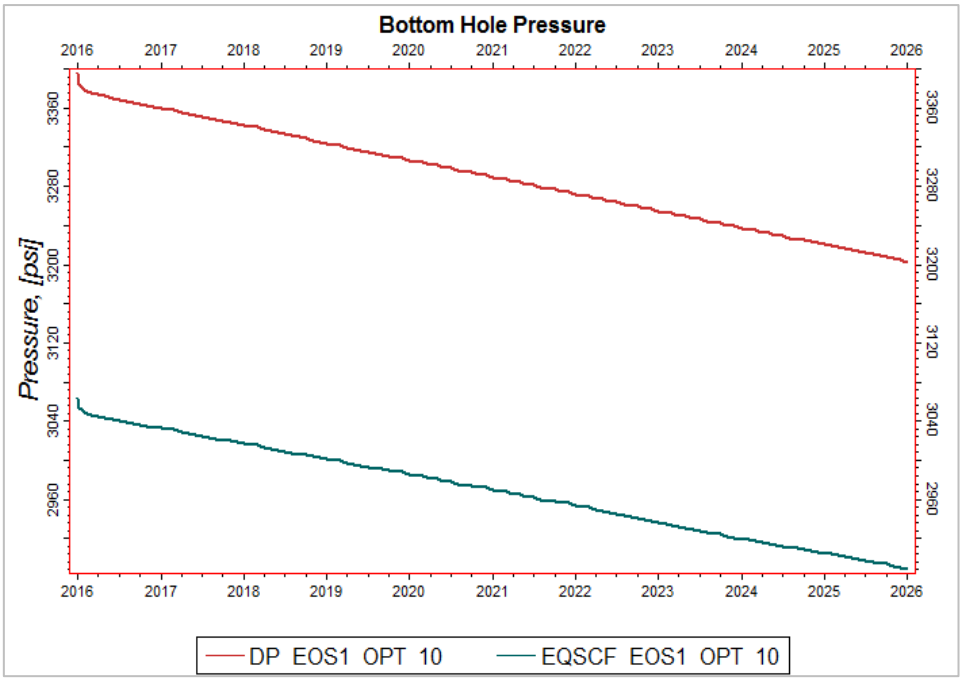

Figure 5.11 Effect of Fracture to Matrix Permeability Ratio on BHP.

The fracture to matrix permeability ratio might play an important role on the effectiveness of ESM approach. It is recommended that it may work well up to 250 times totally in this case, but if it is above that, the representation gets worse and dual porosity model can be preferred for those cases. The findings define the limitation of ESM approach as well.

5.2 Comparison of Lumped Models

The original fluid sample having 16 components is represented with EOS-1 and additional 5 fluid models are also chosen from the cluster of automated lumping schemes. As it is mentioned before, the high number of components overburdens the simulator too much not only for pressure matrix solution but also for flash calculations. One of the main purpose in compositional simulation is to reduce the number of component in a proper way. The most important indicators are the shape of the phase diagram and the critical values of the fluid samples to make sure whether the grouped fluid sample is characterized accurately or not. (All details of PVT simulation are given and explained in the section 4.3.) Also, the simulation results are another control point and it should be identical for all cases irrespective of the component numbers. In the light of this information, the equivalent single medium and dual porosity cases were run with 6 different predefined lumped fluid models.

Figures 5.12 and 5.13 illustrate the average grid and bottom-hole pressures for dual porosity cases in terms of 5 different EOS models respectively. The average grid pressures of 5 EOS models overlap perfectly. As for the bottom hole pressures, they tend to increase a little bit while the number of components decrease. The difference between EOS-1 and EOS-5 is only 5.5 psia at the end of the ten-year production period. It means that the least number of component model brings only 0.17 % error to the bottom-hole pressure calculations.

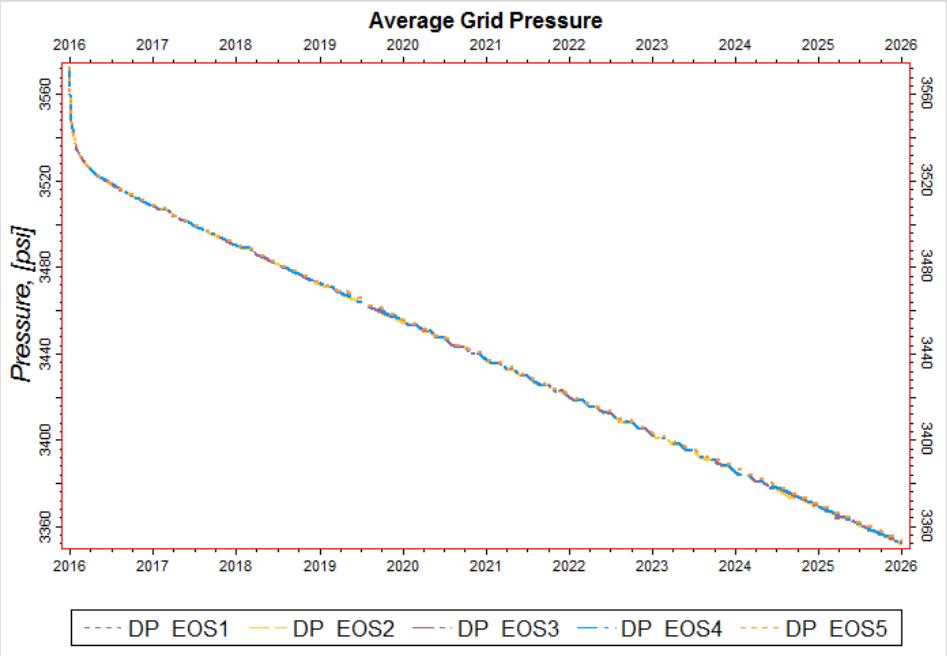

Figure 5.12 Average Grid Pressure of Dual Porosity Lumped Models.

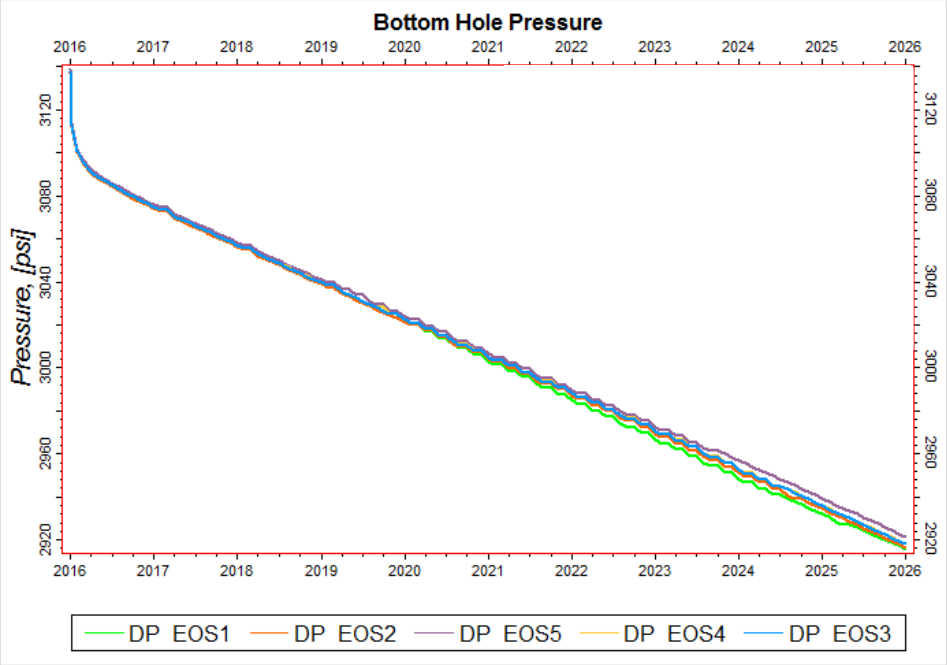

Figure 5.13 Bottom Hole Pressure of Dual Porosity Lumped Models.

For the equivalent single porosity runs, the deviation of average grid pressure values range from 1 to 3 psia especially after the condensation occurs in the reservoir (Figure 5.14) but overall performance of lumped procedure is still favorable. As it is addressed in the previous part, the equivalent single porosity is not capable of representing the

bottom-hole pressure without any near wellbore modeling facility. Thus, generalized pseudo pressure runs are plotted to evaluate the performance of the lumped methodology on the bottom-hole pressures of the single medium approach in figure 5.15. The bottom-hole pressure values vary within a narrow range between 0.5 and 7 psia. Accordingly, the equivalent single porosity model with generalized pseudo pressure represents the lumped fluid models efficiently.

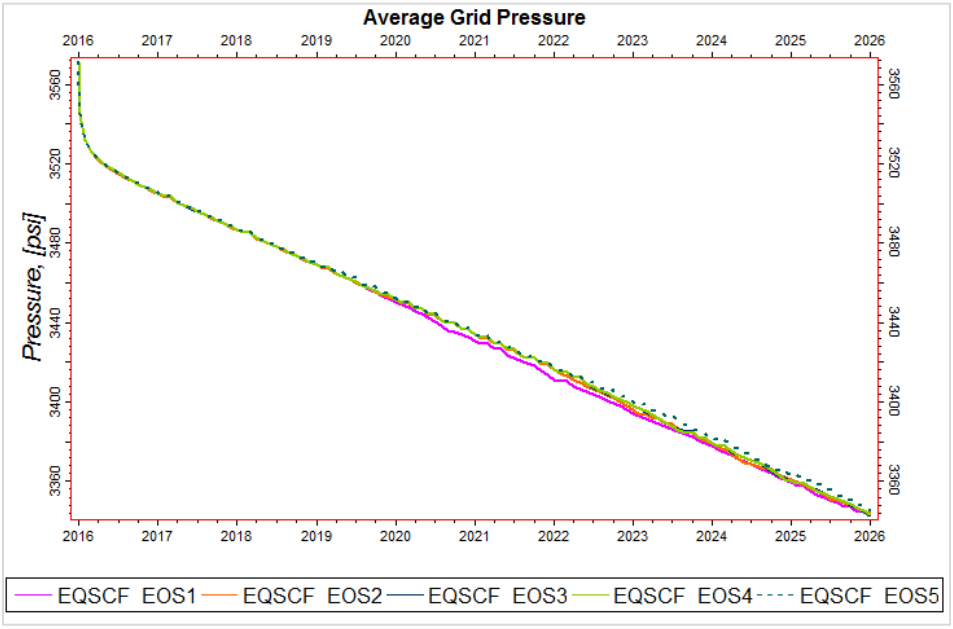

Figure 5.14 Average Grid Pressure of Equivalent Single Porosity Lumped Models.

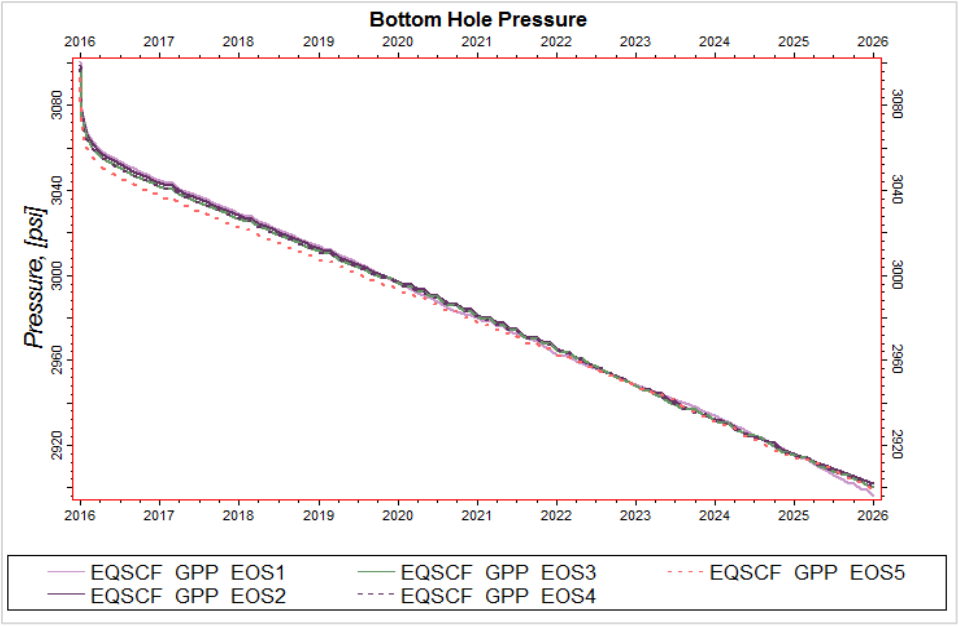

Figure 5.15 Bottom Hole Pressure of Equivalent Single Porosity Lumped Models.

Although the results of 5 different EOS models are in accordance with each other, the EOS 6 deviates from the general trend drastically with respect to average grid and bottom-hole pressure values for the dual porosity and equivalent single medium systems. This deviation indicates that the 6th fluid model having only 5 components is not suitable for the simulation and does not represent the original fluid sample successfully. That may also be predictable comparing the phase diagrams but the simulation was run in order to be sure about that. According to the findings, the minimum number of component should not be less than 7 and the 5th fluid model (EOS-5) is the most optimum fluid model with the optimum component number according to our limitations. The inappropriate representation of the average grid pressure of EOS 6 is plotted in figure 5.16 and 5.17 for dual and equivalent single porosity systems.

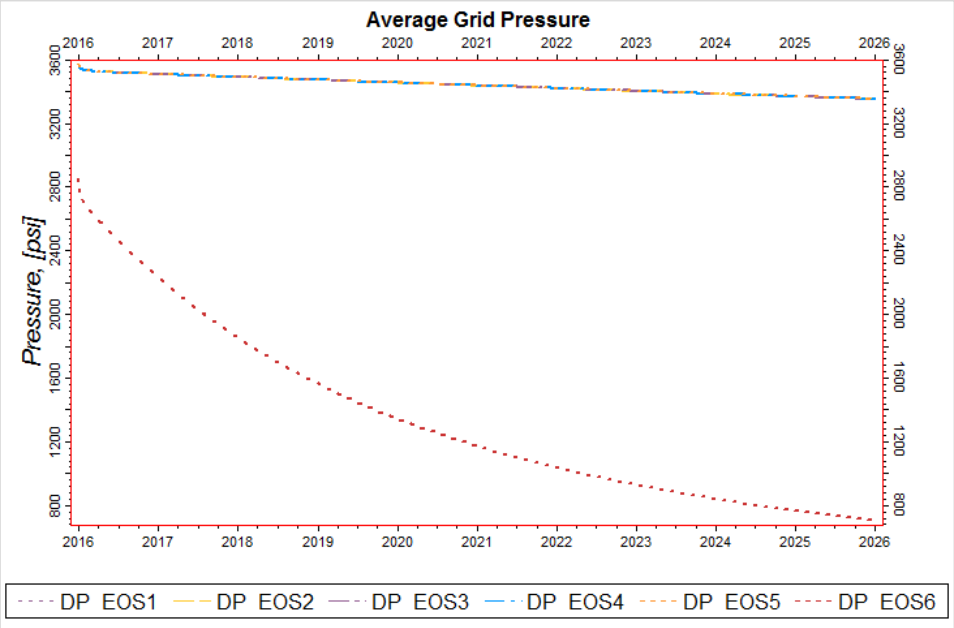

Figure 5.16 Average Grid Pressure of all Lumped Models for Dual Porosity.

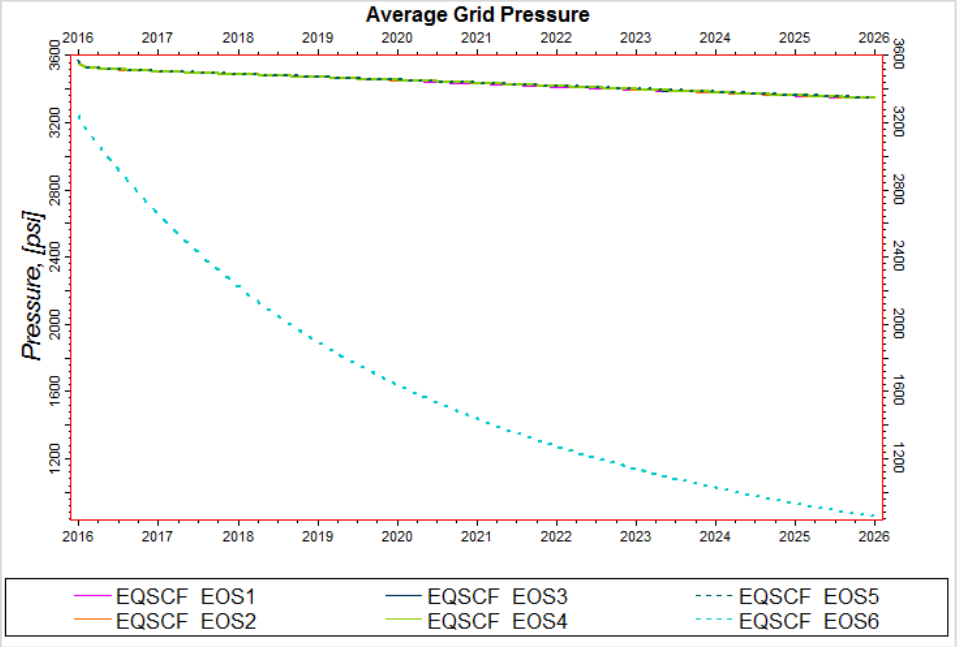

Figure 5.17 Average Grid Pressure of all Lumped Models for Single Porosity.

Similarly, both systems with different EOS models give satisfactory results. Automated lumped methodology works well for the dual porosity systems as well. EOS-5 fluid model case only underestimates the cumulative condensate production amount and the error is less than 0.2 %. The others give almost same results (Figure 5.18). For equivalent single porosity system, the cumulative condensate production values vary within a narrow range while the number of components decreases (Figure 5.19).

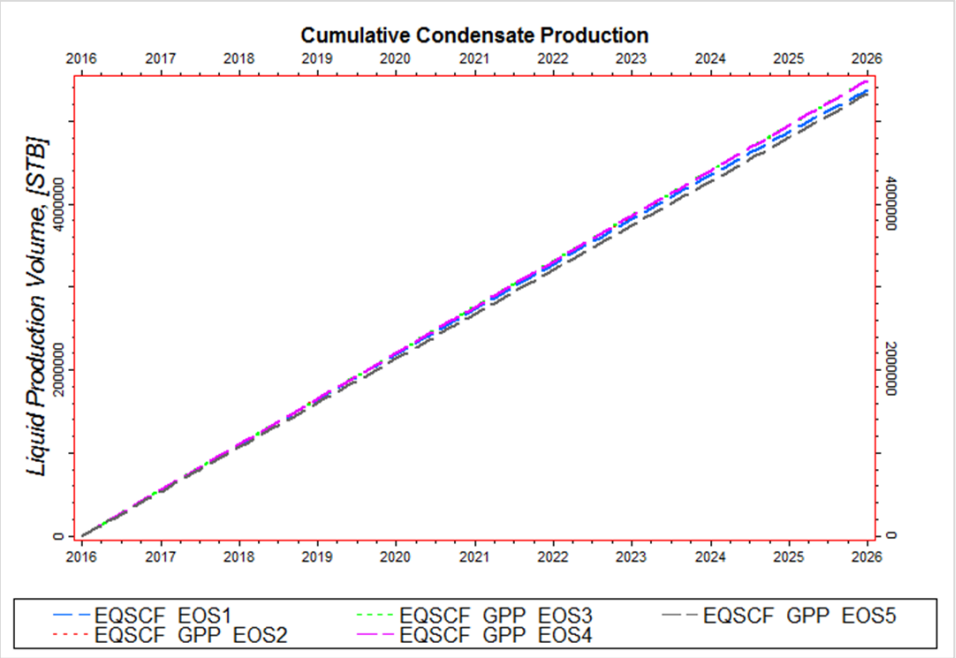

Figure 5.18 Cumulative Condensate Production of Dual Porosity Lumped Models.

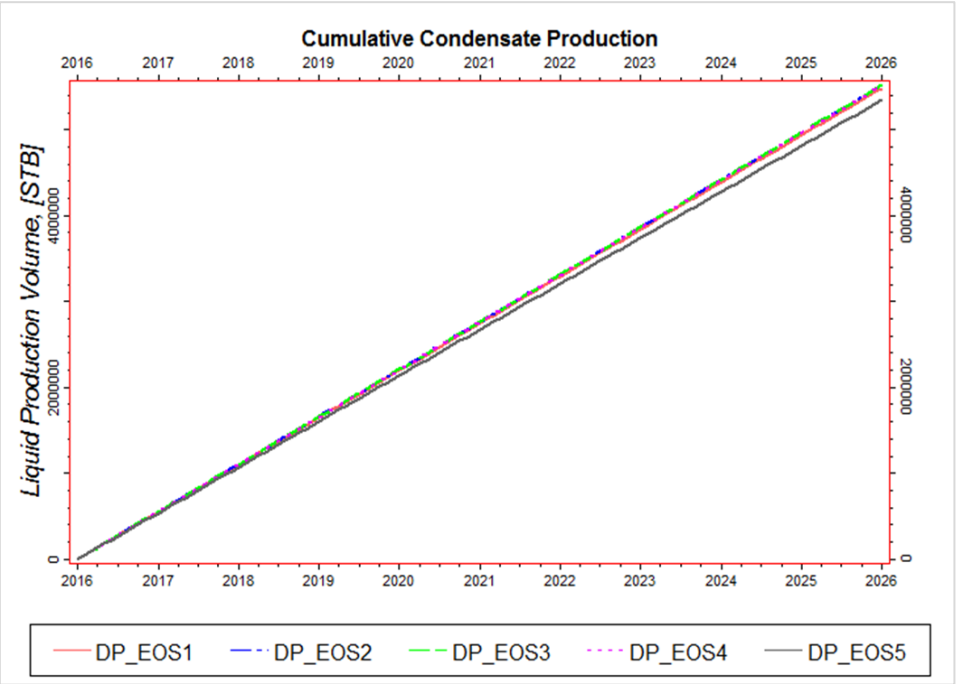

Figure 5.19 Cumulative Condensate Production of Equivalent Single Porosity Lumped Models.

5.3 Comparison of Time Efficiency

In the study, the one of objectives is to minimize the simulation time of naturally fractured gas condensate reservoir by applying the equivalent single medium approach in an innovative way to represent the dual porosity system with a small margin of error and the second one is to reduce the number of components by means of the proposed automated lumping methodology. The representation ability of the equivalent single medium method and the accuracy of lumped fluid models have been already explained in the previous parts. Besides that implementation of both techniques enable us to save the execution time of compositional simulation remarkably. Figure 5.20 indicates the comparison of dual and equivalent single porosity systems with respect to cumulative elapsed time of the simulation for the original fluid sample or EOS-1. The execution time difference between the equivalent single and dual porosity models is definitely large and the ratio of the cumulative time is around 10 for this case.

Figures 5.21 and 5.22 show the effect of different lumped fluid models on the total simulation time. Expectedly, the less number of components are used, the less simulation time is required.

The advantage of the implementing of grouping procedure is seen clearly for both the dual and the single porosity systems and the simulation time can be decreased considerably by this way.

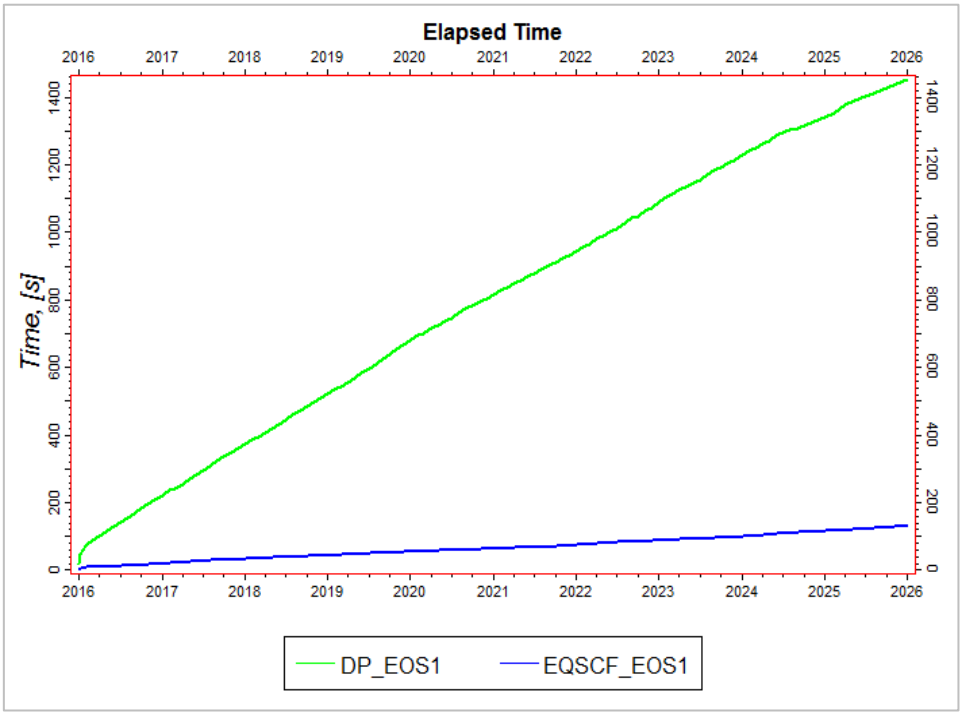

Figure 5.20 Elapsed time of Equivalent Single Porosity and Dual Porosity Models.

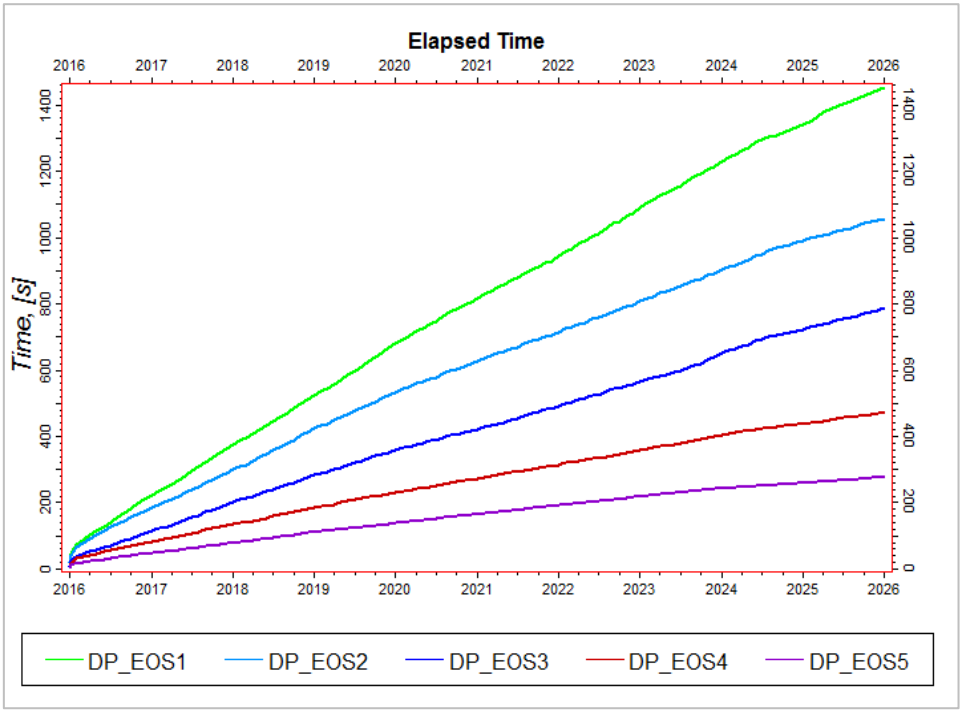

Figure 5.21 Elapsed time of Dual Porosity System with Different Lumped Samples.

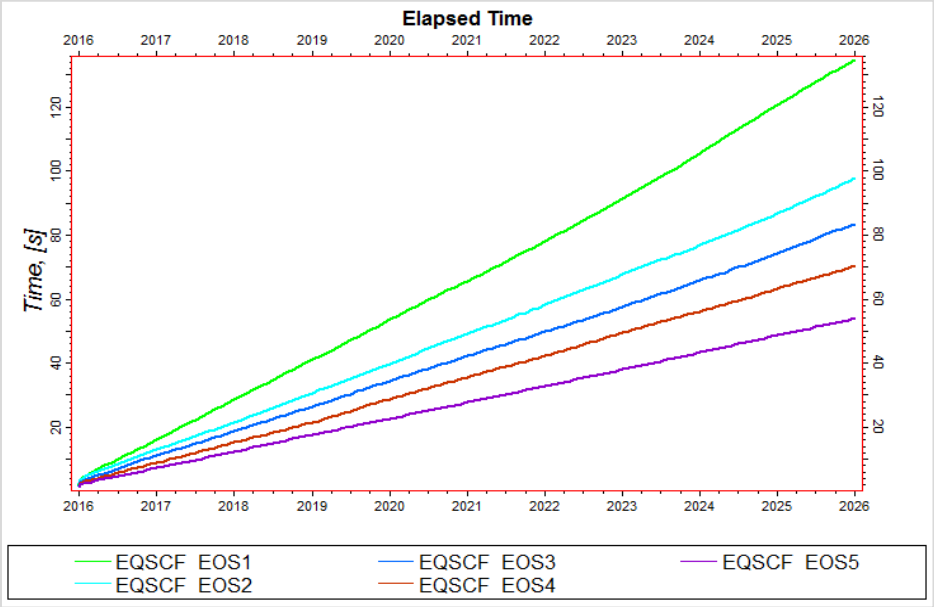

Figure 5.22 Elapsed time of Single Porosity System with Different Lumped Samples

In our case, the execution time can be reduced 5 times with EOS-5 model for dual porosity case and It can reduces the simulation time around 3 times and it is always less than the results of dual porosity cases. Hence, the positive effect of lumping methodology of equivalent single medium model is limited compared to dual porosity system.

The component number versus total simulation time of different lumped fluid samples relationship is given for dual and single porosity systems in figure 5.23 and 5.24. The reduction in component number has a positive effect on simulation time of single porosity system clearly. However, the efficiency of lumping technique on elapsed time does not show the similar linear trend as the component numbers decreases. The slope of the line is higher initially and it tends to decline with less amount of components. Especially, the change on trend line is observed after 13^{th} number of component and it follows a descending line of slope. It means that the performance of the simulation time does not improve at the same speed while the component number gets smaller.

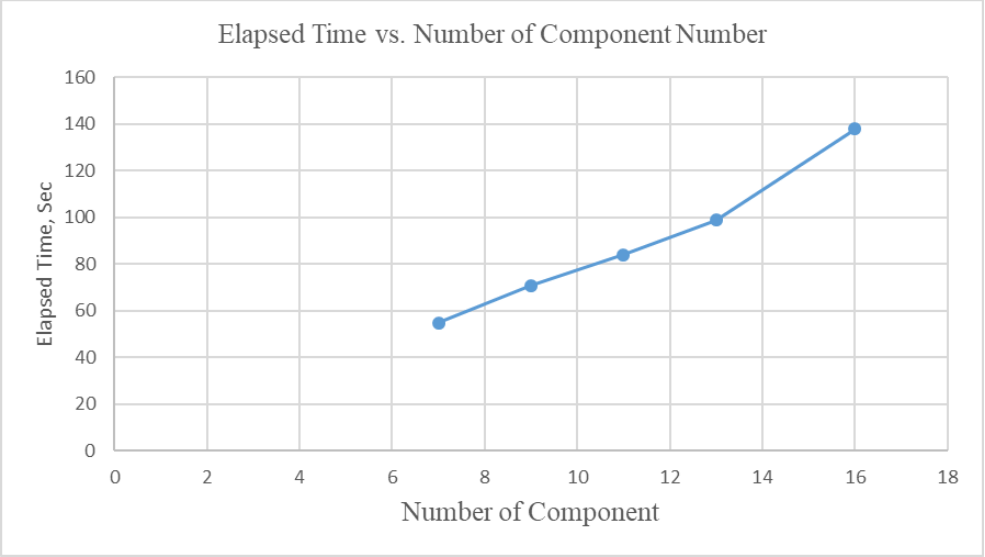

Figure 5.23 Elapsed Time vs. # Component Number for Single Porosity System.

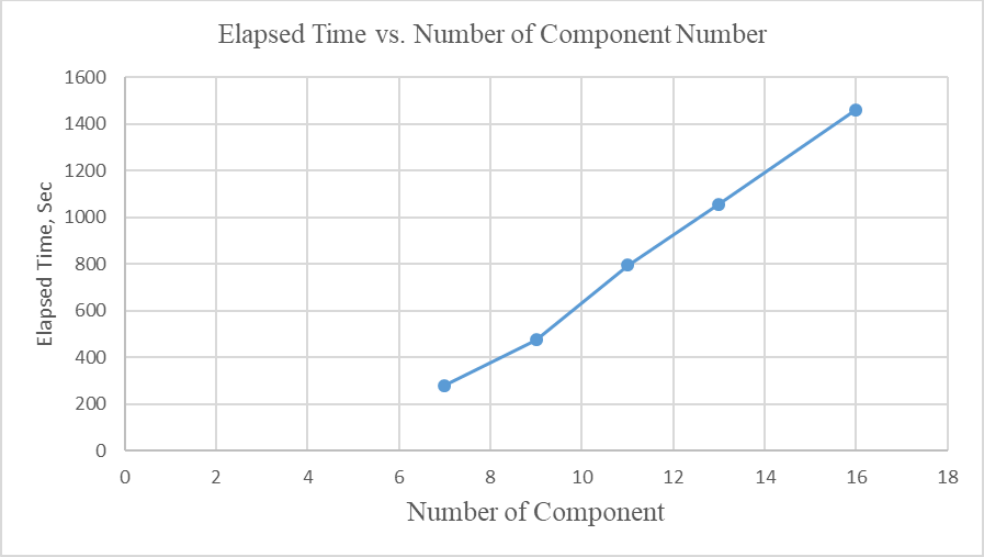

Figure 5.24 Elapsed Time vs. # Component Number for Dual Porosity System.

The reduction in component number has more positive effect on simulation time of dual porosity system and the effectiveness of the lumping approach on elapsed time is better compared to the equivalent single porosity model and that provides more advantage as the slope of line decreases sharply. That arises from the nature of dual porosity approach since the number of grid size is doubled and the calculation of each component is made for the fracture media as well. For this case, the change on the trend line is observed after 9^{th} number of component and it follows less descending line of slope. Similarly, it means that the performance of the simulation time does not

improve at the same speed while the component number gets smaller. Although applying of lumping methodology increase the efficiency of simulation study in terms of elapsed time, the equivalent single porosity and dual porosity models have different characteristics and efficiencies.

Table 5.1 Simulation Time of Some Cases

Name of Case	Simulation Time, Sec	
	DP	ESM
EOS-1	1463	138
EOS-2	1058	99
EOS-3	797	84
EOS-4	476	71
EOS-5	280	55

Table 5.2 Number of Component of Cases

Name of Case	# Component
EOS-1	16
EOS-2	13
EOS-3	11
EOS-4	9
EOS-5	7

The simulation time of some cases for dual porosity and equivalent single medium are tabulated in table 5.1 and the number of component is also given as per case name in table 5.2. The positive effect of equivalent single medium approach is seen clearly on the simulation time. In order to highlight the combined effect of equivalent single medium approach and proposed lumping methodology, the bar chart is constructed and given in figure 5.25.

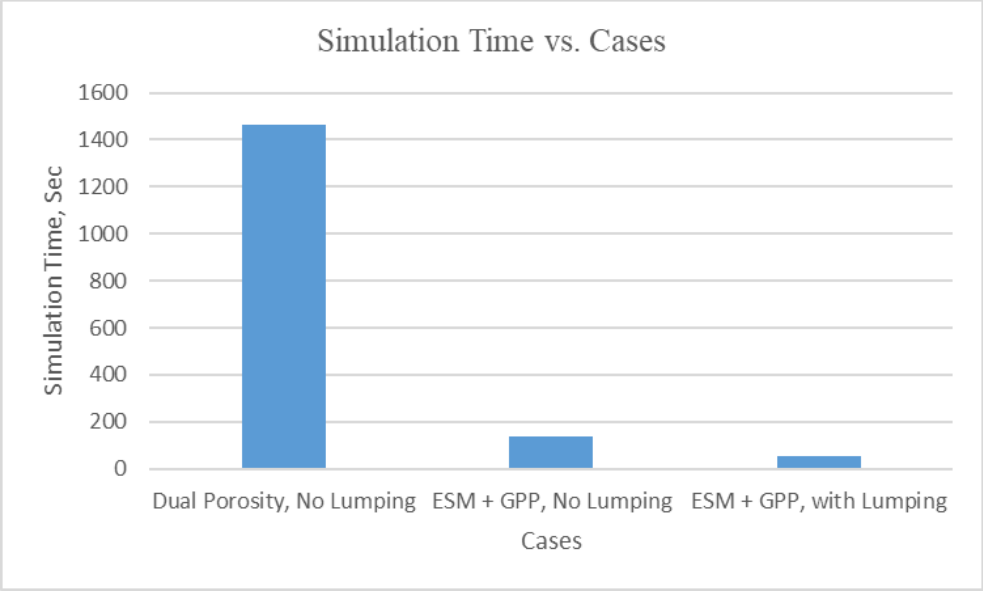

Figure 5.25 Simulation Time vs Cases.

In figure 5.25, the effect of the combination of ESM+GPP with optimum lumping schmes on simulation time is being illustrated. As it is seen on the plot, if the equivalent single medium appoach including GPP facility and pseudo components with the help of lumping are performed together, it is possible to receieve 28-fold decrease on the simulaiton run time.

5.4 Analysis of Automated Lumped EOS Models

The RMS values of all lumped alternatives are constructed separately for each predefined phase with respect to proposed algorithm and analysis of grouped fluid samples are given in the following tables. The main purpose of the automated lumping methodology is to obtain the most appropriate lumped fluid model with the minimum number of component by considering the physical and reliable constraints.

Before we start to apply proposed lumping methodology, the maximum margin of error is defined as 0.2 % and then all lumped models are compared to the original fluid sample in order to determine the margin of error for the each lumping procedure. It is deduced that the simulation results of modified fluid models correspond to that of original one up to 7.2 as reference RMS value but they are liable to deviate

remarkably. After, the suggested algorithm which is already mentioned earlier is applied in a stepwise manner.

In the first step, the plus fraction of fluid sample are handled to reach the optimum grouped configuration. Component number of plus fraction are reduced gradually with respect to proposed algorithm. The available component number are decreased from six to one. Following tables show all the possible alternatives of lumped models and their RMS values in a descending number of component order.

Table 5.3 Error Values of Lumped Plus Fraction for Component Reduction Level 1

Fluid Composition																	Scenario	# total component	RMS Error
C1	N2	C2	CO2	C3	IC4	NC4	IC5	NC5	C6	C7	C8	C9	C10	C11	C12+		1	16	-
C1	N2	C2	CO2	C3	IC4	NC4	IC5	NC5	C6	C7	C8	C9	C10	C11	C12+		2	15	1.73
C1	N2	C2	CO2	C3	IC4	NC4	IC5	NC5	C6	C7	C8	C9	C10	C11	C12+		3	15	1.48
C1	N2	C2	CO2	C3	IC4	NC4	IC5	NC5	C6	C7	C8	C9	C10	C11	C12+		4	15	1.13
C1	N2	C2	CO2	C3	IC4	NC4	IC5	NC5	C6	C7	C8	C9	C10	C11	C12+		5	15	1.01
C1	N2	C2	CO2	C3	IC4	NC4	IC5	NC5	C6	C7	C8	C9	C10	C11	C12+		6	15	0.95

Table 5.3 shows the contiguous couple component of plus fraction and it has very low statistical error but the reduction of component number is only one by this way. The error values decreases for the lighter couple component of plus fraction for all scenarios. They are all lower than reference error value and not suitable to be grouped in this way since there is no big benefit and the more promising alternatives should be assessed.

Table 5.4 Error Values of Lumped Plus Fraction for Component Reduction Level 2

Fluid Composition																	Scenario	# total component	RMS Error
C1	N2	C2	CO2	C3	IC4	NC4	IC5	NC5	C6	C7	C8	C9	C10	C11	C12+		1	14	2.89
C1	N2	C2	CO2	C3	IC4	NC4	IC5	NC5	C6	C7	C8	C9	C10	C11	C12+		2	14	3.56
C1	N2	C2	CO2	C3	IC4	NC4	IC5	NC5	C6	C7	C8	C9	C10	C11	C12+		3	14	5.06
C1	N2	C2	CO2	C3	IC4	NC4	IC5	NC5	C6	C7	C8	C9	C10	C11	C12+		4	14	5.35
C1	N2	C2	CO2	C3	IC4	NC4	IC5	NC5	C6	C7	C8	C9	C10	C11	C12+		5	14	5.38
C1	N2	C2	CO2	C3	IC4	NC4	IC5	NC5	C6	C7	C8	C9	C10	C11	C12+		6	14	6.01
C1	N2	C2	CO2	C3	IC4	NC4	IC5	NC5	C6	C7	C8	C9	C10	C11	C12+		7	14	7.50
C1	N2	C2	CO2	C3	IC4	NC4	IC5	NC5	C6	C7	C8	C9	C10	C11	C12+		8	14	6.60
C1	N2	C2	CO2	C3	IC4	NC4	IC5	NC5	C6	C7	C8	C9	C10	C11	C12+		9	14	6.15
C1	N2	C2	CO2	C3	IC4	NC4	IC5	NC5	C6	C7	C8	C9	C10	C11	C12+		10	14	4.35

Table 5.4 indicates possible alternatives of the component number reduction level two and their corresponding error values. The cluster includes some couple and triple combinations. The coupled alternatives give less amount of error values compared to triple ones. The scenario 1 has lowest root mean squared value. However, it is still not reasonable to lump the plus fraction with these alternative because all error values are below the reference value and the limit should be tested with the configuration having the less amount of component numbers.

Table 5.5 Error Values of Lumped Plus Fraction for Component Reduction Level 3

Fluid Composition																Scenario	# total component	RMS Error
C1	N2	C2	CO2	C3	IC4	NC4	IC5	NC5	C6	C7	C8	C9	C10	C11	C12+	1	13	9.63
C1	N2	C2	CO2	C3	IC4	NC4	IC5	NC5	C6	C7	C8	C9	C10	C11	C12+	2	13	8.20
C1	N2	C2	CO2	C3	IC4	NC4	IC5	NC5	C6	C7	C8	C9	C10	C11	C12+	3	13	7.41
C1	N2	C2	CO2	C3	IC4	NC4	IC5	NC5	C6	C7	C8	C9	C10	C11	C12+	4	13	6.58
C1	N2	C2	CO2	C3	IC4	NC4	IC5	NC5	C6	C7	C8	C9	C10	C11	C12+	5	13	19.23
C1	N2	C2	CO2	C3	IC4	NC4	IC5	NC5	C6	C7	C8	C9	C10	C11	C12+	6	13	13.64
C1	N2	C2	CO2	C3	IC4	NC4	IC5	NC5	C6	C7	C8	C9	C10	C11	C12+	7	13	10.28
C1	N2	C2	CO2	C3	IC4	NC4	IC5	NC5	C6	C7	C8	C9	C10	C11	C12+	8	13	4.64

Table 5.5 demonstrates the possible alternatives of the component number reduction level three and their corresponding error values. The cluster includes some couple, triple, and quadruple combinations. It is seen that the quadruple grouped brings too much error compared to couple, triple and both. Therefore, the gathering of couple and triple lumped seems to be more logical to obtain more representative case with the less amount of error values. The worst scenarios are 5^{th}, 6^{th} and 7^{th} with quadruple grouped components and they have very big error values and exceed the reference error value. The rest of the cases are relatively low error values but the scenario 8^{th} is only within the acceptable range of error. Therefore, the optimum component number reduction level of plus fraction can be three provided that the more compact lumping configuration under the reference error values is not achieved in the further component reduction level of plus fraction. The lumping scheme of scenario 8 is called as PF (Plus Fraction) for the final lumping phase.

Table 5.6 Error Values of Lumped Plus Fraction for Component Reduction Level 4

Fluid Composition																Scenario	# total component	RMS Error
C1	N2	C2	CO2	C3	IC4	NC4	IC5	NC5	C6	C7	C8	C9	C10	C11	C12+	1	12	14.31
C1	N2	C2	CO2	C3	IC4	NC4	IC5	NC5	C6	C7	C8	C9	C10	C11	C12+	2	12	10.64
C1	N2	C2	CO2	C3	IC4	NC4	IC5	NC5	C6	C7	C8	C9	C10	C11	C12+	3	12	41.81
C1	N2	C2	CO2	C3	IC4	NC4	IC5	NC5	C6	C7	C8	C9	C10	C11	C12+	4	12	19.84

Table 5.6 demonstrates the possible alternatives of the component number reduction four and their corresponding error values. The cluster includes some couple, triple, quadruple and quintuplet combinations. Unfortunately, all possible alternatives have higher error values than the predefined reference limit. Even if the scenario 2nd provides less amount of error, it is already above the reference value. This section of plus fraction lumping confirms that the maximum number of component reduction has to be three. Thus, the lumping of the plus fraction can be completed at this point. However, for the sake of formality, the most compact form of plus fraction lumping is also analyzed. Table 5.7 depicts the component number reduction level five and its corresponding error value. Expectedly, it has the highest error value among the set of lumped components and it should be discarded.

Table 5.7 Error Value of Lumped Plus Fraction for Component Reduction Level 5

Fluid Composition																Scenario	# total component	RMS Error
C1	N2	C2	CO2	C3	IC4	NC4	IC5	NC5	C6	C7	C8	C9	C10	C11	C12+	1	11	60.91

It is observed that the reduction in component number increases the RMS values bringing the margin of error up above 60. The recommended number of component reduction should not exceed three for the plus fraction of the original fluid sample to keep the error less than 7.2. According to RMS results, scenario 8th of the component number reduction level three configuration come to the forefront. It has the lowest RMS value and it is the best candidate to be combined with the lumped alternatives of other phases.

In the second step, the isomers are combined and same procedure is done with the previous step to reduce the component number and get the most compact configuration taking into account the RMS values (Table 5.8). The most representative lumped fluid model of isomers are determined and transferred into last phase similarly. As seen from Table 5.8, the lumping of isomers gives very low error once they lessen the component number of original fluid sample. The lumping scheme of scenario 1 and 2 are called as C4+ and C5+ respectively.

Table 5.8 Error Value of Lumped Isomers

Fluid Composition																Scenario	# total component	RMS Error
C1	N2	C2	CO2	C3	IC4	NC4	IC5	NC5	C6	C7	C8	C9	C10	C11	C12+	1	15	0.15
C1	N2	C2	CO2	C3	IC4	NC4	IC5	NC5	C6	C7	C8	C9	C10	C11	C12+	2	15	0.20

In the third step, non-hydrocarbons are kept as pure compounds and grouped with the predefined hydrocarbons accordingly. Table 5.9 indicates RMS values. The margin of error have slightly larger than that of the previous step (isomer lumping) but they also give low error values as the lumping of non-hydrocarbon reduces the component number. The lumping scheme of scenario 1 and 2 are called as X1 and X2 respectively.

Table 5.9 Error Value of Lumped Non-Hydrocarbons

Fluid Composition																Scenario	# total component	RMS Error
C1	N2	C2	CO2	C3	IC4	NC4	IC5	NC5	C6	C7	C8	C9	C10	C11	C12+	1	15	0.36
C1	N2	C2	CO2	C3	IC4	NC4	IC5	NC5	C6	C7	C8	C9	C10	C11	C12+	2	15	0.25

In the final step, the main issue is to have fewer components as much as possible and find the ideal/optimum component number for the compositional simulation study of the equivalent single and dual porosity approaches. With the help of three phases, the total component number has already been reduced from 16 to 9 and the additional treatment is investigated to achieve the less amount of component number.

For this reason, all possible alternatives are evaluated with the predefined constraints. In this case, the most appropriate lumped scheme of the first phase (plus fraction) is kept constant for all other lumped models and then it is tried to come up with the solution lowering the total component number gradually.

In this part, the remaining light hydrocarbons that are not classified in the previous phases are lumped with their contiguous carbon numbers. Later on, the grouped components of the second and third steps are assembled in itself to decrease the component number more.

Table 5.10 Error Values of Final Lumping Schemes

Fluid Composition																	Scenario	# total component	RMS Error
C1	N2	C2	CO2	C3	IC4	NC4	IC5	NC5	C6	C7	C8	C9	C10	C11	C12+		1	11	5.94
C1	N2	C2	CO2	C3	IC4	NC4	IC5	NC5	C6	C7	C8	C9	C10	C11	C12+		2	11	6.07
C1	N2	C2	CO2	C3	IC4	NC4	IC5	NC5	C6	C7	C8	C9	C10	C11	C12+		3	9	6.12
C1	N2	C2	CO2	C3	IC4	NC4	IC5	NC5	C6	C7	C8	C9	C10	C11	C12+		4	8	6.32
C1	N2	C2	CO2	C3	IC4	NC4	IC5	NC5	C6	C7	C8	C9	C10	C11	C12+		5	7	7.49
C2	N2	C2	CO2	C3	IC5	NC5	IC6	NC6	C6	C7	C8	C9	C10	C11	C12+		6	7	7.85
C1	N2	C2	CO2	C3	IC4	NC4	IC5	NC5	C6	C7	C8	C9	C10	C11	C12+		7	7	7.20
C1	N2	C2	CO2	C3	IC4	NC4	IC5	NC5	C6	C7	C8	C9	C10	C11	C12+		8	6	14.48
C1	N2	C2	CO2	C3	IC4	NC4	IC5	NC5	C6	C7	C8	C9	C10	C11	C12+		9	6	15.25
C1	N2	C2	CO2	C3	IC4	NC4	IC5	NC5	C6	C7	C8	C9	C10	C11	C12+		10	5	27.05

As seen from table 5.10, the scenario 1 with the 11 components has the lowest RMS value. Once the remainder light hydrocarbons come into picture separately, the component number can be reduced for each scenario and the error values increase gradually. The scenarios from 2 to 4 show this situation and the total number of component decreases to 8. If the lumping of them are performed by their contiguous carbon numbers, one more component is able to be reduced by means of the scenario 5-7 with 7 total components. Expectedly, that boosts the error values as well. However, the scenario 7 with the 7 pseudo-components brings the grouped isomers with their relevant contiguous carbon atoms and gives the satisfactory results. The scenario 8 considering the lumping scheme of all light carbon numbers enable to decrease component number one more but the RMS value exceeds the reference limit. The scenario 9 taking into account groping of non-hydrocarbons together is another option to reach 6 components as total number of component. However, it makes the

error values worse compared to scenario 8. The scenario 10 having the lowest number of component is the most compact form of grouping and that can be achieved by 5 total components with the highest error values in the final phase of automated lumping procedure. Hence, it is inadequate to represent the original fluid sample in a proper way.

Once RMS error values versus the number of pseudo component are plotted for fluid sample 1 and 2, it is observed that change of trend leads us to determine the optimum number of pseudo components after all lumped schemes RMS errors were estimated as per our proposed lumping methodology. Figure 5.26 & 5.27 depict the relationship between them and how to decide the minimum number of component. The intersecting point of two trend lines corresponds to ending of acceptable correlation between RMS error and number of component. It is expected that extra reduction in component number will cause a large change on RMS error and also simulation results.

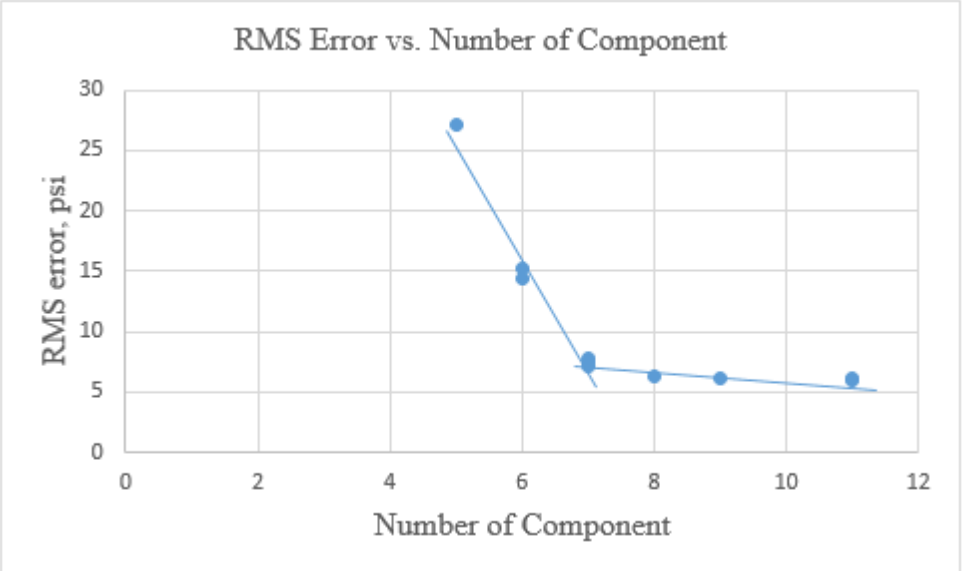

Figure 5.26 RMS Error vs. Number of Pseudo Components (sample 1)

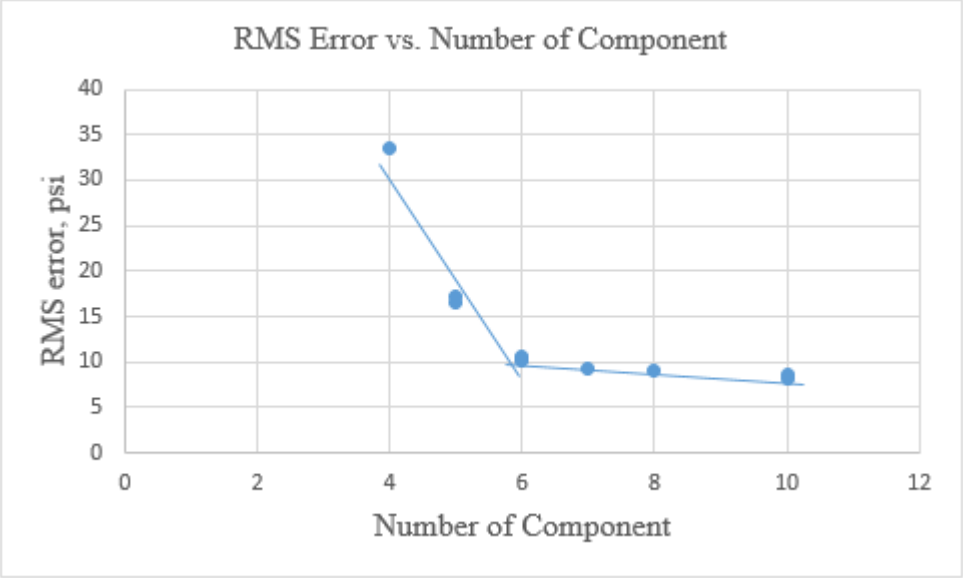

Figure 5.27 RMS Error vs. Number of Pseudo Components (sample 2)

It is understood that the appropriate fluid model with the optimal pseudo-component number and acceptable margin of error should not have less than 7 pseudo-component. The scenario 7 has totally 7 pseudo components and the lowest RMS value in the last phase of lumping methodology and it may be chosen as the best lumping scheme among the set of all plausible combinations and also tested to make sure the accuracy of the compositional simulation run.

The analysis of the lumped fluid models are based on the pressure difference between the phase diagrams at the same temperature and it is evaluated for the different quality lines of phase diagram that intersect them at the reservoir temperature as reference temperature. Once the RMS values are plotted against the error of simulation results, the correlation between them is seen in figures 5.28 and 5.29. As a result, the graph shows that the accurate or more representative lumping model with low RMS value can give insight regarding the simulation results. If the RMS value gets bigger, the simulation results tend to give large amount of error. This relationship seems to be linear (figure 5.28) up to a critical point of RMS value but it does not continue for higher RMS values and the error on simulation results deviates steeply and breaks the linear correlation and follow logarithmic trendline (figure 5.29). The approach works well until the optimum component number of grouped fluid model and then the extra

reduction on component number brings extremely high amount of error. If the lumping gets continued irrespective of simulation and RMS error values, the stabilization may be seen with respect to both trend lines. However, the number of pseudo components and RMS error values do not provide the desired simulation results.

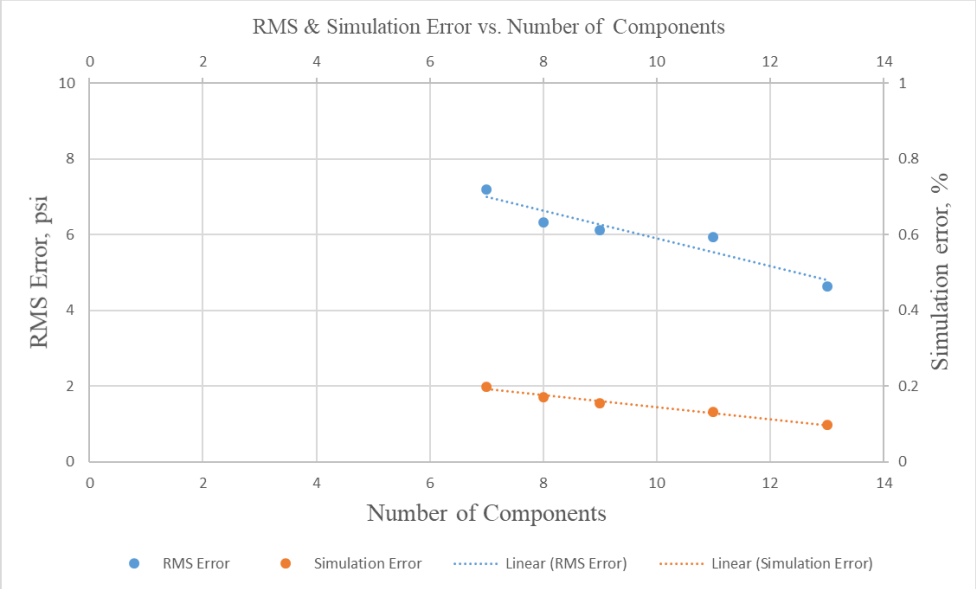

Figure 5.28 RMS & Simulation Error vs. Number of Pseudo Components

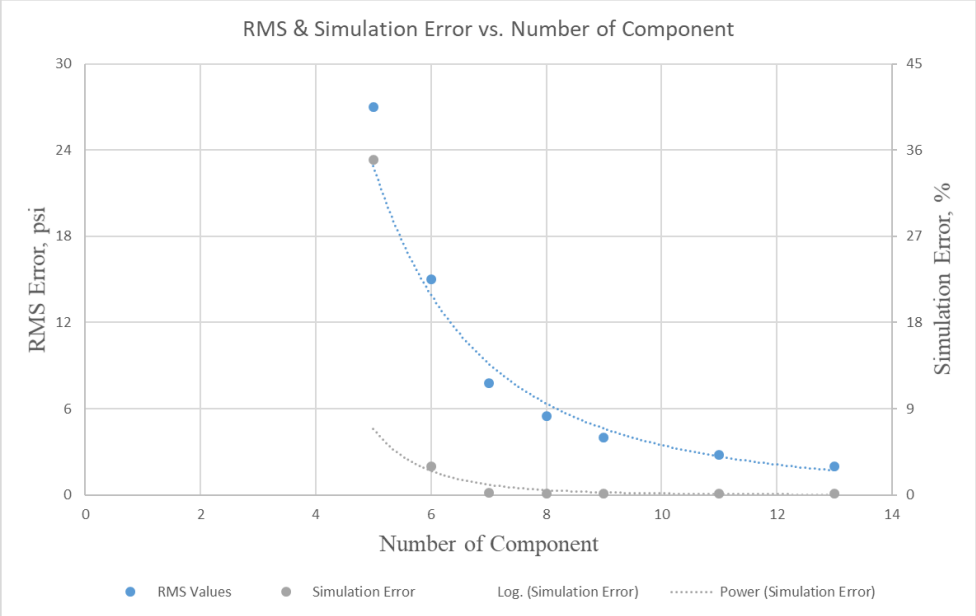

Figure 5.29 RMS & Simulation Error vs. Number of Pseudo Components

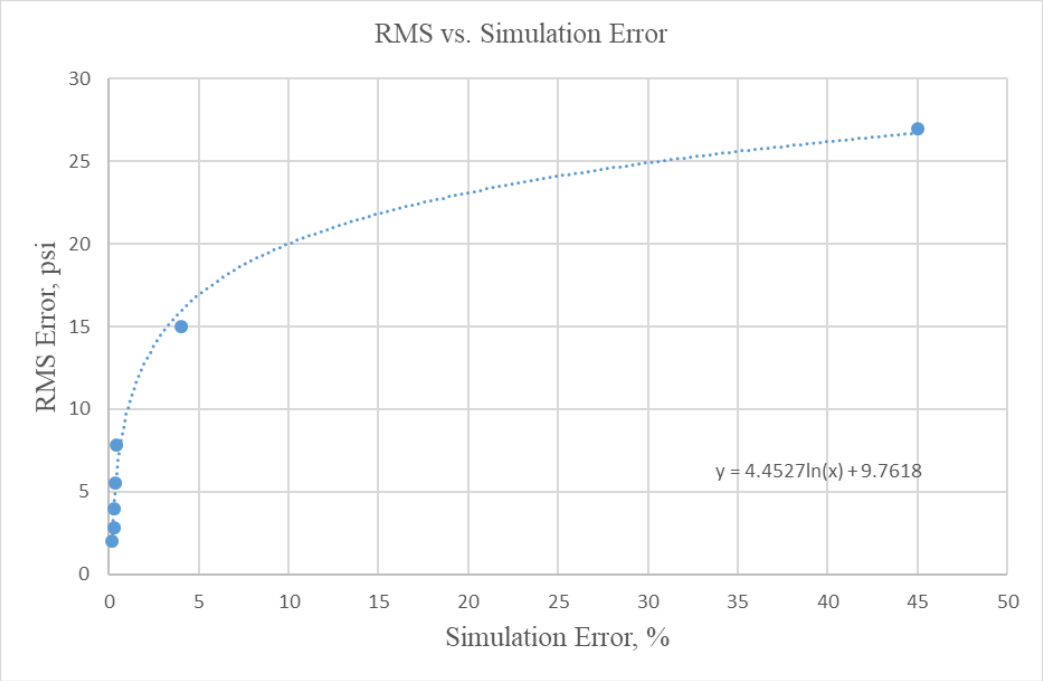

Figure 5.30 RMS vs Simulation Error

Finally, the relationship between RMS error and simulation results are investigated. As seen on figure 5.30, the plot supports the previous findings of the study. In other words, the proposed lumping methodology based on RMS error of phase diagram differences considering the intersection of quality lines at isothermal depletion condition lead us to determine the optimum number of component for lumping and better understand the effect of lumping on simulation results in advance of running. According to plot, the response of simulation error is limited to RMS increase to some extent and then the simulation error starts to increase steeply. Both variables can be correlated logarithmically. The change of behavior is in line with the optimum number of component as well. In fact, the relationship between RMS error of lumping procedure and simulation results can be used as a proxy before performing a compositional simulation study, thus it enables to determine constraints of using pseudo components on simulation results by saving time and cost.

The proposed algorithm has also been applied to a different fluid composition (fluid sample-2) to observe the general trend of the similar lumped schemes. The same methodology used for this study gives a reasonable insight and similar results compared to aforementioned findings. The properties of second fluid sample and all possible grouped models have been given in following figures and tables.

Table 5.11 Composition of Second Fluid Sample

Component Name		**mol %**
CO2	Carbon Dioxide	2.42
N2	Nitrogen	0.47
C1	Methane	68.22
C2	Ethane	11.80
C3	Propane	5.46
IC4	Isobutane	0.83
NC4	n-Butane	1.74
IC5	Isopentane	0.72
NC5	n-Pentane	0.74
C6	Hexanes	1.07
C7	Heptanes	1.09
C8	Octanes	1.47
C9	Nonanes	0.95
C10	Decanes	0.65
C11+	Undecanes plus	2.47
Plus fraction - MW: 217, SG: 0.836		

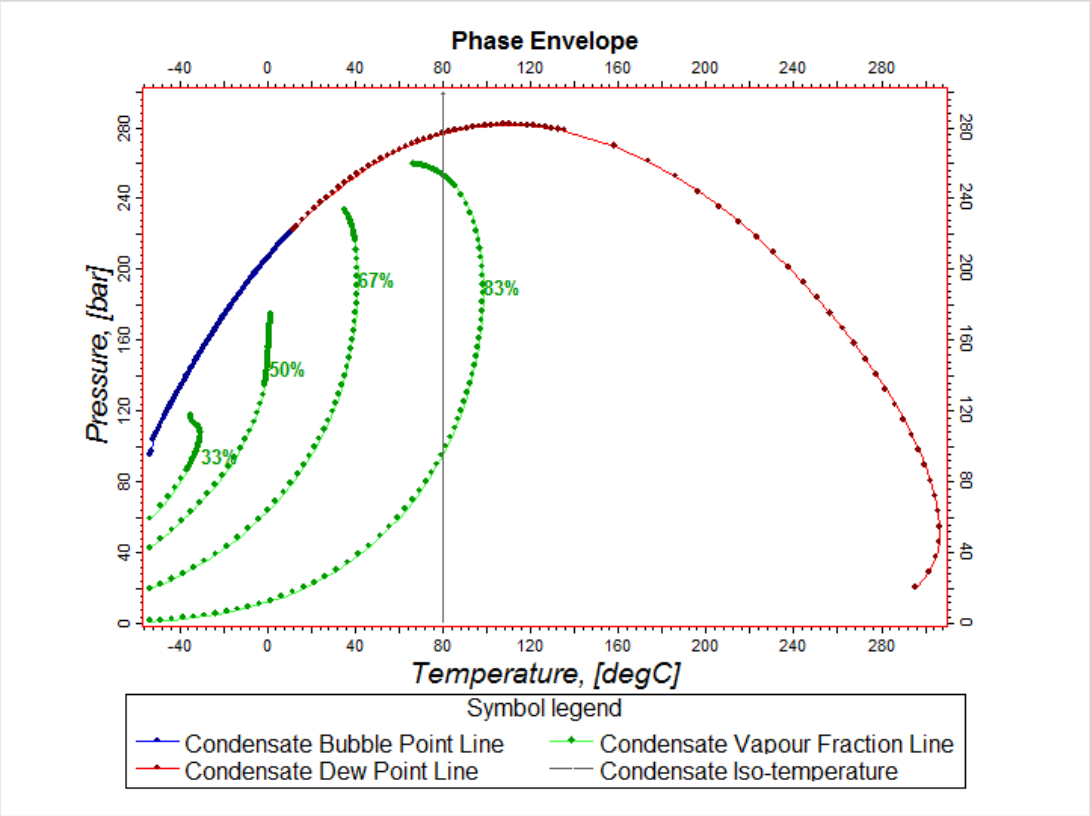

Figure 5.31 Phase diagram of second fluid sample (gas condensate)

Table 5.12 Error Values of Lumped Plus Fraction for Component Reduction Level 1

Fluid Composition															Scenario	# total component	RMS Error
C1	N2	C2	CO2	C3	IC4	NC4	IC5	NC5	C6	C7	C8	C9	C10	C11+	1	15	-
C1	N2	C2	CO2	C3	IC4	NC4	IC5	NC5	C6	C7	C8	C9	C10	C11+	2	14	1.84
C1	N2	C2	CO2	C3	IC4	NC4	IC5	NC5	C6	C7	C8	C9	C10	C11+	3	14	1.42
C1	N2	C2	CO2	C3	IC4	NC4	IC5	NC5	C6	C7	C8	C9	C10	C11+	4	14	1.27
C1	N2	C2	CO2	C3	IC4	NC4	IC5	NC5	C6	C7	C8	C9	C10	C11+	5	14	1.19

Table 5.13 Error Values of Lumped Plus Fraction for Component Reduction Level 2

Fluid Composition															Scenario	# total component	RMS Error
C1	N2	C2	CO2	C3	IC4	NC4	IC5	NC5	C6	C7	C8	C9	C10	C11+	1	13	3.75
C1	N2	C2	CO2	C3	IC4	NC4	IC5	NC5	C6	C7	C8	C9	C10	C11+	2	13	4.63
C1	N2	C2	CO2	C3	IC4	NC4	IC5	NC5	C6	C7	C8	C9	C10	C11+	3	13	6.58
C1	N2	C2	CO2	C3	IC4	NC4	IC5	NC5	C6	C7	C8	C9	C10	C11+	4	13	6.96
C1	N2	C2	CO2	C3	IC4	NC4	IC5	NC5	C6	C7	C8	C9	C10	C11+	5	13	7.01
C1	N2	C2	CO2	C3	IC4	NC4	IC5	NC5	C6	C7	C8	C9	C10	C11+	6	13	7.82

Table 5.14 Error Values of Lumped Plus Fraction for Component Reduction Level 3

Fluid Composition															Scenario	# total component	RMS Error
C1	N2	C2	CO2	C3	IC4	NC4	IC5	NC5	C6	C7	C8	C9	C10	C11+	1	12	11.48
C1	N2	C2	CO2	C3	IC4	NC4	IC5	NC5	C6	C7	C8	C9	C10	C11+	2	12	19.10
C1	N2	C2	CO2	C3	IC4	NC4	IC5	NC5	C6	C7	C8	C9	C10	C11+	3	12	14.39

Table 5.15 Error Values of Lumped Plus Fraction for Component Reduction Level 4

Fluid Composition															Scenario	# total component	RMS Error
C1	N2	C2	CO2	C3	IC4	NC4	IC5	NC5	C6	C7	C8	C9	C10	C11+	1	11	62.71

Table 5.16 Error Value of Lumped Isomers

Fluid Composition															Scenario	# total component	RMS Error
C1	N2	C2	CO2	C3	IC4	NC4	IC5	NC5	C6	C7	C8	C9	C10	C11+	1	14	0.38
C1	N2	C2	CO2	C3	IC4	NC4	IC5	NC5	C6	C7	C8	C9	C10	C11+	2	14	0.23

Table 5.17 Error Value of Lumped Non-Hydrocarbons

Fluid Composition															Scenario	# total component	RMS Error
C1	N2	C2	CO2	C3	IC4	NC4	IC5	NC5	C6	C7	C8	C9	C10	C11	1	14	0.35
C1	N2	C2	CO2	C3	IC4	NC4	IC5	NC5	C6	C7	C8	C9	C10	C11	2	14	0.48

Table 5.18 Error Values of Final Lumping Schemes

Fluid Composition															Scenario	# total component	RMS Error
C1	N2	C2	CO2	C3	IC4	NC4	IC5	NC5	C6	C7	C8	C9	C10	C11+	1	10	8.29
C1	N2	C2	CO2	C3	IC4	NC4	IC5	NC5	C6	C7	C8	C9	C10	C11+	2	10	8.72
C1	N2	C2	CO2	C3	IC4	NC4	IC5	NC5	C6	C7	C8	C9	C10	C11+	3	8	9.05
C1	N2	C2	CO2	C3	IC4	NC4	IC5	NC5	C6	C7	C8	C9	C10	C11+	4	7	9.27
C1	N2	C2	CO2	C3	IC4	NC4	IC5	NC5	C6	C7	C8	C9	C10	C11+	5	6	10.13
C2	N2	C2	CO2	C3	IC5	NC5	IC6	NC6	C6	C7	C8	C9	C10	C11+	6	6	10.35
C1	N2	C2	CO2	C3	IC4	NC4	IC5	NC5	C6	C7	C8	C9	C10	C11+	7	6	10.57
C1	N2	C2	CO2	C3	IC4	NC4	IC5	NC5	C6	C7	C8	C9	C10	C11+	8	5	16.51
C1	N2	C2	CO2	C3	IC4	NC4	IC5	NC5	C6	C7	C8	C9	C10	C11+	9	5	17.18
C1	N2	C2	CO2	C3	IC4	NC4	IC5	NC5	C6	C7	C8	C9	C10	C11+	10	4	33.48

CHAPTER 6

CONCLUSION

In the study, the first innovative approach is to make the PVT lumping/grouping statistically based on the phase diagram comparison considering the all available schemes under the physical constraints and then to calculate the RMS error of each scenario compared to that of original quality lines of phase plot with isothermal depletion assumption. The stepwise manner approach gives insight into the error relationship between simulation and PVT lumping results and it leads to understanding of the optimal number of components to be used prior to running the compositional simulation for both rich gas condensate fluid samples.

Lumping of components or use of pseudo components plays an important role on simulation time.

- Heuristic lumping can pose a problem thus the lumping should be performed in a methodological way.
- The proposed lumping methodology is based on a stepwise algorithm.
- It is possible to find the optimum number of components by the proposed algorithm which compares the isothermal phase diagram differences for rich gas condensate reservoirs.

The second one is to construct the equivalent single media which has not been used to represent the naturally fractured gas condensate reservoirs before instead of doubled number of cells representing the dual-medium matrix/fracture system. It is also integrated with the near well bore modeling facilities to capture the fluid flow occurring through the near wellbore region. That gives reasonable results and reduces the execution time of simulation remarkably.

The equivalent single medium approach can represent the dual porosity model to some extent.

- It should be modified by incorporating the near wellbore modeling techniques to honor the proper bottom-hole pressure behavior.
- Generalized Pseudo Pressure as a near wellbore modeling technique improves the overall accuracy of equivalent single porosity approach especially for BHP.
- Limitation of Generalized Pseudo Pressure is dependent on the ratio of fracture to matrix permeability and it also defines the extent of equivalent single medium approach. The acceptable ratio is less than 25 in this study.

The running of dynamic simulation of naturally fractured gas condensate reservoirs can be conducted by reducing the simulation time drastically with the help of the equivalent single medium approach and proposed lumping methodology.

- ESM approach is able to reduce the execution time drastically compared to DP model. It is possible to save about 10 times less simulation time in this study.
- Lumping Methodology can decrease the elapsed time further for both models and total reduction reached to 28 times using the example composition in this study.

REFERENCES

Afidick, D., Kaczorowski, N., and Bette, S.: "Production Performance of a Retrograde Gas: A Case Study of the Arun Field," Paper SPE 28749 presented at SPE Asia Pacific Oil and Gas Conference, Melbourne, Australia, 1994.

Ahmed, T.: "Equation of State and PVT Analysis," Gulf Publishing Company, Houston, Texas, 2007.

Al Hussainy, R., Ramey, H. and Crawford, P.: "The flow of real gases through porous media," J. Pet. Tech. 237, pp. 624–636, 1966.

Ali, J.K., McGauley, P.J. and Wilson, C.J.: "Experimental studies and modelling of gas condensate flow near the wellbore", Paper SPE 39053 presented at Latin American and Caribbean Petroleum Engineering Conference, 30 August-3 September, Rio de Janeiro, Brazil, 1997.

Allen, F.H., and Roe, R.P.: "Performance characteristics of volumetric condensate reservoir", AIME transaction 189, pp. 83-90., 1950.

App, J.F. and Mohanty, M.: "Gas and Condensate Relative Permeability at Near Critical Conditions: Capillary and Reynolds Number Dependence", Journal of Petroleum Science and Engineering, pp. 111-126, 2002.

Barenblatt, G.I: "On the equilibrium cracks due to brittle fracture. Straight-line cracks in flat plates", Journal of Applied Mathematics and Mechanics 23, pp. 434, 1959.

Barker, J. W.: "Experience with simulation of Condensate Banking Effects in Various Gas Condensate Reservoirs", Paper IPTC presented at International Petroleum Technology Conference, Doha, Qatar, 2005.

Barnum, R., Brinkman, F., Richardson, T., and Spillette, A.: "Gas Condensate Reservoir Behavior: Productivity and Recovery Reduction Due to Condensation," Paper SPE 30767 presented at SPE Annual Technical Conference and Exhibition, Dallas, 1995.

Bear, J. and Buchlin, J-M.: “Modelling and Application of Transport Phenomena in Porous Media,” (Chapter 1), Kluwer Academic Publishers, Dordrecht, 1991.

Bear, J.: “Dynamics of Fluids in Porous Media”, American Elsevier, New York, pp. 784, 1972.

Beckner, B.L.: “Improved Modeling of Imbibition Matrix/Fracture Fluid Transfer in Double Porosity Simulators”, PhD Dissertation at Stanford University, 1990.

Behrens, R.A. and Sandler S.I: “The use of Semicontinuous Description to Model the C7+ Fraction in Equation of State Calculations”, Paper SPE 14925 presented at the 5th Symposium on EOR, Tulsa, 1986.

Bengherbia, M. and Tiab, D.: “Gas-Condensate Well Performance Using Compositional Simulator: A Case Study”, Paper SPE 75531 presented at SPE Gas Technology Symposium, 30 April-2 May, Calgary, Alberta, Canada, 2002.

Blom, S.M.P., Hagoort, J., & Soetekouw, D.P.N.: “Relative Permeability at Near Critical Conditions”, Paper SPE 3835 presented at Ann. Tech. Conf., San Antonio, October, 1997.

Bourbiaux, B., Basquet, R., Cacas, M-C., Daniel, J-M., Sarda, S.: “An Integrated Workflow to Account for Multi-Scale Fractures in reservoir simulation models: Implementation and Benefits”, Paper SPE 78489 presented at Abu Dhabi International Petroleum Exhibition and Conference, Abu Dhabi, United Arab Emirates, October, 2002.

Bourbiaux, B.J. and Limborg, S.: “An Integrated Experimental Methodology for a Better Understanding of Gas Condensate Flow Behaviour,” Paper SPE 28931 presented at 69th SPE Annual Technical Conference and Exhibition, 25-28 September, New Orleans, Louisiana, 1994

Chopra, A. and Carter, R.: “Proof of the two-phase steady-state theory for flow through porous media,” Paper SPE 14472 presented at International Petroleum Technology Conference, Bangkok, Thailand, 1985.

Coats, K. “An equation of state compositional model”. Journal of Petroleum Science and Engineering October, pp. 363–367, 1980.

Coats, K. H.: “An Equation of State Compositional Model”, SPEJ, Oct, 1980.

Coats, K. H.: “Simulation of gas condensate reservoir performance”, JPT pp. 1870–1886, 1988.

Coats, K.H., and Smart, G.T.: “Application of a Regression-Based EOS PVT Program to Laboratory Data”, SPE Res. Eng. pp. 277-299, May, 1986.

Danesh, A. Xu, D.H. and Todd, A.C.: “A Grouping Method to Optimize Oil Description for Compositional Simulation of Gas-Injection Processes", SPE Res Eng. pp. 343-348, 1992.

Dennis, J.E. and Schnabel, R.B.:“Numerical Methods for Unconstrained Optimisation and Non-linear Equations”, Prentice-Hall Inc., New Jersey, 1983.

Dershowitz, W. S., Einstein, H.H., “Characterizing rock joint geometry with joint system models” Rock Mechanics and Rock Engineering, January-March, pp. 21-51, 1988.

Dershowitz, W.S., and Doe, T.W.: “Practical applications of discrete fracture approaches in hydrology, mining, and petroleum extraction”, Proceedings of International Conference on Fluid Flow in Fractured Rocks, pp. 381-396, Atlanta, 1998.

El-Banbi, A.H and McCain W.D.: “Investigation of Well Productivity in Gas-Condensate Reservoirs”, Paper SPE 59773 at SPE/CERI gas Technology Symposium, Calgary, Canada, 2000.

El-Banbi, A.H and McCain W.D.: “Investigation of Well Productivity in Gas-Condensate Reservoirs”, Paper SPE 59773 presented at SPE/CERI gas Technology Symposium, Calgary, Canada, 2000.

Estrada, C. A. and Settari, A.: “Critical Evaluation of Existing Methods for Accounting for Multiphase Effects Around Producers in Depleting Gas Condensate

Reservoirs", Paper SPE 100497 Presented at SPE Gas Technology symposium, Calgary, Alberta, Canada, 2006.

Fevang, O. and Whitson, C.: "Modeling Gas-Condensate Well Deliverability," SPE Reservoir Engineering, pp. 221–230, 1996.

Fevang, O.: "Gas Condensate Flow Behavoir and Sampling," Ph.D. thesis, University of Trondheim, 1995.

Fussell, D.: "Single-Well Performance Predictions for Gas Condensate Reservoirs," JPT July, pp. 860–870, 1973.

Gonzalez, E., Colonomos, P. and Rusinek, I: "A New Approach for Characterizing Oil Fractions and For Selecting Pseudocomponents of Hydrocarbons", JCPT, 78-84, 1986.

Henderson, G. D., Danesh, A., Tehrani, D. H. and Peden, J. M.: "The effect of velocity and interfacial tension on relative permeability of gas–condensate fluids in the wellbore region", Presented at Proceedings of the 8th European IOR Symposium, Vienna, pp. 201–208, 1995.

Henderson, G.D., Danesh, A., Tehrani, D.H. and Al-Kharusi, B.: "The Relative Significance of Positive Coupling and Inertial Effects on Gas Condensate Relative Permeabilities at High Velocity", SPE Paper 62933 presented at Annual Technical Conference and Exhibition, 1-4 October, Dallas, Texas, 2000.

Hinchman, S. and Barree, R.: "Productivity Loss in Gas condensate Reservoirs," Paper SPE 14203 presented at SPE Annual Technical Conference and Exhibition, Las Vegas, Nevada, 1985.

Hong, K.C: "Lumped-Component Characterization of Crude Oils for Compositional Simulation", Paper SPE 10691 presented at the 3rd Joint Symposium on EOR, Tulsa, 1982.

Jacoby, R.H., Koeller, R.C. and Berry, U.J: "Effect of Composition and Temperature on Phase Behavior and Depletion Performance of Rich Gas-Condensate Systems", Trans. AIME, 216, 406-411, 1959.

Joergensen, M. and Stenby, E.H.: “Optimization of pseudo-component selection for compositional studies of reservoir fluids”, SPE Paper 30789 presented at 70th Annual SPE Technical conference & exhibition, Dallas TX, 1995.

Kazemi, H., J. R. Gilman and Elsharkawy, A.M.: “Analytical and Numerical Solution of Oil Recovery From Fractured Reservoirs With Empirical Transfer Functions”, SPE Reservoir Engineering, Volume 7, Issue 2, Pages 219 – 227, 1992.

Kazemi, H., Vestal, C. R., and Shank, G.D.: “An Efficient Multi-component Numerical Simulator", SPE 6890 Journal Paper, pp. 355-368, October 1969.

Kniazeff, V.J. and Naville, S.A.: “Two-Phase Flow of Volatile Hydrocarbons,” Journal Paper SPEJ 37, Trans., AIME, 234, 1965.

Lai, B., Miskimins, J.L, and Wu, S.W.: “Non-Darcy Porous Media Flow According to the Barree and Conway Model: Laboratory and Numerical Modeling Studies”, Paper SPE 122611 presented at SPE Rocky Mountain Petroleum Technology Conference, 14-16 April, Denver, Colorado, 2009.

Li, Y.K, and Nghiem, L.X., and Siu, A. 1984: “Phase Behavior Computation for Reservoir Fluid: Effects of Pseudo Component on Phase Diagrams and Simulation Results”, Paper presented at the Petroleum Soc. Of CIM Annual Meeting, Calgary, June 10-13, 1984.

Li, Y.K, and Nghiem, L.X.: "The Development of a General Phase Envelope Construction Algorithm for Reservoir Fluid Studies" SPE Paper 11198 presented at the 57th Technical Conference and Exhibition, New Orleans, Sept 26-29, 1982.

Li, Y-K., Nghiem, L.X and Siu, A: “Phase Behavior Computations for Reservoir Fluids: Effect of Pseudo-Components on Phase Diagrams and Simulation Results”, JCPT, 29-36, 1988.

Lingen, V.P., Sengul, M., Daniel, J. M., Cosentino, L.: “Single Medium Simulation of Reservoirs with Conductive Faults and Fractures”, Paper SPE 68165 presented at SPE Middle East Oil Show, Manama, Bahrain, March, 2001.

Liu, K.: “Reduce the Number of Components for Compositional Reservoir Simulation”, SPE Paper 66363 presented at the SPE Reservoir Simulation Symposium, Houston, Texas, 11-14 February, 2001.

McKeen, S. A., et al.: Assessment of an ensemble of seven real-time ozone forecasts over eastern North America duringthe summer of 2004, J. Geophys. Res., 110, 21307, 2005.

Michelsen, M.L.: “The Isothermal Flash Problem. Part I. Stability”, Fluid Phase Equillibria, Vol. 9, pp. 1-19, 1982.

Montel, F. and Sandler, S.I: “A new Lumping Scheme of Analytical Data for Composition Studies”, Paper SPE 13113 presented at Proc. Of 59th Ann. Conf., 1984.

Muscat, M.: “Physical Principles of Oil Production,” McGraw-Hill Book Company, Inc., 1949.

Nelson, R. A.: “Geologic Analysis of Naturally Fractured Reservoirs,” Gulf Professional Publishing, Boston, Massachusetts, 2001.

Newly, T.M.J. and Merrill Jr’ R.C: “Pseudocomponent Selection for Compositional Simulation”, Paper SPE 19638 presented at Proc. Of 64th Ann. Conf., 1984.

Nikravesh, M. and Soroush, M.: “Theoretical Methodology for Prediction of Gas-Condensate Flow Behavior”, Paper SPE 36704 presented at Presentation at SPE Annual Technical Conference and Exhibition, Denver, USA, 1996.

O’Dell, H.G. and Miller, R.N.: “Successfully Cycling a Low Permeability, High-Yield Gas-Condensate Reservoir,” JPT 41, Trans., AIME, 240, 1967.

Pedersen, S.K., and Christensen. L.P.: “Phase Behavior of Petroleum Reservoir Fluids”, Taylor and Francis Group LLC, Florida, 2007.

Peng., D.Y. and Robinson “A New Two Constant Equation of State”, Ind Eng. Chem. Fundan, 15(1), pp. 59-64, 1976.

Raghavan, R., Chu, W. C. and Jones, J. R.: “Practical considerations in the analysis of gas-condensate well tests”, Paper SPE 30576 presented at SPE Annual Technical Conference and Exhibition, 22-25 October, Dallas, Texas, 1995.

Riemens, W. and de Jong, L.: “Birba Field PVT Variations Along the hydrocarbon Column and Confirmatory Field Tests,” Paper SPE 13719 presented at SPE Middle East Oil Technical Conference, Bahrain, 1985.

Roebuck, I.F., Ford, W.T., Henderson, G.E., Doughlas, J.: “The Compositional Reservoir Simulator; Case IV – The Two Dimensional Model”, Paper SPE 2235 presented at Annual Meeting, Houston, Texas, 1968.

Rosenberg, V.: “Local Mesh Refinement for Finite Difference Methods”, Paper SPE 10974 presented at SPE Annual Technical Conference and Exhibition, 26-29 September, New Orleans, Louisiana, 1982.

Roussennac, B.: “Gas Condensate Well Test Analysis,” Master’s thesis, Stanford University, Stanford, California, 2001.

Savage, N. H., et al.: Air quality modelling using the Met Office Unified Model (AQUM OS24-26): Model description and initial evaluation, Geosci. Model Dev., 6,353–372, 2013

Schlijper, A.G: “Simulation of Compositional Process, the Use of Pseudocomponents in Equation of State Calculations”, Paper SPE 12633 presented at the SPE/DOE 4th Symposium on EOR, Tulsa, 1984.

Shi, C., Horne, R., and Li, K.: “Optimizing the Productivity of Gas - Condensate Wells,” Paper SPE 103255 presented at Annual Technical Conference and Exhibition, San Antonio, Texas, 2006.

Singh, K and Whitson, C.H.: “Gas Condensate Pseudopressure in Layered Reservoirs”, Paper SPE 117930 presented at Abu Dhabi International Petroleum Exhibition and Conference, 3-6 November, Abu Dhabi, UAE, 2008.

Sognesand, S.: “Long-term testing of vertically fractured gas condensate wells”, Paper SPE 21704 presented at SPE Production Operations Symposium, 7-9 April, Oklahoma City, Oklahoma, 1991.

Spivak, A. and Dixon, T.N.: “Simulation of Gas-Condensate Reservoirs”, Paper SPE 4271 presented at SPE Symposium on Numerical Simulation of Reservoir Performance, 11-12 January, Houston, Texas, 1973.

Vo, D., Jones, J., and Raghavan, R.: “Performance Prediction for Gas Condensate Reservoirs,” SPE Formation Evaluation December, pp. 576–584, 1989.

Vo, D., Jones, J., and Raghavan, R.: “Performance Prediction for Gas Condensate Reservoirs,” SPE Formation Evaluation December, pp. 576–584, 1989.

Warren, J. E. and Root, P. J.: “The Behavior of Naturally Fractured Reservoirs, SPE Journal, pp. 245-255”, Trans. AIME, v. 234, September 1963.

Wheaton, R. and Zhang, H.: “Condensate Banking Dynamics in Gas Condensate Fields: Compositional Changes and Condensate Accumulation around Production Wells,” Paper SPE 62930 presented at Annual Technical Conference and Exhibition, Dallas, Texas, 2000.

Whitson, C. H. and Brule, M. R.: “Phase Behavior”, SPE monograph V. 20, 2000.

Whitson, C. H., Fevang, Oivind, and Saevareid, A.: “Gas Condensate Relative Permeability for Well Calculations”, Transport in Porous Media 52: pp. 279–311, 2003.

Whitson, C. H., Saevareid, A. and Fevang, O.: “An engineering approach to measuring and modeling gas condensate relative permeabilities,” Paper presented at SCA, 2-4 August, Goldon, CO, 1999.

Whitson, C. H.: “Phase Behavior and Flow of Petroleum Reservoir Fluids”, Ph.D. thesis, University of Trondheim, Norwegian Institute of Technology, Department of Petroleum and Chemical engineering, 1982.

Whitson, H. C. and Fevang, Q.: “Generalized Pseudopressure Well Treatment in Reservoir Simulation”, Norwegian University of Science and Technology, 1997.

Wu, S.W., Lai, B., and Miskimins, J.L.: “Simulation of Multiphase Non-Darcy Flow in Porous and Fractured Media”, SPE Paper 122312 presented at Annual Technical Conference and Exhibition, New Orleans, Louisiana, October, 2009.

CURRICULUM VITAE

Name: Mehmet Cihan ERTÜRK

E-mail: mcihanerturk@yahoo.com

Academic Qualifications

- B.Sc. degree in Petroleum and Natural Gas Engineering, Department of Petroleum and Natural Gas Engineering, Middle East Technical University (2002-2007)
- M.Sc. degree in Petroleum and Natural Gas Engineering, Department of Petroleum and Natural Gas Engineering, Middle East Technical University (2010-2013)
- Ph.D. degree in Petroleum and Natural Gas Engineering, Department of Petroleum and Natural Gas Engineering, Middle East Technical University (2013-2018)

Awards

- Performance Award in 2008-2009 academic year, Graduate School of Natural and Applied Science, METU
- Performance Award in 2012-2013 academic year, Graduate School of Natural and Applied Science, METU

Professional Experience

- Reservoir Engineer at Trade of Technology (2007-2009)
- Geomodeller at Halliburton Landmark (2009-2010)
- Senior Reservoir Engineering at Turkish Petroleum Corporation (2010-2018)
- Senior Reservoir Engineering at Genel Energy (2018-present)

Publications

- Erturk, M. C., Sınayuc, C., "Simulation Performance Analysis of Shale Gas and Coal Bed Methane Reservoirs with Different Well Trajectories and Completions Techniques", Presented at AAPG International Conference & Exhibition Istanbul Turkey, 14-17 Sep, 2014
- Erturk, M. C., Sınayuc, C., "Production Performance Analysis of Shale Gas and Coal Bed Methane Reservoirs with Different Well Trajectories and Completions Techniques", Paper SPE 172944 to be presented at the SPE Middle East Unconventional Resources Conference & Exhibition, Muscat Oman, 26-28 Jan, 2015